IT'IS FOUNDATION

Foundation for Research on Information Technologies in Society

Prof. Dr. Niels Kuster

Director Foundation IT'IS
Professor of Swiss Federal Institute of Technology – ETHZ
Phone +41 1 245 9690 · kuster@itis.ethz.ch

Final Report

Project 516

The Effect of the Human Body on Wireless Microphone Transmission

Eugenia Cabot, Myles Capstick

Performed for

BAKOM
Frequency Management Division
Zukunftstrasse 44
P.O. Box 2501
Biel/Bienne

Zurich, July 2015

Contents

List of Figures

1 Introduction

Frequencies assigned for use by wireless microphones are in the VHF and UHF bands. With the recent clearance of the UHF 800 MHz band to broadband mobile, and the potential clearance of the 700 MHz band, wireless microphones are losing the available spectrum [1]. And the remaining spectrum will no longer be able to satisfactorily accommodate the increasing demand for frequencies. Therefore, there is a need to ensure the continuation of wireless microphone services in higher frequency bands as well (such as the 1492 – 1518 MHz band, which is currently being implemented by CEPT working group FM or even higher frequency bands).

1.1 Objectives of the Project

The goal of the study is to quantify the degradation in the wireless microphone transmission performances at higher frequencies as compared to the performances in the UHF band with particular reference to how the radiation pattern of wireless microphones (in the presence of a human body) changes as the transmission frequency increases.

1.2 Scope of the Work

The study has investigated the effect of the antenna placement and its distance from the body on its radiation pattern and consequently, on the link budget loss (body loss) for different frequencies, starting with the VHF band and going up to 6 GHz. This was done using full-wave electromagnetic simulations of three numerical human-body models (obese, average male adult and child), see Figure 1, with a handheld or a body-pack wireless microphone transmitter. As proposed extraction frequencies, 3 frequencies per octave: 235, 300, 375, 470, 595, 750, 945, 1190, 1500, 1890, 2380, 3000, 3780, 4760 and 6000 MHz with specific extractions at 825, 1400 and 1700 MHz.

1.3 Project Plan and Work Packages

1.3.1 Simulation Scenarios

There were two major scenarios studied in this project:

Scenario 1: Handheld Wireless Microphone (see Appendix A)
In this scenario, the human model is posed into a representative posture so as to hold the microphone in one hand close to its mouth and with an inclination angle of 45 degrees.

Scenario 2: Body-Pack Wireless Microphone (see Appendix B)
In this scenario, we will concentrate on the case where a microphone is connected via cable to the bodypack transmitter that is:

- Attached to the belt on the human model's front side
- Attached to the belt on the human model's back side

2 Methods

Simulations using SEMCAD X FDTD EM solver of lossless antennas in typical wireless microphone packages either in free space or in conjunction with a human model were performed. For the purpose of simulation the frequencies were split into 4 different bands, 235 – 825 MHz, 945 – 1890 MHz, 2380 – 3780 MHz and 4760 – 6000 MHz.

2.1 Models

2.1.1 Human Models

Three models were chosen to represent users with different body mass indices, or in other words, small to large users, namely spanning users of 30 to 120 kg weight and 1.35 to 1.78 m tall as a reasonable proxy for the entire user population. The models used in the study can be seen in Figure 1.

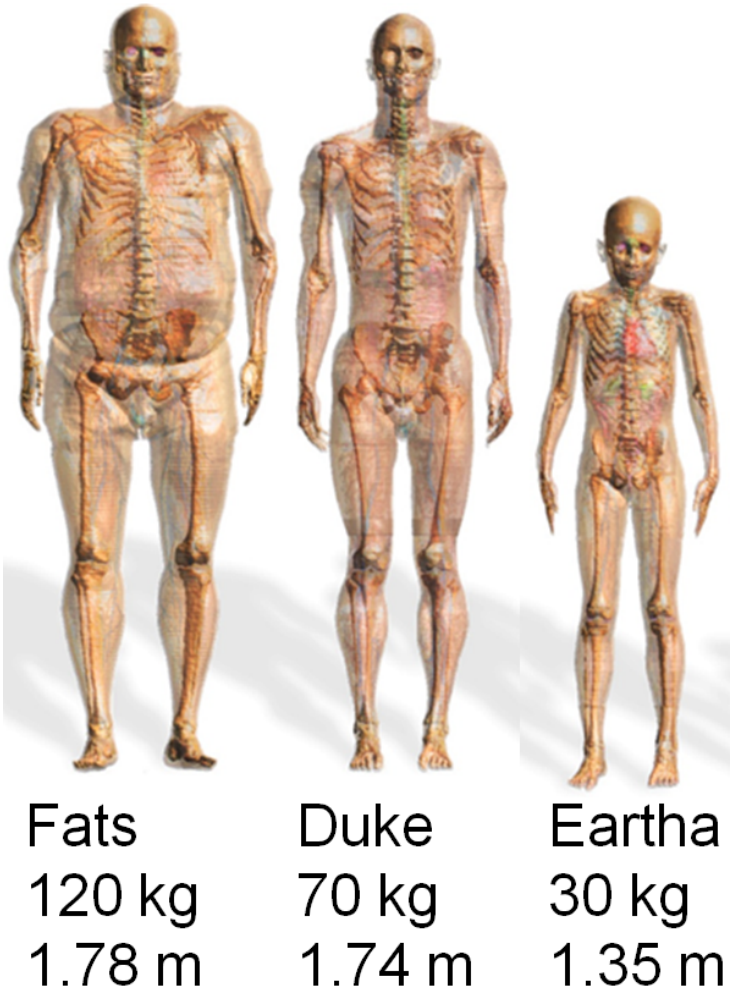

Figure 1: Human Models.

The human models are based on high resolution magnetic resonance images of healthy volunteers. More than 80 different tissues were distinguished during the segmentation of the models [2]. For the simulations, the tissues are assigned with the corresponding dielectric properties, as defined in the database available online [3].

2.1.2 Handheld Microphone Model

The antenna selected for the handheld microphone setup was a short monopole (length $< \lambda/4$). Given this constrain, the lengths of the monopole for the different frequency bands were chosen as:

- Band 1 (235 – 825 MHz): 40 mm
- Band 2 (945 – 1890 MHz): 40 mm
- Band 3 (2380 – 3780 MHz): 16 mm
- Band 4 (4760 – 6000 MHz): 10 mm

The handheld microphone structure combined with the monopole corresponding to each band are depicted in Figure 2. The length of the device is 253 mm, and the diameter of the microphone body is 35 mm. The diameters of the head and cap vary from the microphone body as indicated in Figure 2. The parts of the microphone marked as A and B in Figure 2 were simulated as Perfect Electrical Conductor (PEC), whereas the dielectric cap marked as C was simulated as lossless dielectric with relative permittivity $\epsilon_r = 3$.

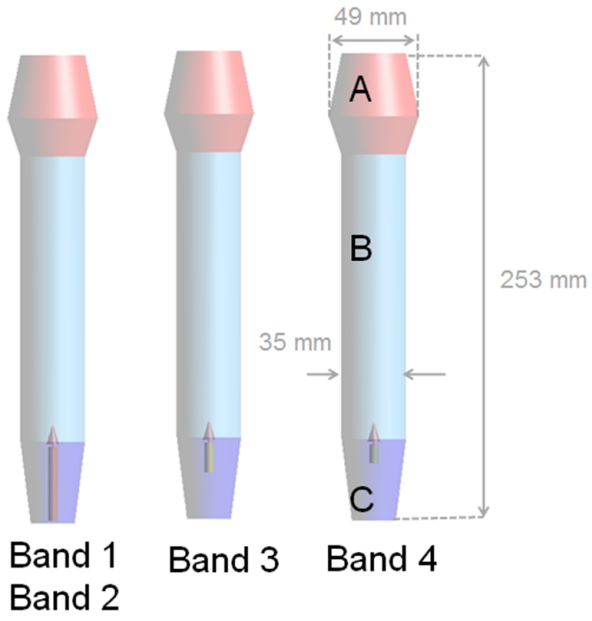

Figure 2: Handheld microphone model.

2.1.3 Bodypack Microphone Model

The antennas in the Bodypack Microphones were simulated as short monopoles, whose lengths were selected according to the frequency band as in the handheld microphone case, see Section 2.1.2. The bodypack microphone system has been modeled as a bodypack, a cable and a small lavalier microphone. The bodypack is a metallic rectangular box, coated with 2 mm thick insulation layer. The cable is grounded to the bodypack metal as shown in Figure 3, and was routed from the bodypack up to the upper torso of the models, keeping 5 mm distance from the body surface along most of the cable length. For model simplicity, the cable has been modeled using a thin wire approximation, and no insulation is covering the metal lead. This approximation reduces considerably the simulation size and run time. The materials used in the simulations were PEC for the monopole, enclosure and microphone lead, and lossless dielectric for the coating of the bodypack ($\epsilon_r = 3$).

2.2 Postures

For the case where the microphone is handheld, an angle of 45° with respect to the axes was chosen as being a representative posture and the human model posed to give a natural arm position, see Figure 4. For the case where a bodypack was used, a typical 1.2 m long lavalier microphone was used and routed close to the body from the lapel as shown in Figure 5.

2.3 Extracted Parameters

The 3D radiation patterns have been extracted with a resolution of 1 degree. The files containing these data form part of the deliverables of the project, and have been sent to BAKOM. In this report, however, some plots of the 3D radiation patterns are shown for illustration, at a lower resolution. The 2D radiation patterns for the three planes XY, YZ and XZ were extracted. Due to the large amount of data, a selection

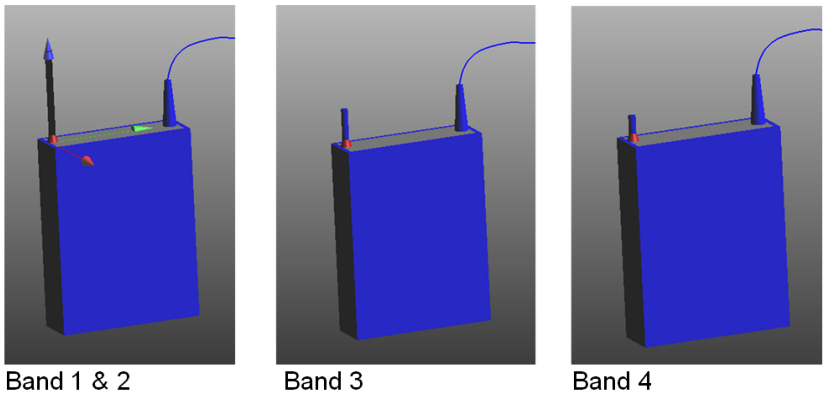

Figure 3: Bodypack microphone model.

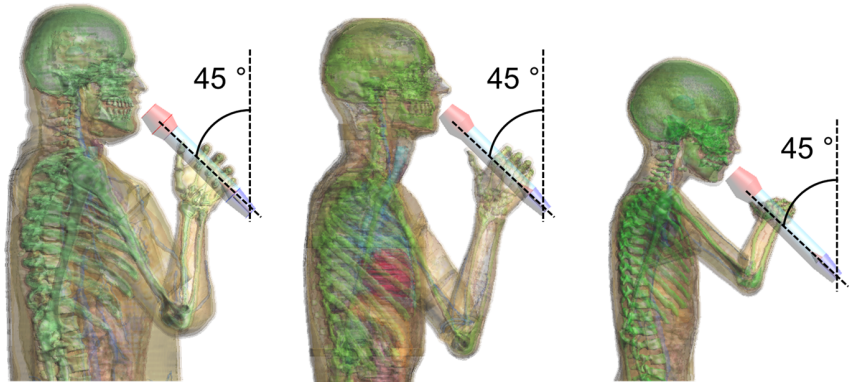

Figure 4: Postures for handheld microphone simulations.

of the 2D radiation pattern plots is included in the main body of the report in Section 3. For the sake of completeness, all the 2D radiation pattern plots (three planes, three human models, and all frequencies) are documented in Appendix A for the handheld microphone and in Appendix B for the bodypack microphone.

Another important aspect that has been investigated in the course of the project is the ratio of the absorbed power in the body versus the radiated power as a function of frequency. At the same time, Specific Absorption Rate (SAR) extractions have been performed, which illustrate power absorption mechanisms.

The results will be shown in reference to the free space case, where the pattern is not affected by the body, and also will be discussed with reference to performance in the bands currently allocated for professional wireless microphones.

All results shown in this report are referenced to 1 W delivered power to the antenna, disregarding mismatch at the feed point. This assumption also implies that the same power is delivered to the antenna in any loading conditions, be the antenna in free space or in the presence of the body. The detuning of the antennas due to the presence of the body has not been studied.

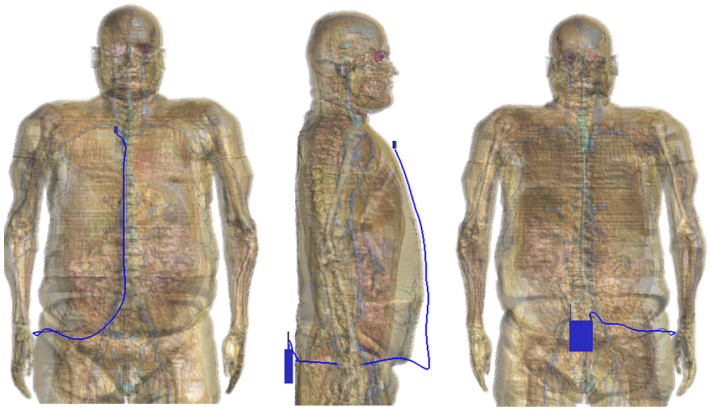

(a) Fats back position

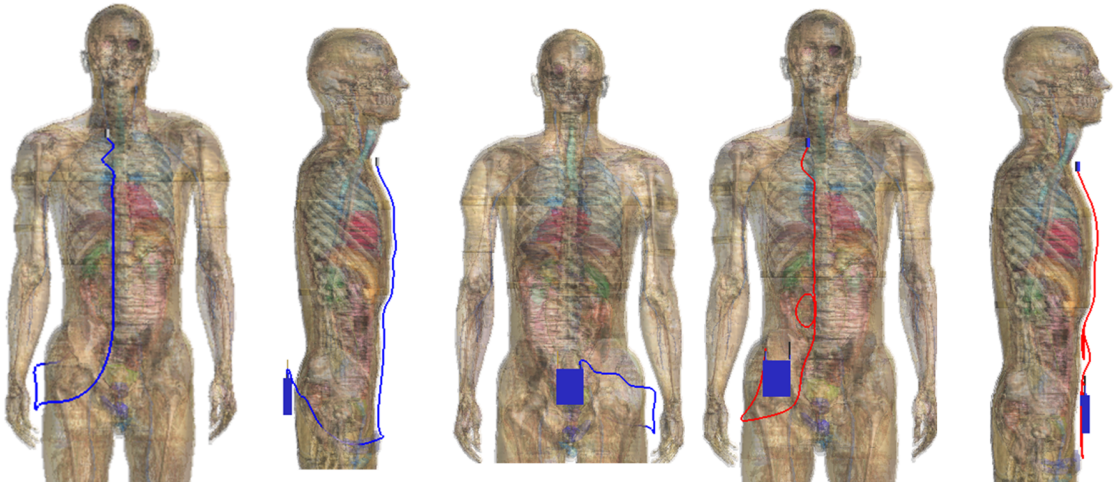

(b) Duke back position

(c) Duke front position

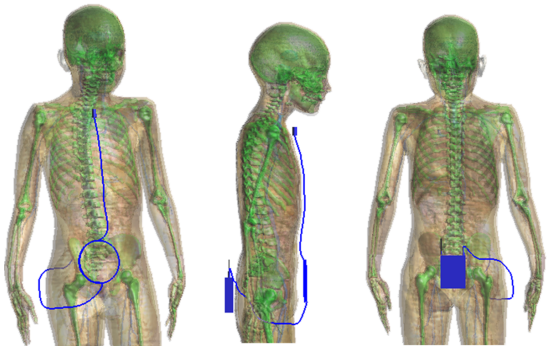

(d) Eartha back position

Figure 5: Lavalier microphone and bodypack positioning.

3 Results

3.1 Handheld Microphones

The handheld microphone was modeled by a conductive tube with a dielectric cover at the bottom containing a monopole fed against the tube as a counterpoise. Figure 6 shows the free space patterns for the microphone monopole combination over the full frequency range of the study.

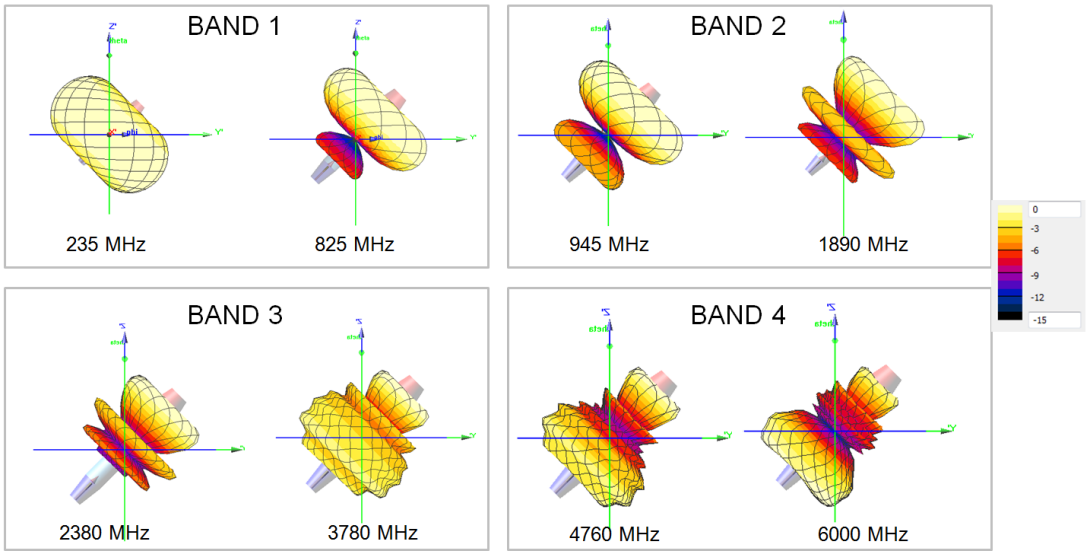

Figure 6: Free space handheld microphone radiation patterns. Scale referenced to peak gain.

The radiation pattern becomes increasingly complex when the microphone body is used as the counterpoise for a monopole element. Effective length for a 40 mm monopole including microphone would be ∼ 266 mm, Figure 7, which is a half wave at ∼ 565 MHz. Above this frequency it will be expected that additional side lobes are introduced, even though the monopole is at, or below, resonance. The simulations clearly show the effect, Figure 6, with the first side lobes becoming evident above at 750 MHz and significant by 825 MHz and increasingly complex at higher frequencies. The radiation patterns when the microphone is held by the hand will be dampened with respect to the microphone in free space.

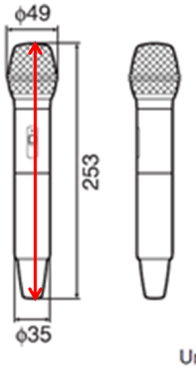

Figure 7: Effective length of the monopole in the handheld microphone.

Figure 8 to Figure 15 show the radiation patterns and how they change between 235 MHz and 6 GHz.

At the lowest frequencies the body and hand/arm do not shadow the radiation pattern. In fact, the interaction acts to modify the radiation pattern and remove some of the nulls that are seen in the free space case. This is due to the hand acting as part of the antenna counterpoise. The loss in the hand also reduces the gain seen but not dramatically. By 845 MHz, Figure 9, the hand continues to act to damp the

nulls, but we see that there is the introduction of some additional nulls in the radiation pattern. It is not completely clear if the origin is due to shadowing or the distribution of RF currents on the microphone and arm.

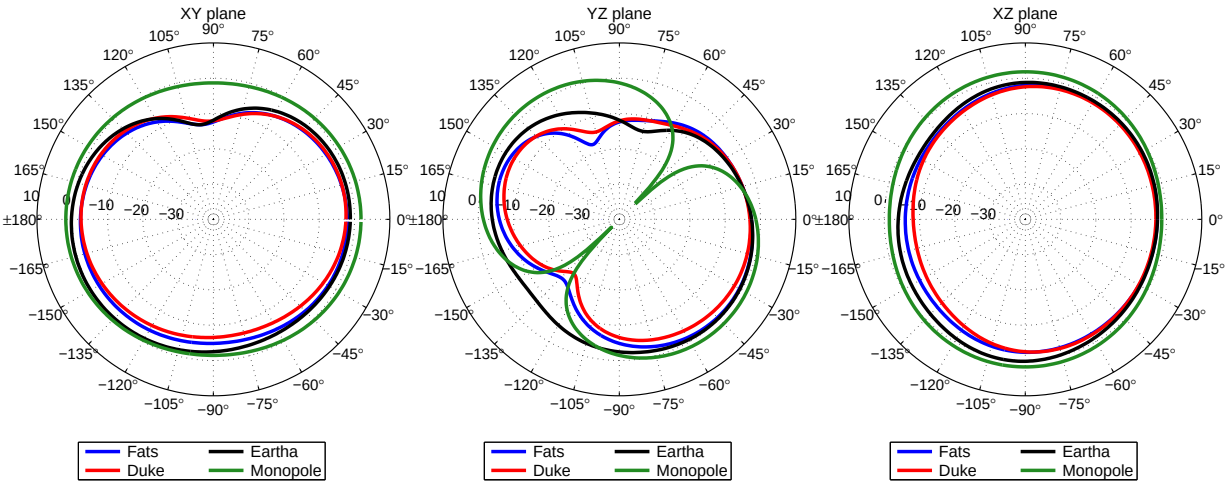

Figure 8: Radiation patterns for the microphone held by the 3 human models and the free space case at 235 MHz.

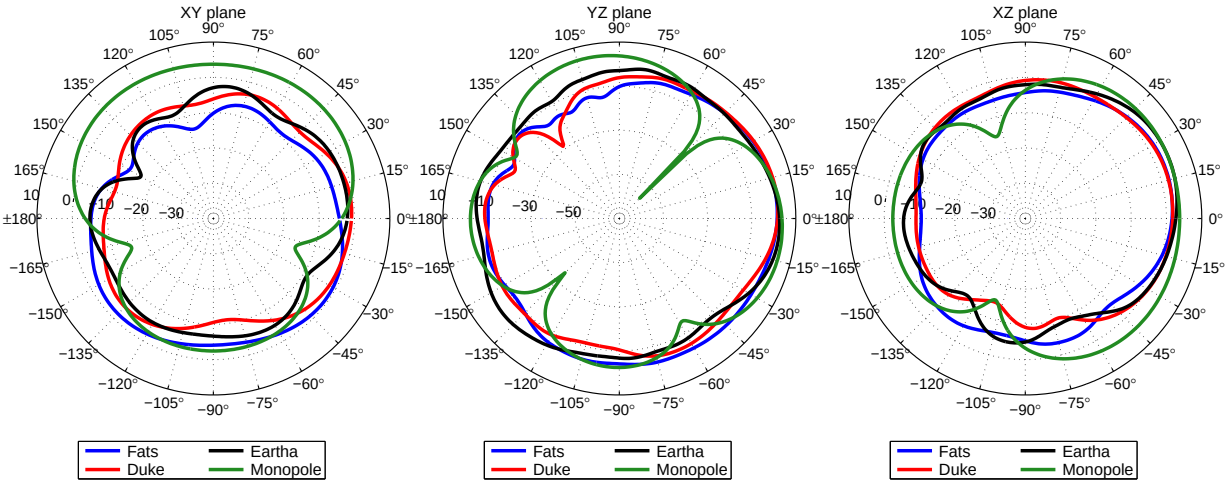

Figure 9: Radiation patterns for the microphone held by the 3 human models and the free space case at 845 MHz.

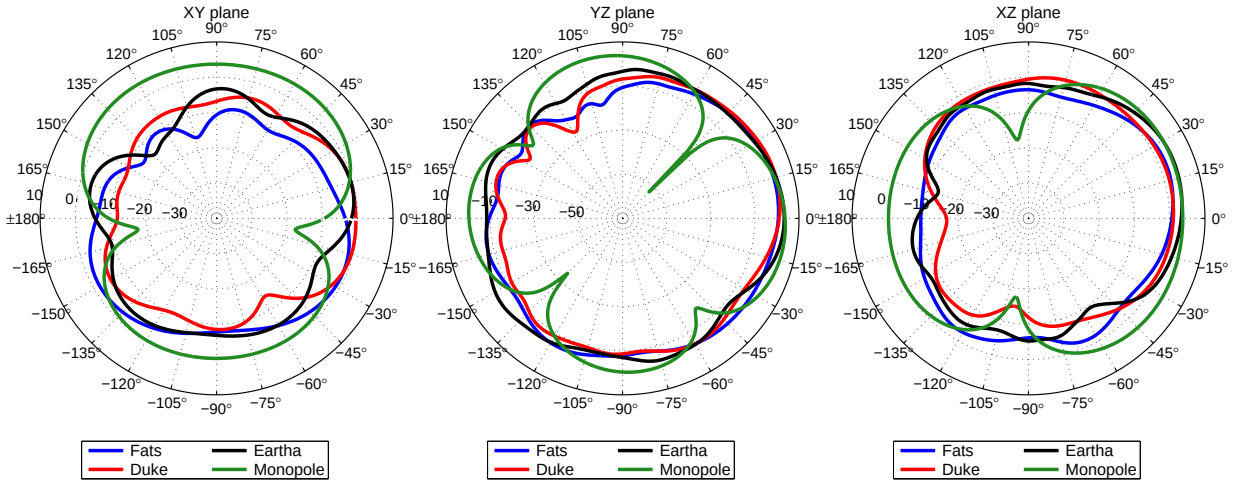

Figure 10: Radiation patterns for the microphone held by the 3 human models and the free space case at 945 MHz.

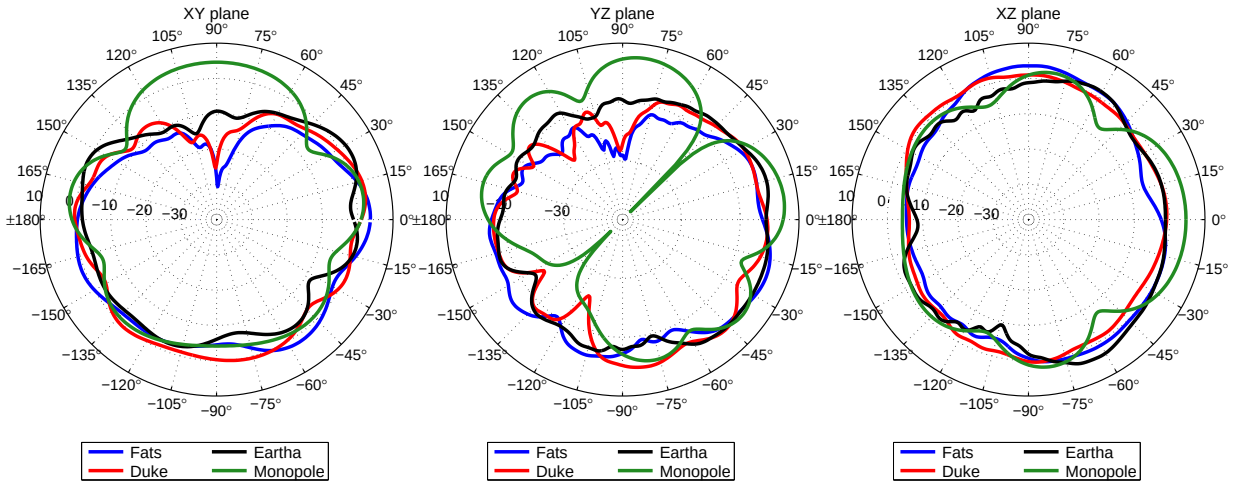

Figure 11: Radiation patterns for the microphone held by the 3 human models and the free space case at 1890 MHz.

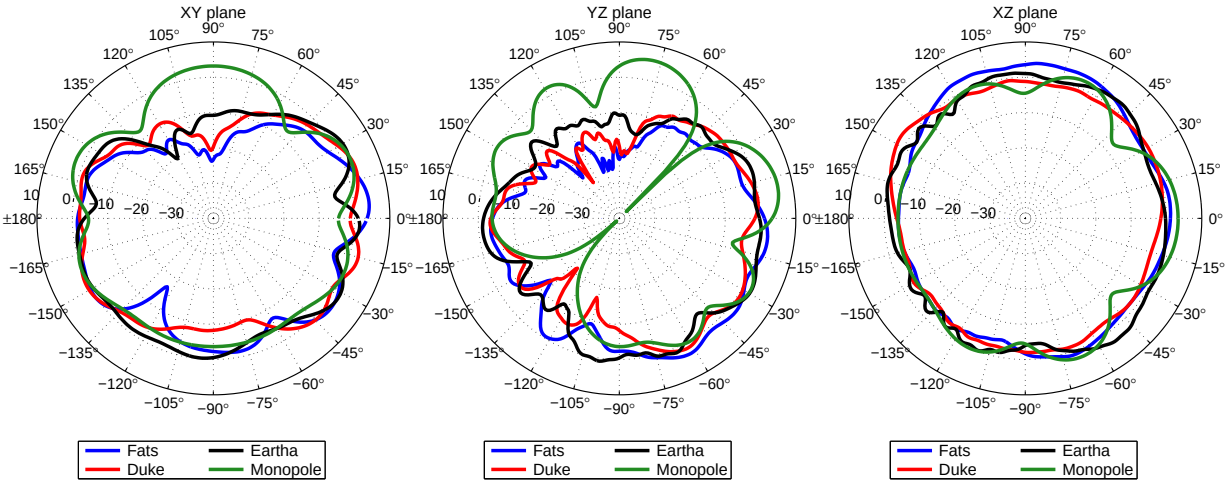

Figure 12: Radiation patterns for the microphone held by the 3 human models and the free space case at 2380 MHz.

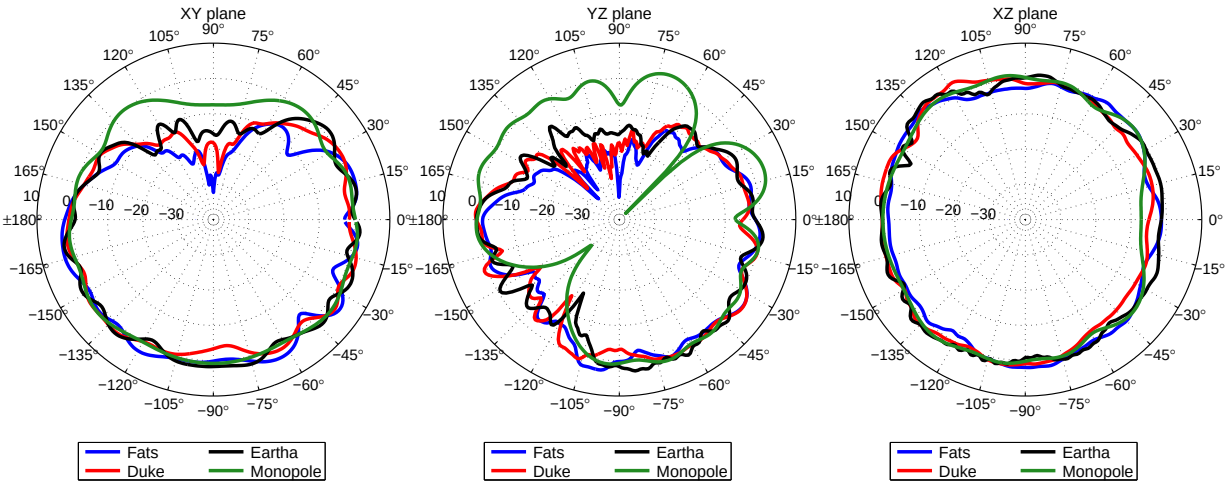

Figure 13: Radiation patterns for the microphone held by the 3 human models and the free space case at 3780 MHz.

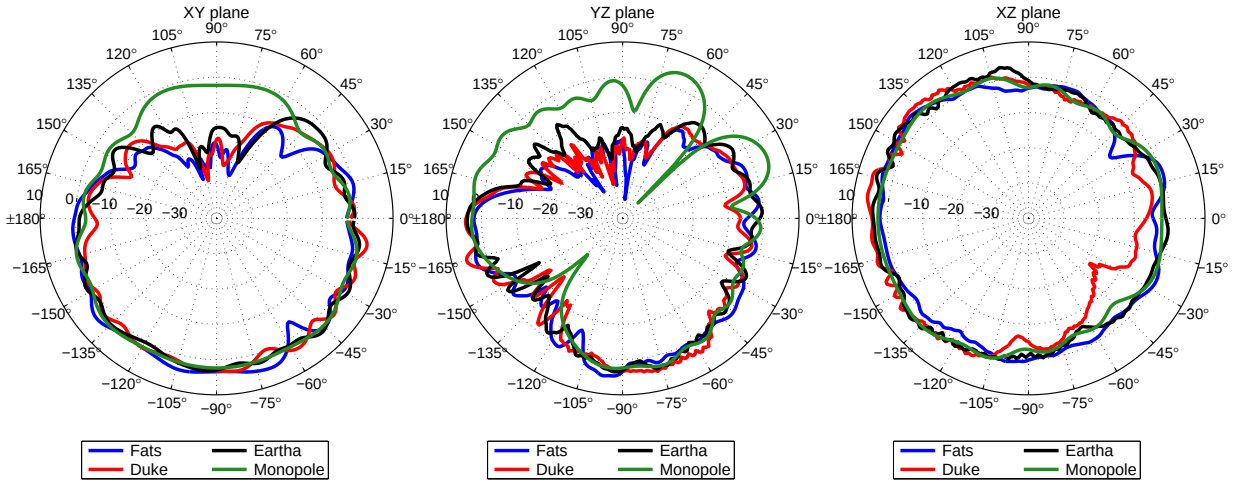

Figure 14: Radiation patterns for the microphone held by the 3 human models and the free space case at 4760 MHz.

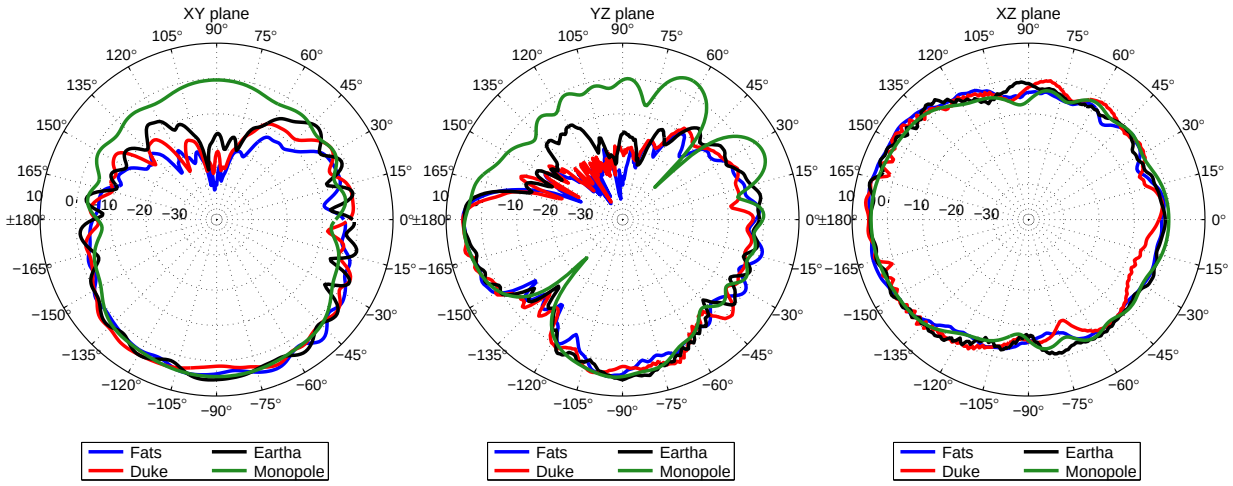

Figure 15: Radiation patterns for the microphone held by the 3 human models and the free space case at 6000 MHz.

The nulls are no deeper than those in the free space case. At 945 and 1890 MHz, Figure 10 and Figure 11, we see a similar pattern to the lower frequencies some gain reduction due to losses in the hand, variations in the radiation patterns with changes in the direction of the nulls, but at 1890 MHz we see the first clear indication of a shadow in the direction of the head and body, which increases in depth as the person gets larger (Figure 11 left plot). As the frequency increases up to the highest frequency of 6 GHz the plots are similar. The horizontal and vertical plots, left and middle plots respectively in Figure 12 to Figure 15, the shadowing of the body is evident, the trend is to slightly more shadowing at higher frequencies but this is not a strong trend. The number of ripples in the patterns increase, as the frequency increases, due to the scattering and multipath mechanisms, the nulls in the patterns are not so related to those of the free space microphone but more directly to the shadowing of the body.

At the lowest frequencies there is a reduction of gain in all directions, whereas at the higher frequencies the gain reduction is only in the directions shadowed by the body. The reason for this can be seen from the power balance, Figure 16, as there is much more loss in the body at low frequencies. The principle reason is that the antenna is then electrically small and the hand and arm play an important role in extending the effective counterpoise of the antenna: The RF current flows along the arm, and the arm being lossy then absorbs a significant amount of power. This mechanism becomes less and less important as the frequency increases and the antenna is no longer electrically small. The specific absorption rate (SAR) at the surface of the body, seen in Figure 17 to Figure 19 for the three body models as a function of frequency, confirms the frequency dependent power balance (more absorption at low frequencies). Also, the SAR in a central slice of the body (plane yz, for x = 0) was extracted for the Duke model at frequencies 825 MHz, 3000 MHz, and 4760 MHz, and it is depicted in Figure 20: The penetration depth is clearly higher at low frequencies and thus the power absorption in the body decays as frequency grows.

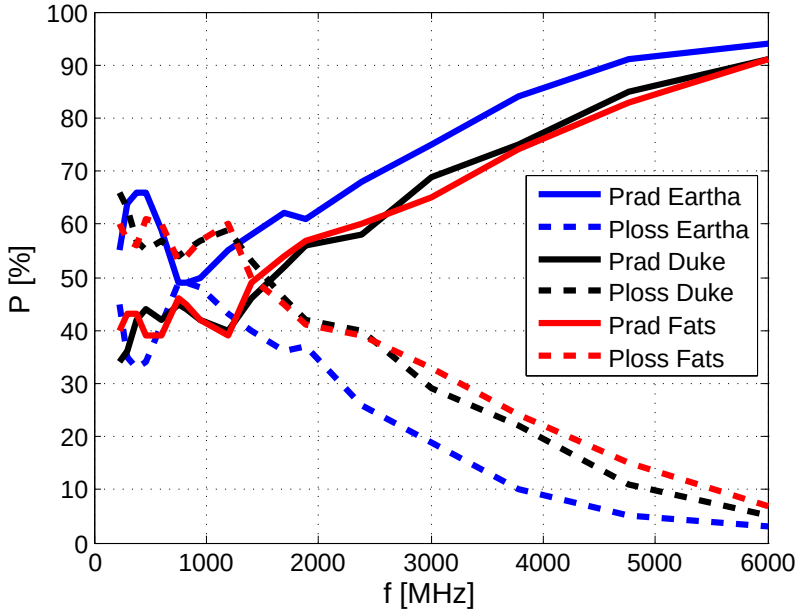

Figure 16: Radiated versus loss power (in %) as a function of frequency, for 1 W input power.

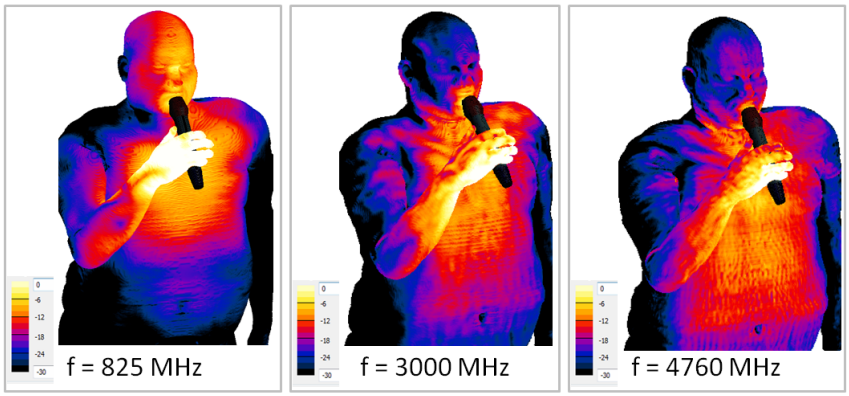

Figure 17: Surface SAR for Fats with the handheld microphone (0 dB = 1 W/kg).

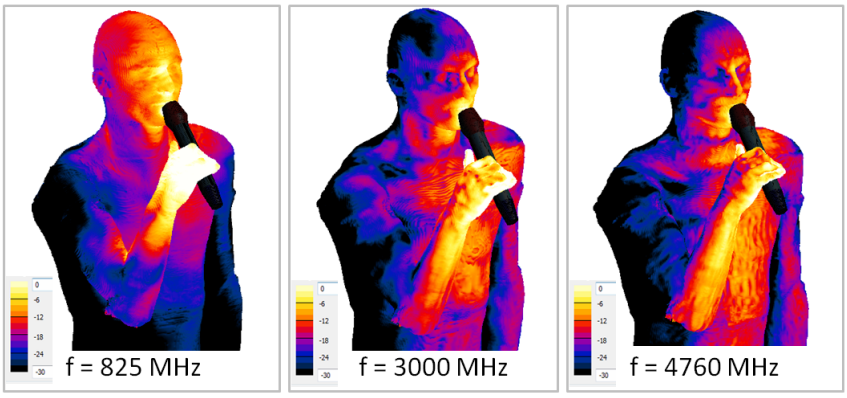

Figure 18: Surface SAR for Duke with the handheld microphone (0 dB = 1 W/kg).

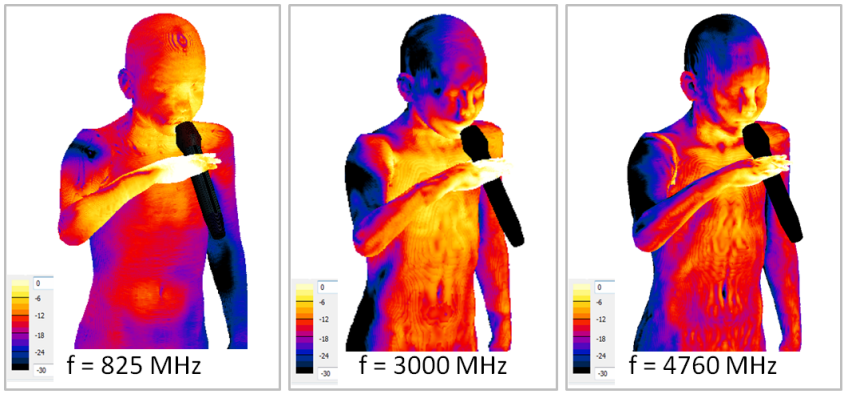

Figure 19: Surface SAR for Eartha with the handheld microphone (0 dB = 1 W/kg).

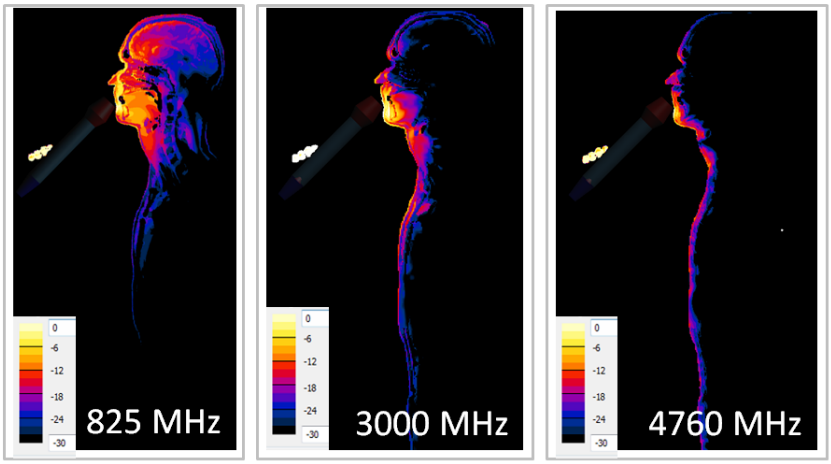

Figure 20: SAR distribution in a profile view of the the Duke model (central slice), showing the absorption in the frontal part of the body due to the antenna radiation at 3 different frequencies. In the scale 0 dB are equivalent to 1 W/kg for 1 W input power.

One question that arises is does the pattern complexity of the free space microphone have significant influence on the results with the body present? Figure 21 shows the simple monopole fed against the microphone body. Figure 22 shows a different configuration with a short dipole, reducing complexity, though reflections from the microphone body still add some ripples. Comparing Figure 23 to Figure 15 we can see that there are some small differences, but the majority of effects are related to the presence of the human body and not to the complexity of the free space pattern when the hand is not present, which confirms the original assumption.

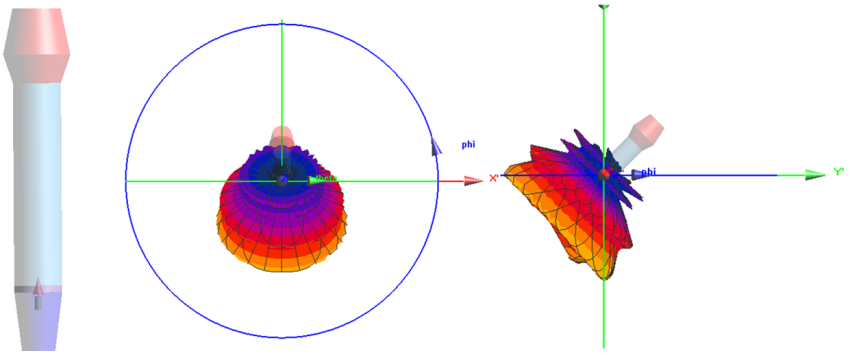

Figure 21: Monopole antenna at 6000 MHz.

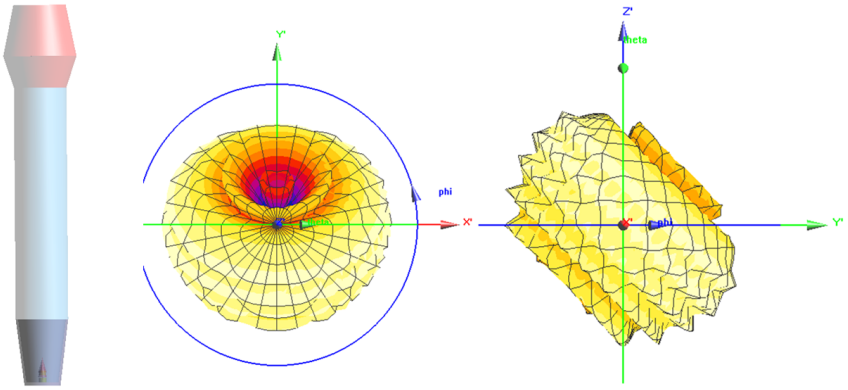

Figure 22: Dipole inside the radome not fed against the microphone body, at 6000 MHz.

Only a subset of the results have been shown here that are sufficient to illustrate the points for discussion. The complete set of simulation results for all frequencies can be found in Appendix A.

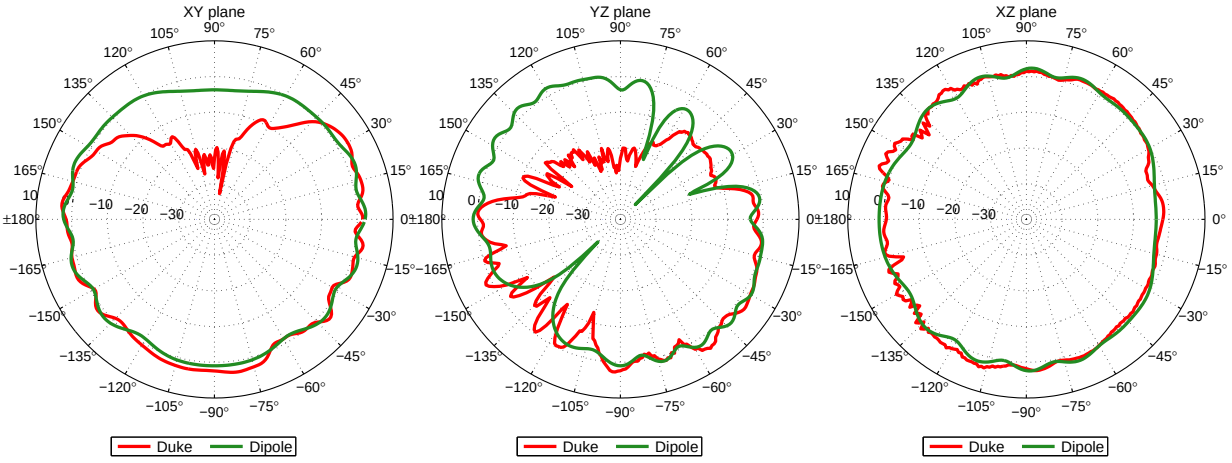

Figure 23: Radiation patterns at 6000 MHz for Duke with handheld microphone with reduced complexity in the reference pattern (as shown in Figure 22).

3.2 Bodypack Microphones

The bodypack with a lavalier microphone was modeled by a conductive case with a dielectric coating to prevent conductive contact to the body and a monopole on the top fed against the case as a counterpoise. The lavalier was modeled as a conductor 1.2 m long with the shield connected to the case "ground". Figure 23 shows the free space radiation patterns of the bodypack with microphone.

At the lowest frequency the microphone lead plays a dominant role in the radiation mechanism as can be seen by the dipole pattern aligned with the lead. As the frequency increases the pattern rotates to be aligned with the monopole - case axis showing that the extension provided by the lead becomes less important. As the frequency increases further the radiation pattern becomes increasingly complex when the microphone case is used as the counterpoise for a monopole element. The complexity is related to the effective length. For a 40 mm monopole including bodypack overall length is ∼152 mm, Figure 24, which is a half wave at ∼985 MHz. Therefore, above this frequency it will be expected that additional side lobes are introduced even though the monopole is at, or below, resonance.

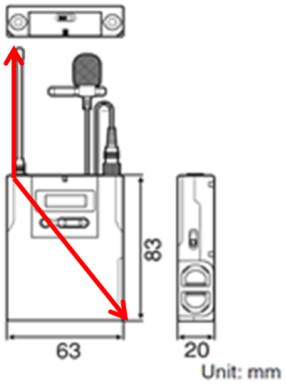

Figure 24: Bodypack model.

Figure 25 to Figure 32 show the radiation patterns and how they change from 235 MHz and 6 GHz when the microphone is at the lapel and bodypack on the belt at the back.

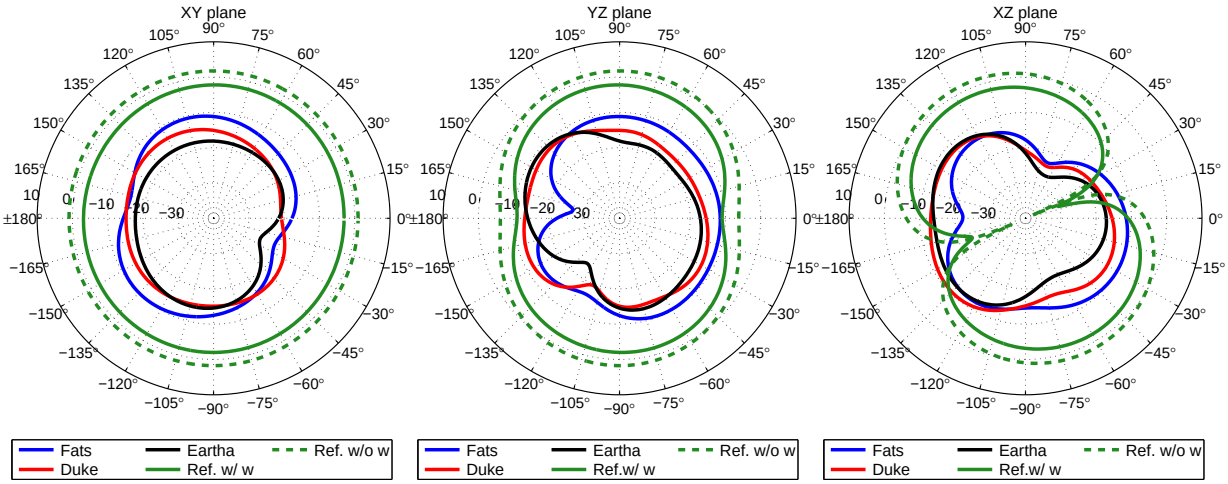

Figure 25: Radiation patterns for the bodypack on the 3 human models and the free space case at 235 MHz.

At the lowest frequency illustrated, Figure 25, the shadowing of the body is not evident however there is a very significant reduction in the gain compared to the free space case in all directions. Both these phenomena are related to each other, we already noted that the microphone lead forms a significant part of the radiating structure and as this goes round to the front of the body radiating along its length there

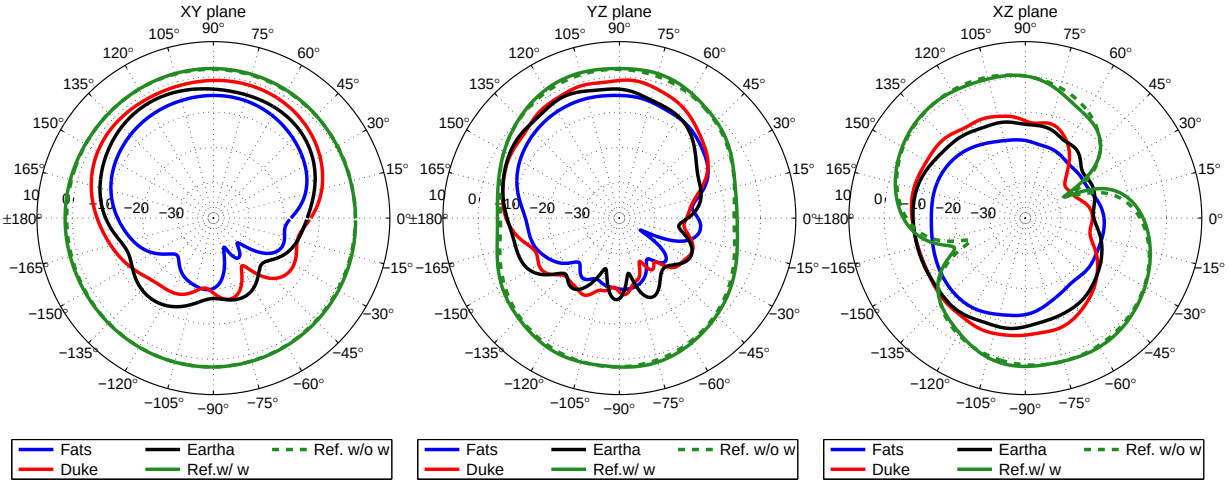

Figure 26: Radiation patterns for the bodypack on the 3 human models and the free space case at 845 MHz.

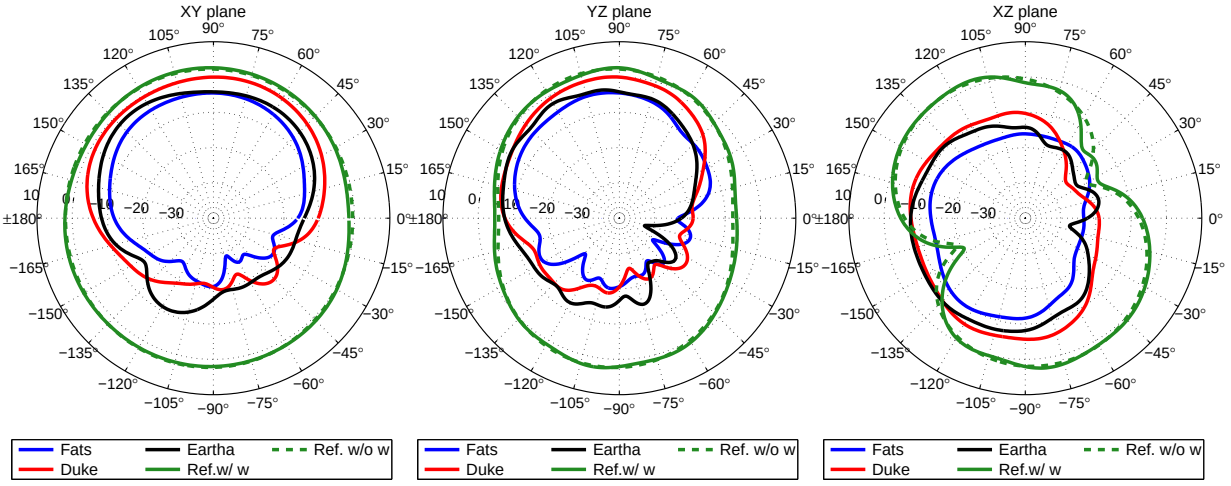

Figure 27: Radiation patterns for the bodypack on the 3 human models and the free space case at 945 MHz.

is no shadow, but the close proximity of the lead to the body gives rise to enhanced interaction and hence loss producing regions of high SAR in the body. As the frequency increases the role of the microphone lead becomes less important and the shadowing of the body increases as there is no radiation to the front from the lead and the gain increases in those directions not shadowed by the body showing that the overall loss in the torso also decreases. The level of shadowing by the body, shown in the left and centre plots, increases with approximately the log of the frequency and the size of the user.

A comparison was then performed between the pack on the back and a front position at the location of one pocket, Figures 5(b) and 5(c) to see if there were any significant differences. Figure 33 to Figure 36 show the comparison of the front and back positions for the median sized adult model Duke.

Firstly, it can be noted that the low frequency performance is poorer due to the fact that pack and lead are now located on the same side of the body: Loss and shadowing are greater at 235 MHz. At 945 MHz we also observe that the radiation from lead and antenna can cause cancellation in some directions with deep nulls possible, but these are hard to predict as they are a function of device and lead positioning. This behavior is not so evident for the rear position, as the lead tends to be routed round orthogonal to the monopole element. At higher frequencies there is little or no difference in performance, just the direction of the shadowing changes, as would be expected.

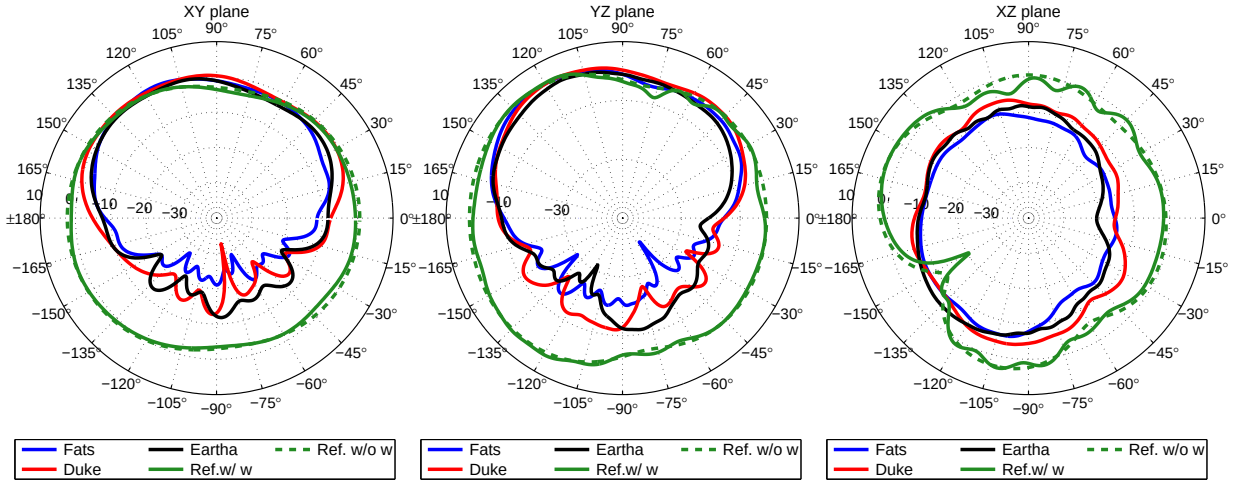

Figure 28: Radiation patterns for the bodypack on the 3 human models and the free space case at 1890 MHz.

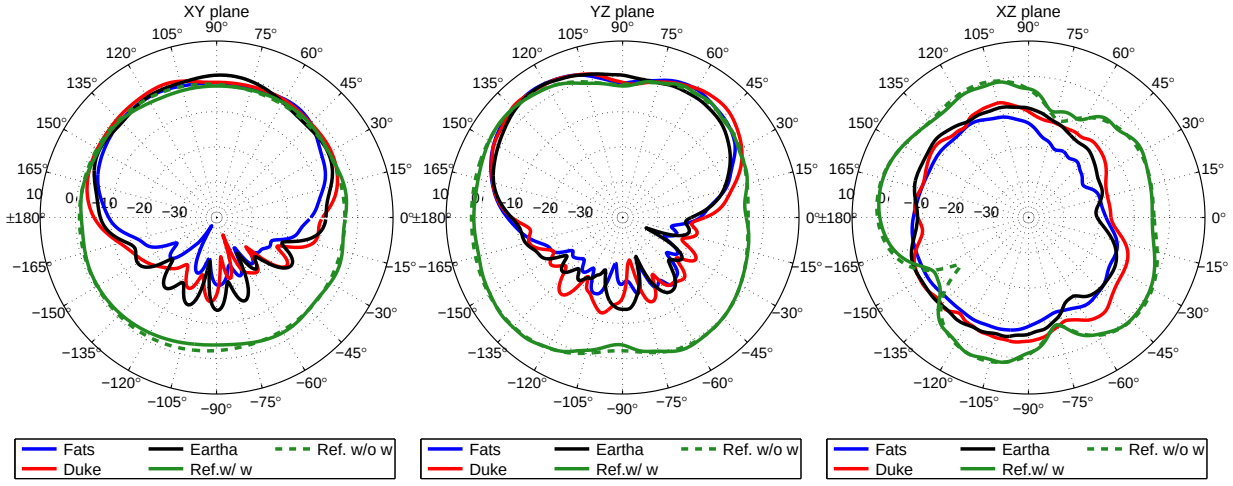

Figure 29: Radiation patterns for the bodypack on the 3 human models and the free space case at 2380 MHz.

The losses in the body, and hence, reduction in gain, are more profound in the bodypack case, as the antenna is in much closer proximity to the body giving rise to body losses due to the reactive near field region of the antenna. Figure 37 shows how as much as 95% of the power can be absorbed at the lowest frequencies. The amount of power loss will however be a strong function of the exact routing and proximity of the microphone cable on the body. Loss decreases as the frequency increases, as the microphone lead plays a less and less important role in extending the counterpoise and the monopole element distance from the body in terms of wavelengths increases, moving it away from the reactive near field region. Furthermore, as the frequency increases the region of strong influence decreases in size as seen in Figures 38, 39 and 40 for the Fats, Duke and Eartha models, respectively. In addition to the surface SAR, the volumetric SAR in a saggital plane was extracted for the Duke model at frequencies 825 MHz, 3000 MHz, and 4760 MHz, as depicted in Figure 41. The plane has been chosen so that the effect of the wire in the front of the body and the antenna at the back are seen at the same time. The penetration depth is higher at low frequencies and thus the power absorption in the body decays as frequency grows.

Only a subset of the results have been shown here that are sufficient to illustrate the points for discussion, the complete set of simulation results for all frequencies can be found in Appendix B.

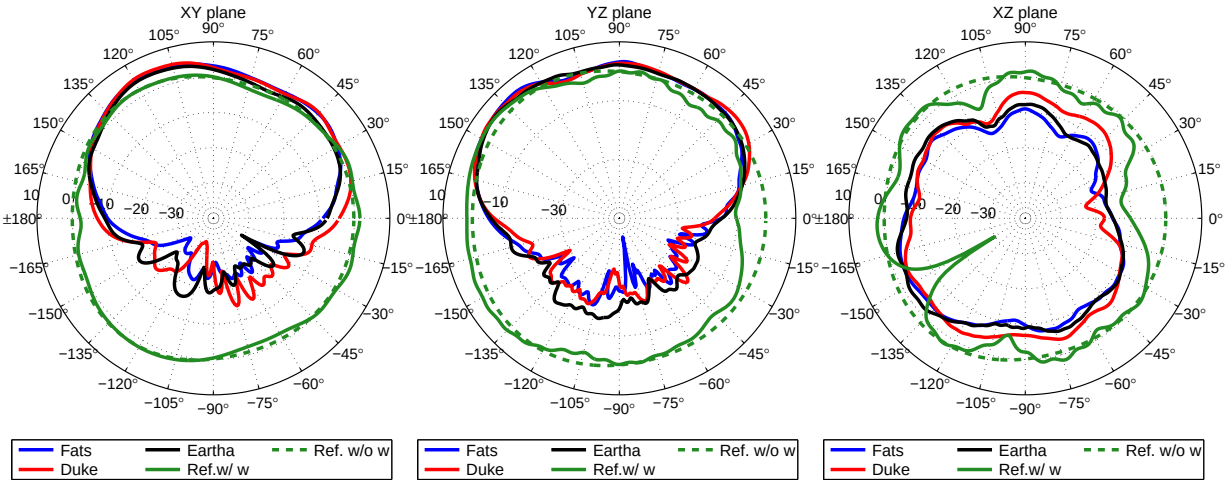

Figure 30: Radiation patterns for the bodypack on the 3 human models and the free space case at 3780 MHz.

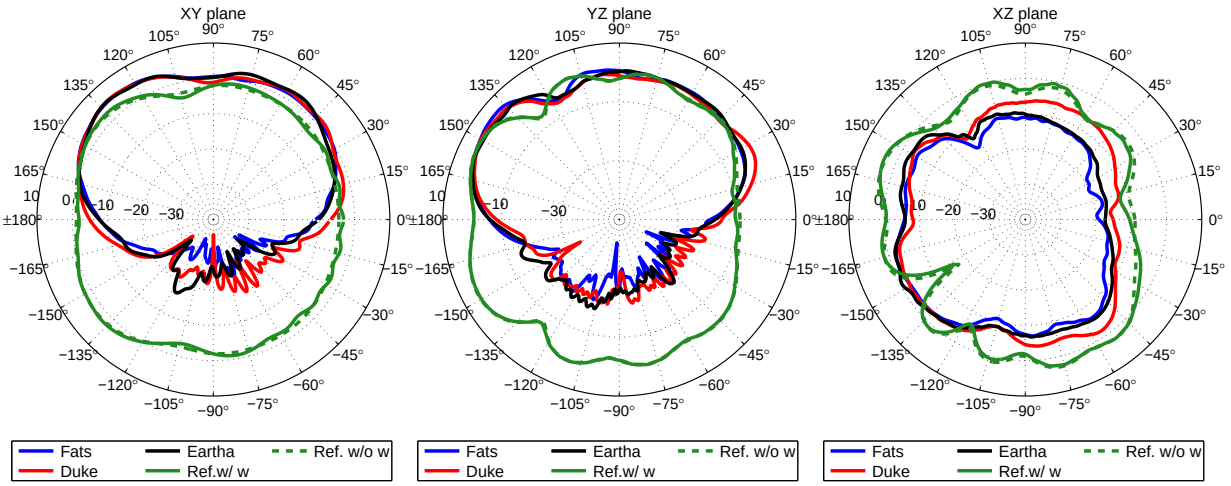

Figure 31: Radiation patterns for the bodypack on the 3 human models and the free space case at 4760 MHz.

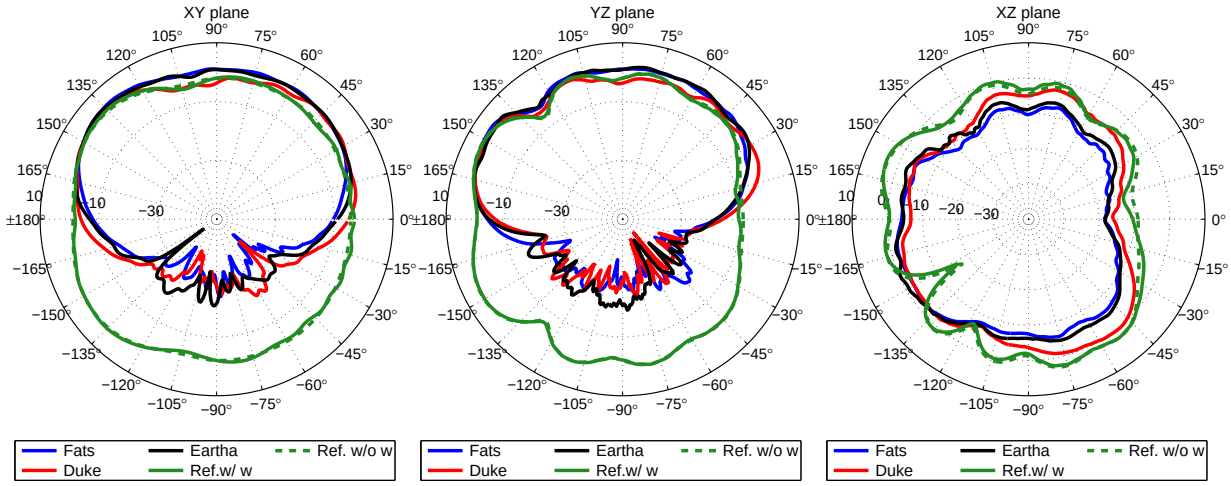

Figure 32: Radiation patterns for the bodypack on the 3 human models and the free space case at 6000 MHz.

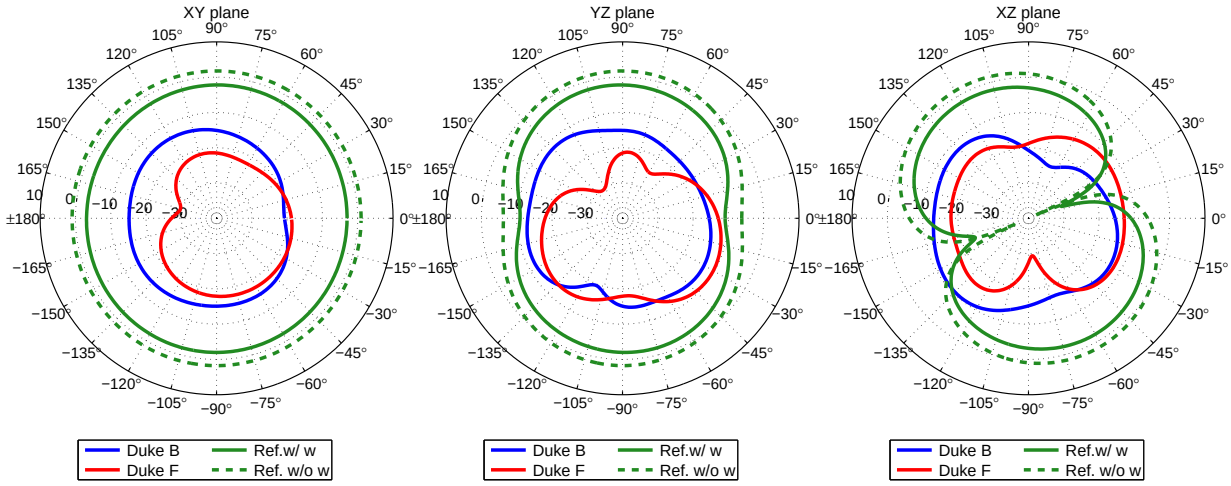

Figure 33: Radiation patterns for the bodypack microphone on front and back of the torso at 235 MHz.

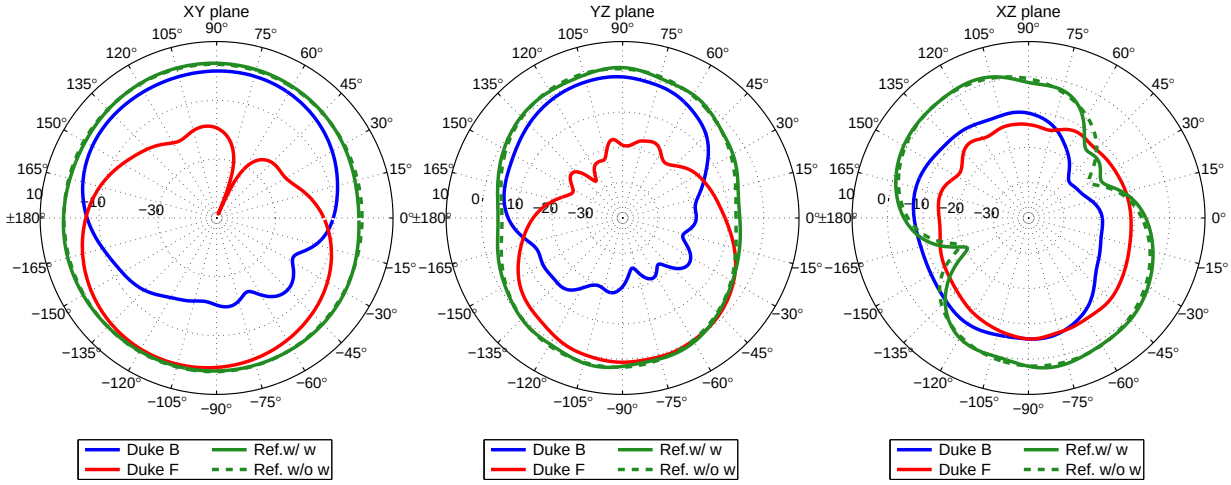

Figure 34: Radiation patterns for the bodypack microphone on front and back of the torso at 945 MHz.

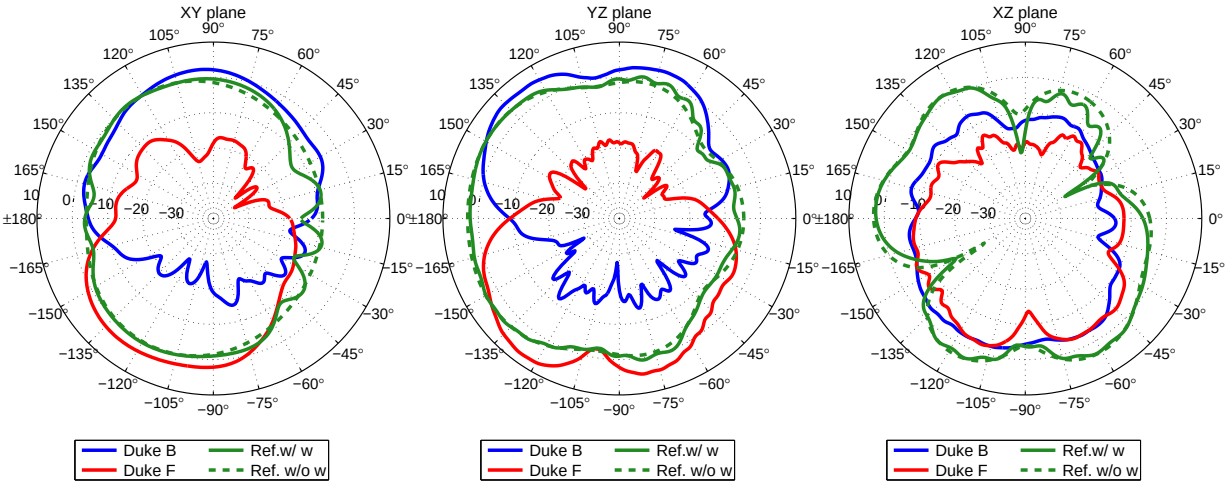

Figure 35: Radiation patterns for the bodypack microphone on front and back of the torso at 3000 MHz.

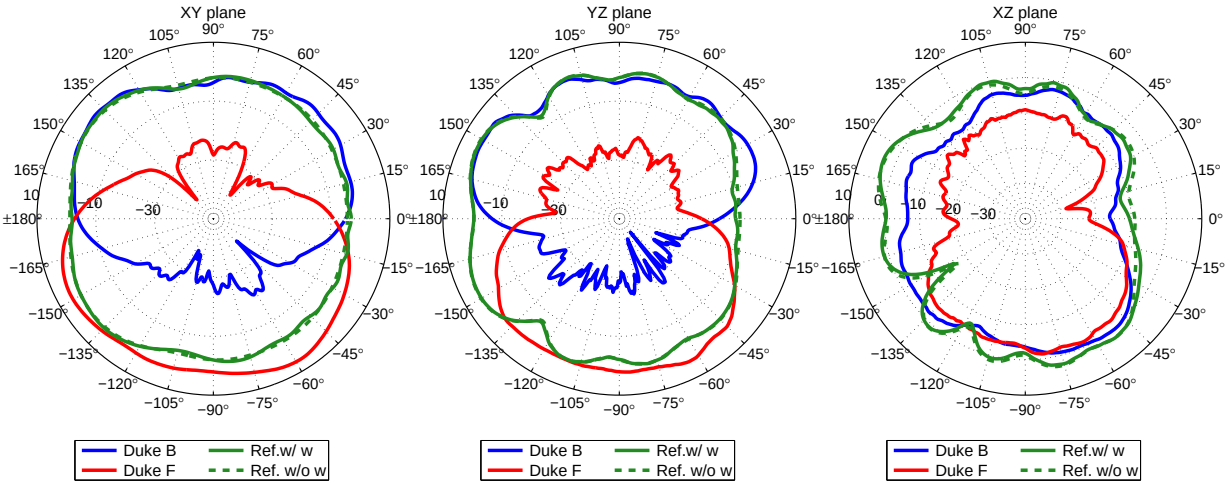

Figure 36: Radiation patterns for the bodypack microphone on front and back of the torso at 6000 MHz.

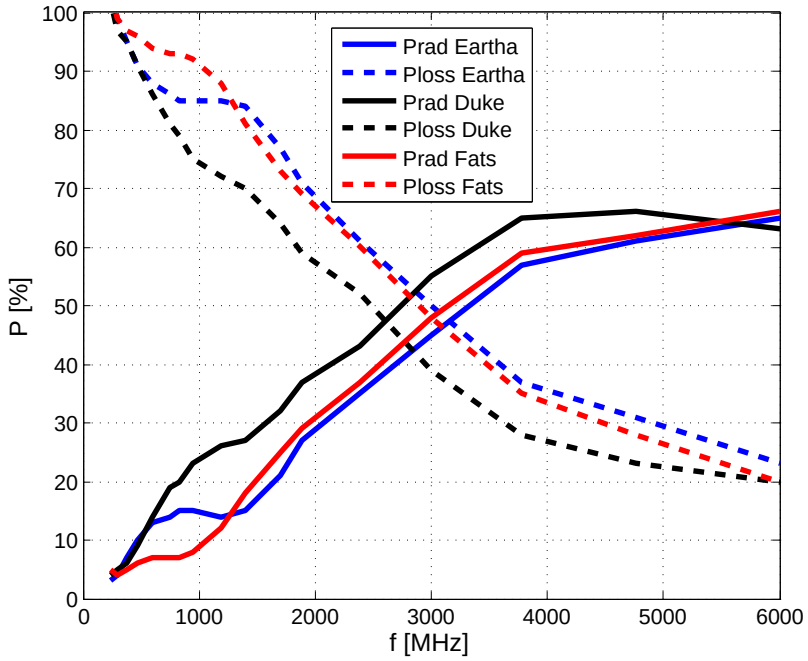

Figure 37: Radiated versus loss power (in %) as a function of frequency, for 1 W input power, for the 3 human models with the bodypack set up.

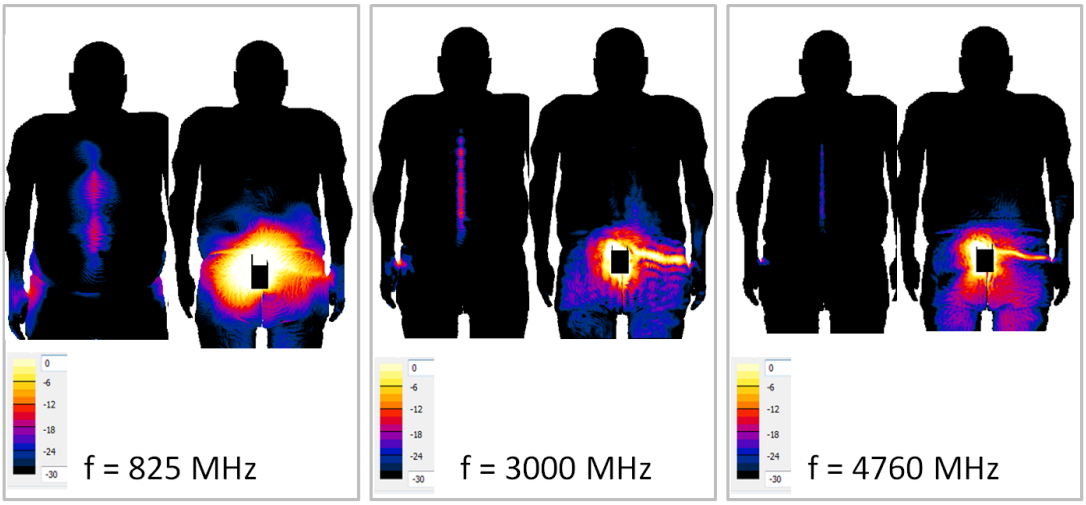

Figure 38: Surface SAR for Fats with the bodypack microphone (0 dB = 1 W/kg).

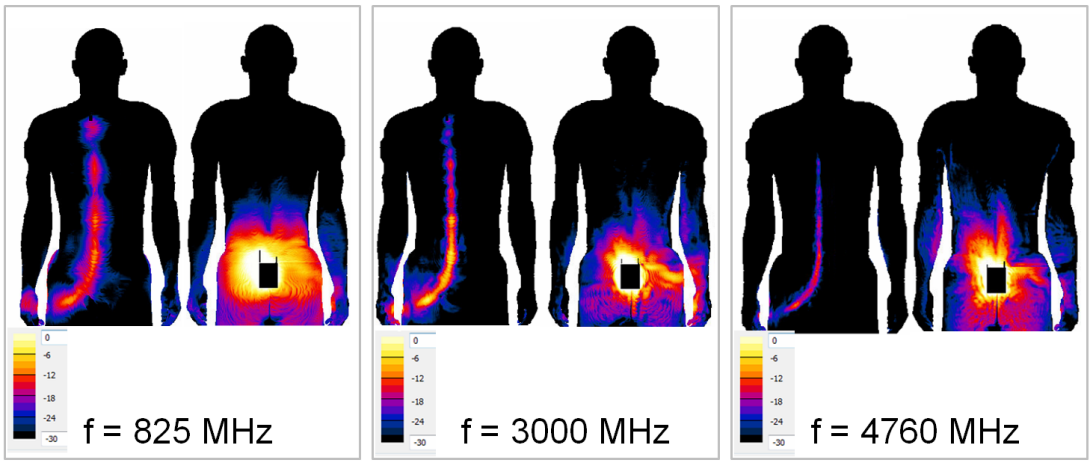

Figure 39: Surface SAR for Duke with the bodypack microphone (0 dB = 1 W/kg).

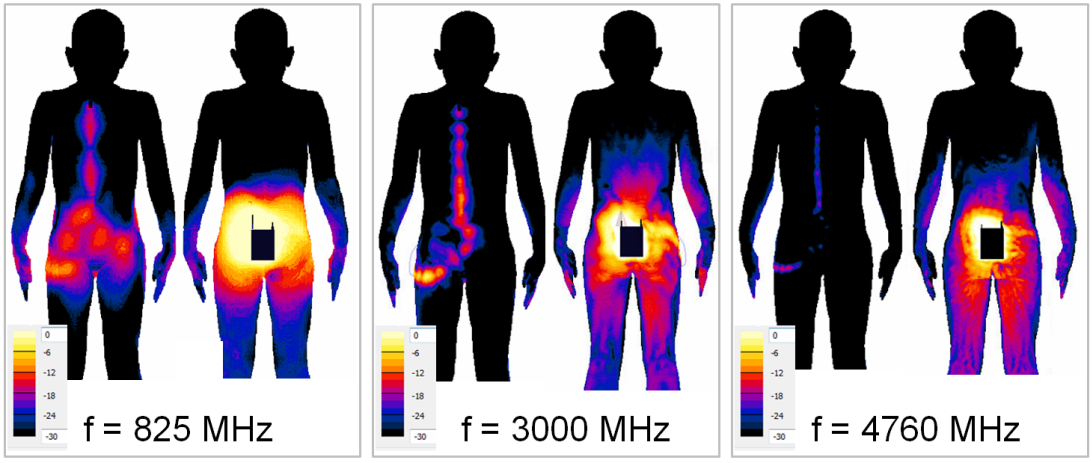

Figure 40: Surface SAR for Eartha with the bodypack microphone (0 dB = 1 W/kg).

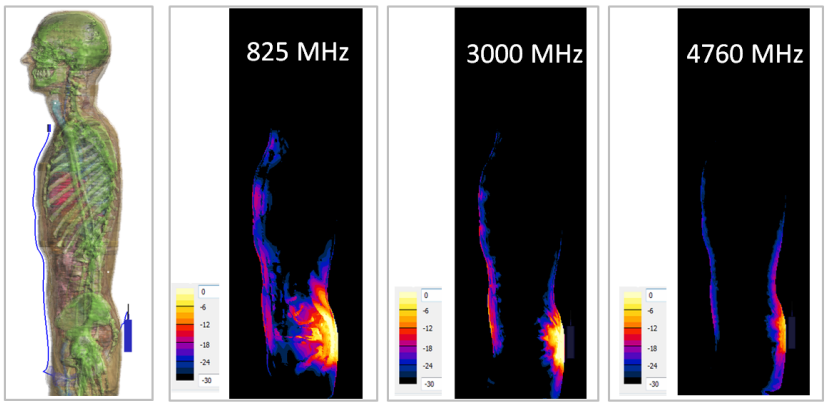

Figure 41: SAR distribution in a profile view of the the Duke model, showing the absorption in the frontal part and back part of the body due to the wire radiation and the antenna radiation, respectively, at 3 different frequencies. In the scale, 0 dB are equivalent to 1 W/kg for 1 W input power.

3.2.1 Distance Variations

The simulations in this study have been performed for a single position of the device with respect to the body. However, the reduction in gain with respect to the free space condition is obviously dependent on the distance of the antenna to the body. In the simulations performed up to this point of the report with the bodypack microphone, the antenna is centered at the middle width of the bodypack, where it stands rigidly parallel to the body axis. Thus, the distance between the antenna and the body is fixed by the bodypack geometry and position. In real life it could well be that the antenna gets closer to the body, for instance, due to the movement of the person using the microphone system, or for an antenna pivoting on its base. The variation of parameters such as distance was out of the scope of this project. However, simulations with the antenna leaning against the body have been run for one model and one frequency band, to ascertain in which way the antenna performance changes due to the distance variation. The modified position of bodypack microphone for the Duke model is shown in Figure 42. In this case the antenna is tilted and closer to the body along its whole length.

The simulations were run for band 2, and the results are depicted for the two extreme frequencies as well as for the central frequency of the band in Figures 43 to 44.

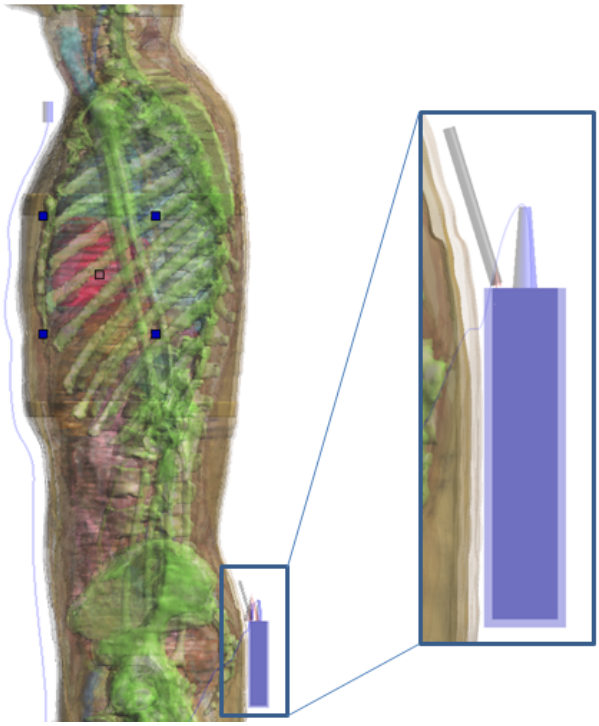

Figure 42: Duke and bodypack microphone positioned closer to the body with the antenna leaning towards the surface of the Duke model.

The closer proximity of the antenna to the body translates into higher power loss in the human, and thus a reduction of the gain in all directions, for all the frequencies in the simulated band (Band 2). The shadowing effect of the body becomes more evident at the higher frequencies, for instance comparing Figures 43 and 44. In the zone affected by the body shadowing, the secondary lobes are more evident when the antenna is tilted towards the body, and the nulls are more pronounced. All in all, the effects of the presence of the body in the antenna behavior are enhanced when the distance from the antenna to the body is reduced, as would be expected. The distance body-antenna and conformance of the antenna to the body may be a topic to have into account in future studies.

3.2.2 Perpendicular Polarization

Having used a short monopole antenna positioned parallel to the body ensures vertically polarized fields for all the bodypack simulations performed in this study. Perpendicular polarization may ameliorate

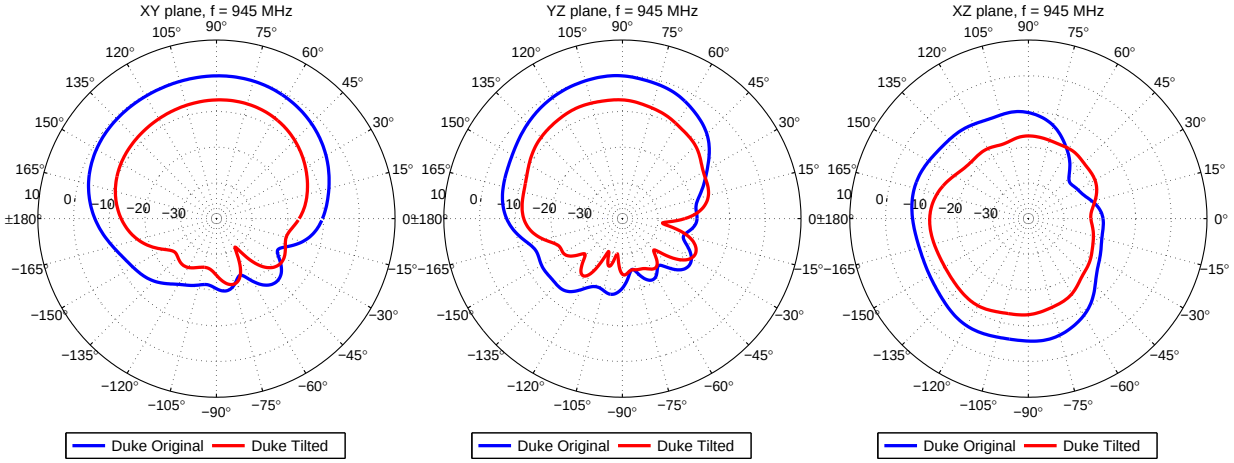

Figure 43: Radiation patterns for the bodypack microphone with the original antenna (blue line) and the antenna leaning towards Duke's body (red line) at 945 MHz.

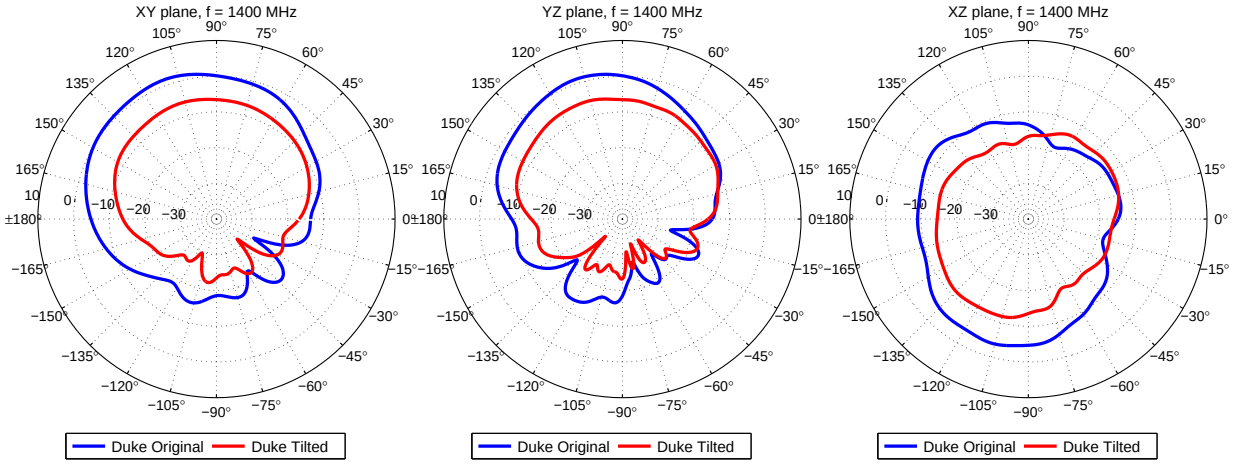

Figure 44: Radiation patterns for the bodypack microphone with the original antenna (blue line) and the antenna leaning towards Duke's body (red line) at 1400 MHz.

the system performance with respect to shadowing, in particular at highest frequencies. For that reason simulations of a modified bodypack with a perpendicularly polarized antenna have been run for band 4 (4760 MHz and 6000 MHz). The modified antenna is shown in Figure 46. One of the bodypack inner walls was turned into a PEC ground plane, and the short monopole positioned at the center of this wall, see the zoomed region in Figure 46.

The radiation patterns obtained for the bodypack microphone with perpendicularly polarized monopole compared to the vertical polarized one have been extracted from simulations and plotted together for comparison, as seen in Figures 47 and 48.

There is an amelioration of performance of the antenna with perpendicular polarization, in particular for the regions shadowed by the body (see for instance plane XY or YZ in Figures 47 and 48). However, intrinsically related to the perpendicularly polarized antenna a null appears at 90 azimuth, which reduces the gain around this direction a minimum of 10 dB. A similar behavior is observed at the two frequencies of Band 4.

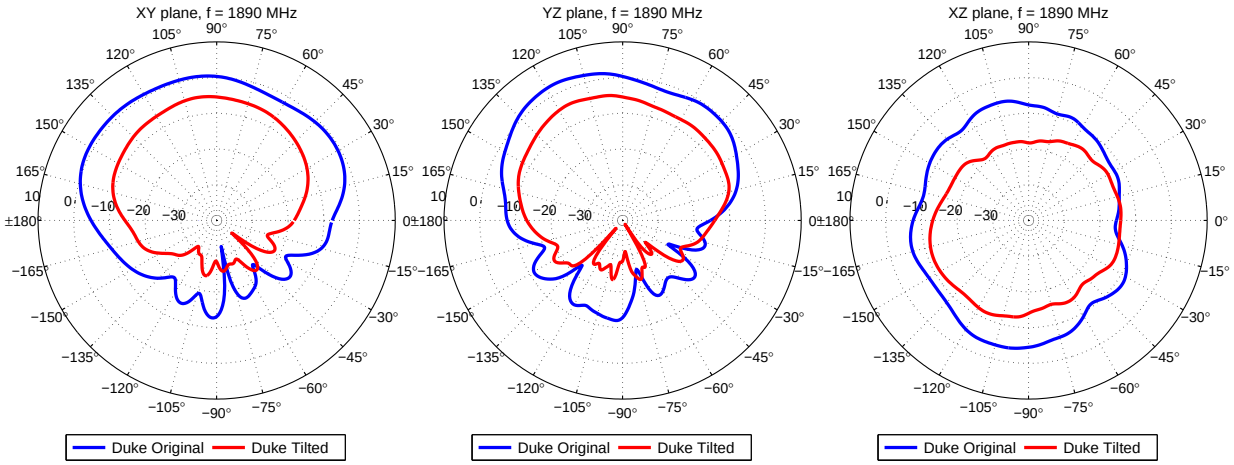

Figure 45: Radiation patterns for the bodypack microphone with the original antenna (blue line) and the antenna leaning towards Duke's body (red line) at 1890 MHz.

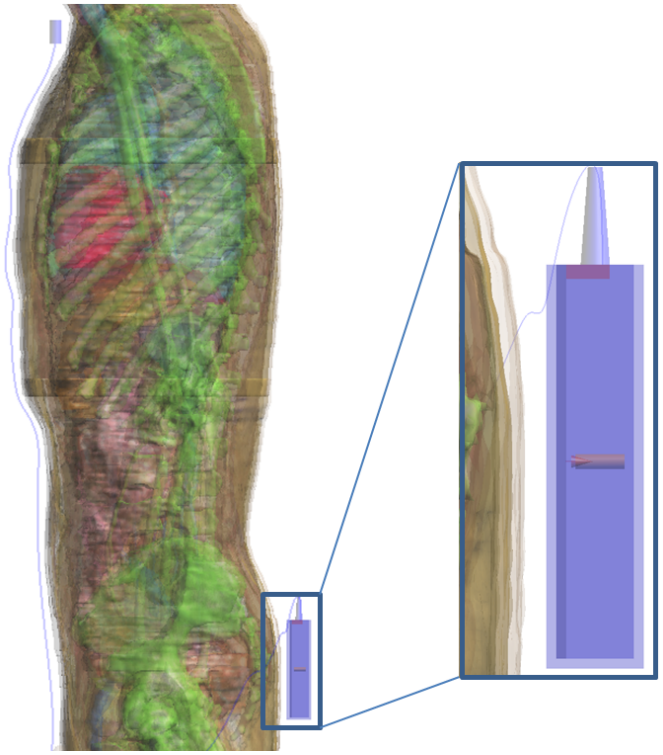

Figure 46: Duke and bodypack microphone with monopole perpendicular to the body.

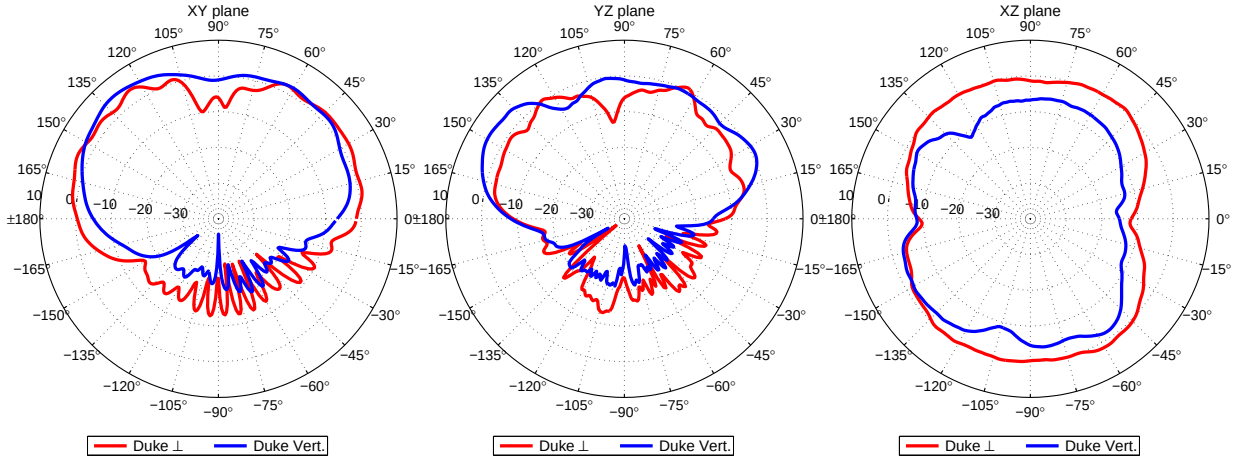

Figure 47: Radiation patterns for the bodypack microphone with perpendicularly polarized antenna compared to vertically polarized antenna (original model) on the back of Duke model torso at 4760 MHz.

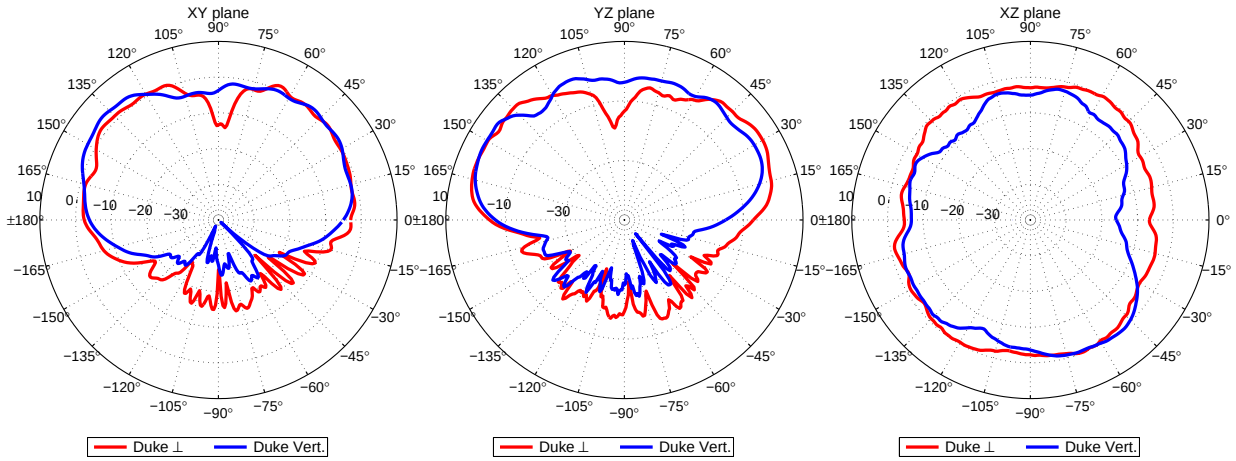

Figure 48: Radiation patterns for the bodypack microphone with perpendicularly polarized antenna compared to vertically polarized antenna (original model) on the back of Duke model torso at 6000 MHz.

4 Discussion

4.1 Handheld Microphones

4.1.1 Comparison to Free Space

To have a global overview on the performance of the handheld microphone in the presence of the human body, a compilation of the results obtained in section 3.1 and Appendix A has been performed, and has been merged into a single plot.

Figure 49(a) represents the gain relative to free space of the monopole antennas mounted in the handheld microphone as a function of frequency, for all radiation directions, for the Duke model. The gain relative to free space is computed from the radiation patterns at each frequency for the microphone model with and without the human model present, with the free space reference being the average gain of all directions at each frequency. A total of 360 points are plotted per frequency, since the resolution of the radiation patterns is 1 degree. The directions belonging to the shadowed regions are plotted in gray, the rest are plotted in red and light blue, as indicated in the schematic of the radiation pattern included in Figure 49. Analogous plots were produced for the other two models, Eartha and Fats, that can be found in Figure 49(b) and 49(c).

The totality of the points yield negative gain with respect to average gain at free space for frequencies below 1000 MHz, for the three models, see Figures 49(a), 49(b) and 49(c), implying that the gain of the antenna is lower when the body is present, as to be expected. At these frequencies shadowing is bounded by a maximum of 13 dB below the average free space reference, consistently for the three models. This suggests that at lower frequencies the gain in the shadow regions is to a lesser extent governed by the size of the human model, since the shadowing at lower frequencies is comparable for the three models. However, for the preferred directions of radiation in azimuth 180° to 360°, plotted in red and blue in Figures 49(a), 49(b) and 49(c), the deviation from the free space reference is clearly less important for the Eartha model, specially in the lower half of Band 1. As a conclusion, at lower frequencies the shadowing is comparable for all body sizes, whereas the gain in the frontal directions diminishes more for the bigger models.

As the frequency grows the shadowing is increasingly higher, reaching values around 30 dB lower than the average at free space for Duke and Fats, whereas for the smallest model Eartha the shadowing at higher frequencies is bounded by -20 dB except for the 2 extreme frequencies, where it can reach 26 dB below the free space reference.

4.1.2 Comparison to 750 MHz

The performance of the antennas with respect to free space has been evaluated previously. However, it is also of great interest to assess the performance of the antenna at the frequency under study with respect to the antenna at a frequency in the bands that are currently assigned to wireless microphones, e.g. 750 MHz. Both study case and reference case are computed in the presence of the body.

Figure 50 shows the gain with respect to the gain at 750 MHz, averaged over all directions, as a function of frequency, for the three human models. For frequencies lower than the reference, the shadowing is comparable to the one at the reference frequency. For higher frequencies, the effect of the shadowing is increasingly higher. The gain deviation from reference starts when the head becomes commensurate with the wavelength. In this way, the enhanced effect of the shadowing starts at a lower frequency for Fats, which is the biggest model, and at the highest frequency for Eartha, the smallest model. For the preferred directions of radiation, the antenna can perform better at higher frequencies, presumably due to the reflections from the body.

Since the radiation pattern of the monopole antenna in the presence of the body at 750 MHz is similar to the pattern in free space, just with lower gain, the graphs in Figures 49 and 50 are very similar, just offset by the gain difference between 750 MHz and free space.

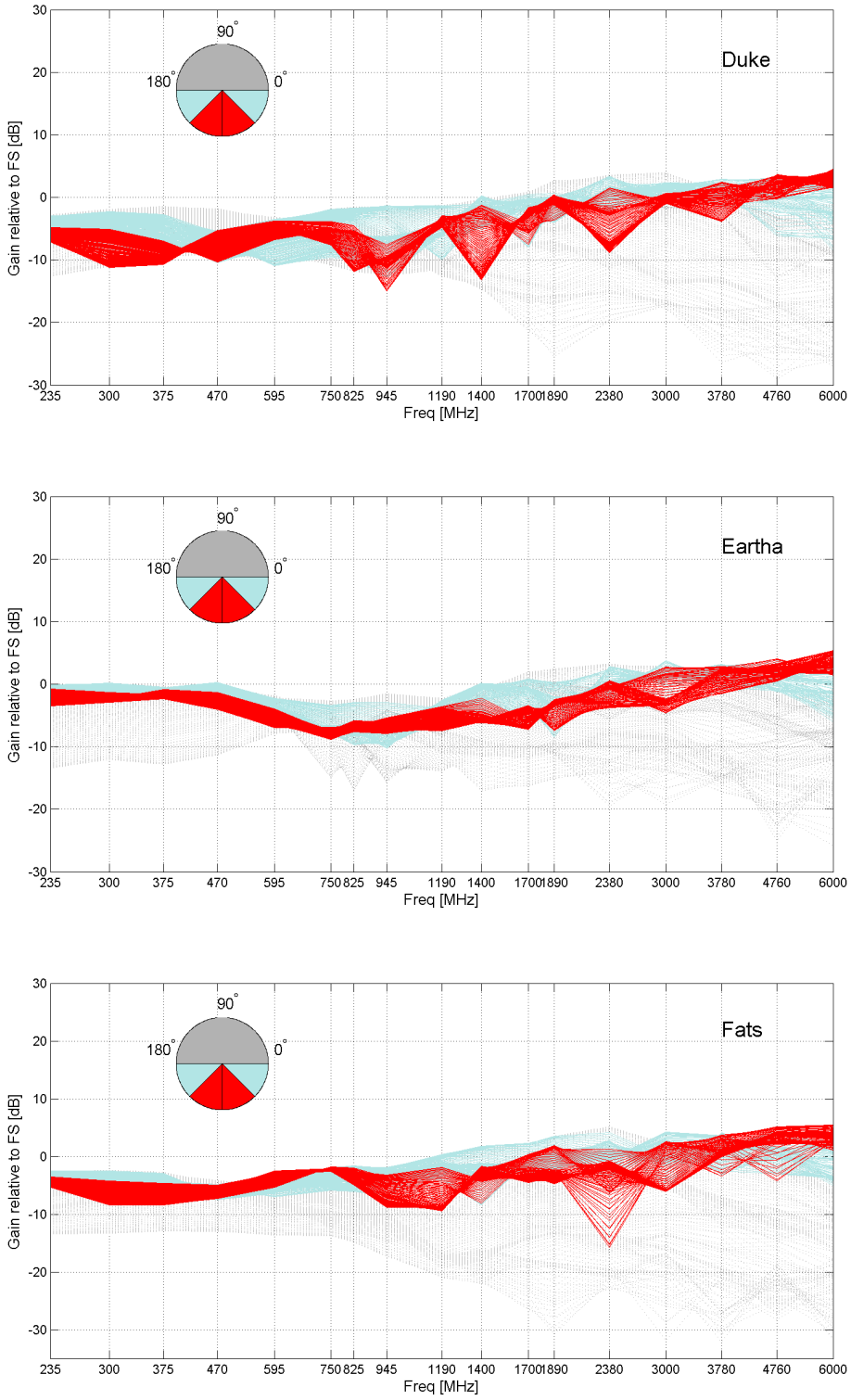

Figure 49: Handheld microphone: Gain at all frequencies relative to free space average in all radiation directions on the XY plane. The color code indicates to which angular sector the depicted points belong: Gray for the shadowed region, red and blue for the rest of XY plane, as indicated in the polar sketch on the figure.

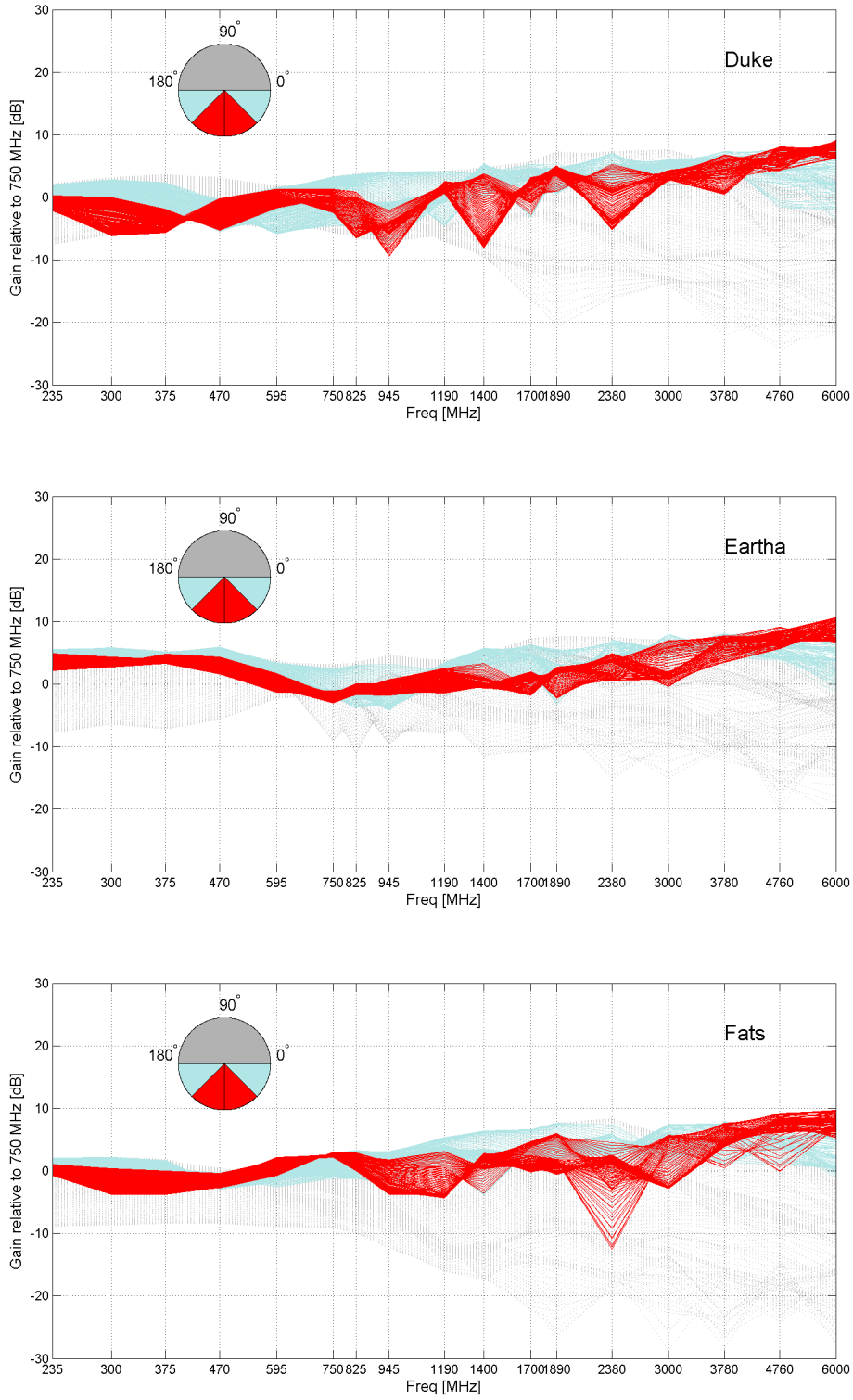

Figure 50: Handheld microphone: Gain at all frequencies relative gain at 750 MHz averaged in all radiation directions on the XY plane. The color code indicates to which angular sector the depicted points belong: Gray for the shadowed region, red and blue for the rest of XY plane, as indicated in the polar sketch on the figure.

4.2 Bodypack Microphones

4.2.1 Comparison to Free Space

Analogously to the handheld microphone case, the totality of the radiation patterns (XY plane) is plotted in a single graph to get the overall picture of the bodypack microphone behavior in the presence of the body as a function of frequency. In a first step, the gain is plotted relative to free space. The free space reference is averaged in all directions for each frequency.

For the bodypack microphone the antenna is much closer to the body than for the handheld microphone, and this reflects in Figure 51, where the gain with respect to free space reaches -30 dB consistently for the three models at much lower frequencies than the handheld microphone. The amount of absorbed power in the body is very sensitive to the distance between microphone and body.

For frequencies lower than 1.7 GHz the gain in all directions is lower in the presence of the body than in free space. As the frequency increases the effects of the shadowing are more pronounced, and the gain reaches values bordering -40 dB. As the radiation on regions shadowed by the body worsens with increasing frequency, some regions with direct radiation benefit of a gain raise due to reflections from the body.

4.2.2 Comparison to 750 MHz

Figure 52 shows the azimutal XY plane of the radiation patterns of the bodypacked antenna at all frequency bands compared to the 750 MHz case (with dashed black line in all four plots), for the Duke model.

The radiation patterns in Figure 52 show a reduction of the gain at frequencies lower than the reference, suggesting that the body acts more as an absorber, and thus part of the power of the system is absorbed in the body, rather than radiated. The shadowing is less predominant at these frequencies, but at the same time the gain in the preferred directions is lower than at the reference frequency.

As the frequency grows the effect is quite the opposite, less power is absorbed in the body and the radiation patterns reach similar levels as the reference, or even get slightly better due to the body acting as a reflector more than as an absorber in the preferred radiation directions, but at the same time the shadowing due to the body is larger.

The antenna performance as a function of frequency can be visualized graphically by plotting the gain at all frequencies relative to the 750 MHz average, see Figure 53. The gain is referenced to the 750 MHz gain, averaged over all directions, and plotted as a function of frequency. The regions of the radiation pattern are identified with different colors: All directions located from 180° to 360° are plotted in gray (shadowed region), whereas the points at $90° \pm 45°$ azimuth are plotted in red and the rest of the space are plotted in light blue. There are 360 points plotted per frequency, since the plots are done with 1 degree resolution in the radiation patterns. The plots are shown for Duke, Eartha and Fats.

The dynamic range of the gain with respect to average at 750 MHz at this very same frequency varies for the three models: Duke ranges from -16 dB to 5 dB, Eartha from -12 dB to 5 dB and Fats from -22 dB to 5 dB. For higher frequencies, the radiation in favorable directions ameliorates with respect to the reference frequency in all cases, reaching up to more than 10 dB at some frequencies for the 3 models. As for the shadowed regions, the gain decreases up to -30 dB for Fats and Duke at high frequencies, but stays bounded by -20 dB in the case of Eartha.

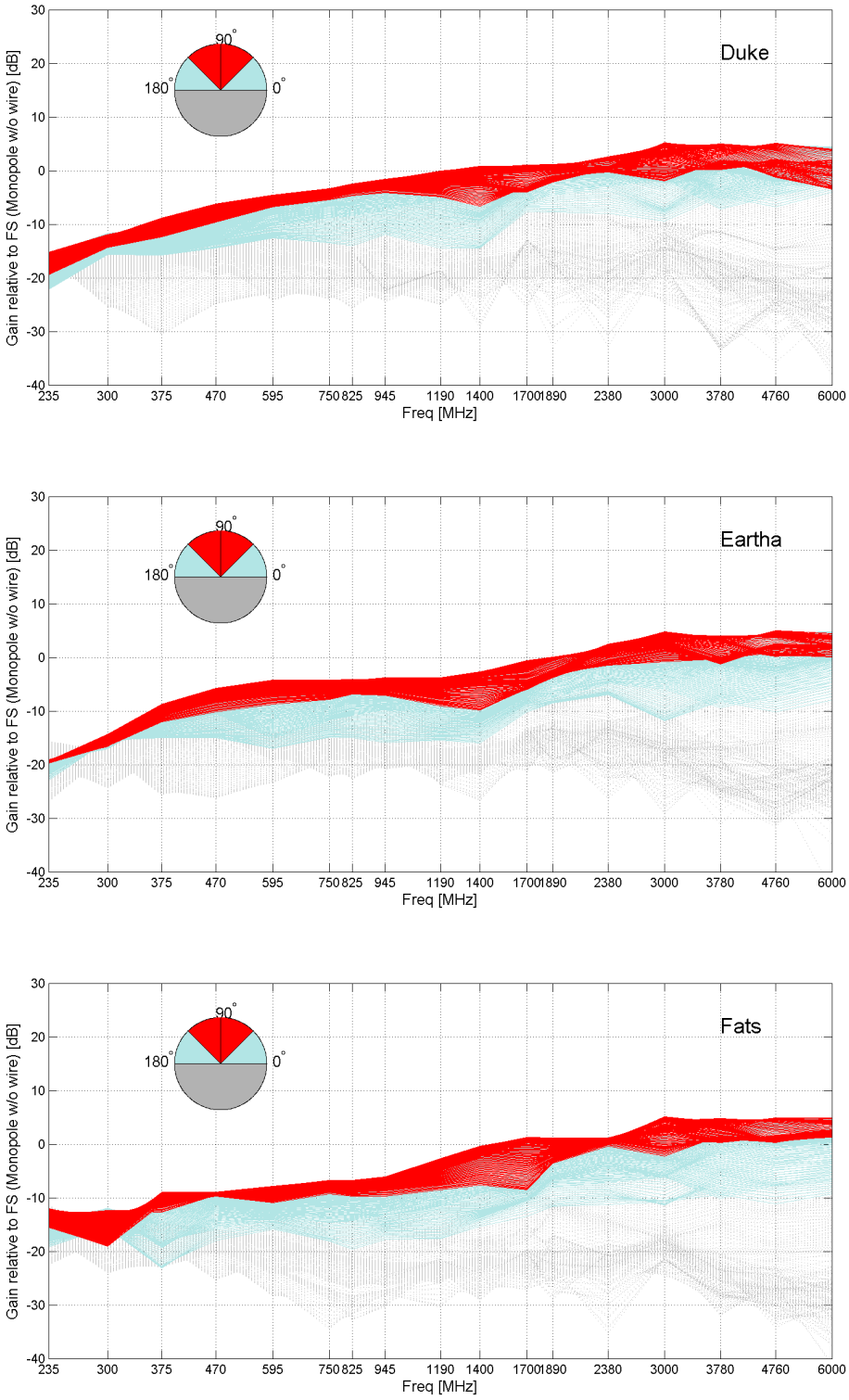

Figure 51: Bodypack Microphone: Gain at all frequencies relative to averaged free space in the XY plane. The color code indicates to which angular sector do the depicted points belong: Gray for the shadowed region, red and blue for the rest of XY plane, as indicated in the polar sketch on the figure.

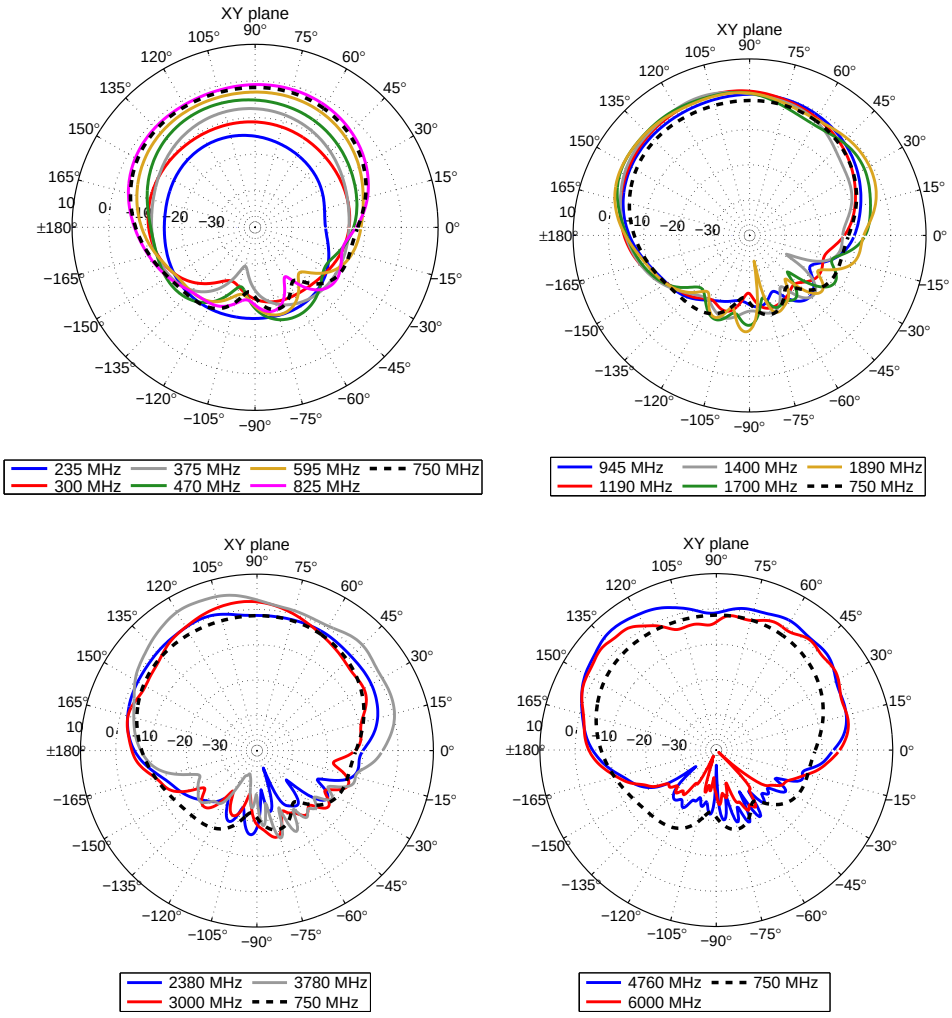

Figure 52: Radiation patterns in the XY plane for the bodypack microphone and the Duke model at all frequencies compared to 750 MHz (black dashed line).

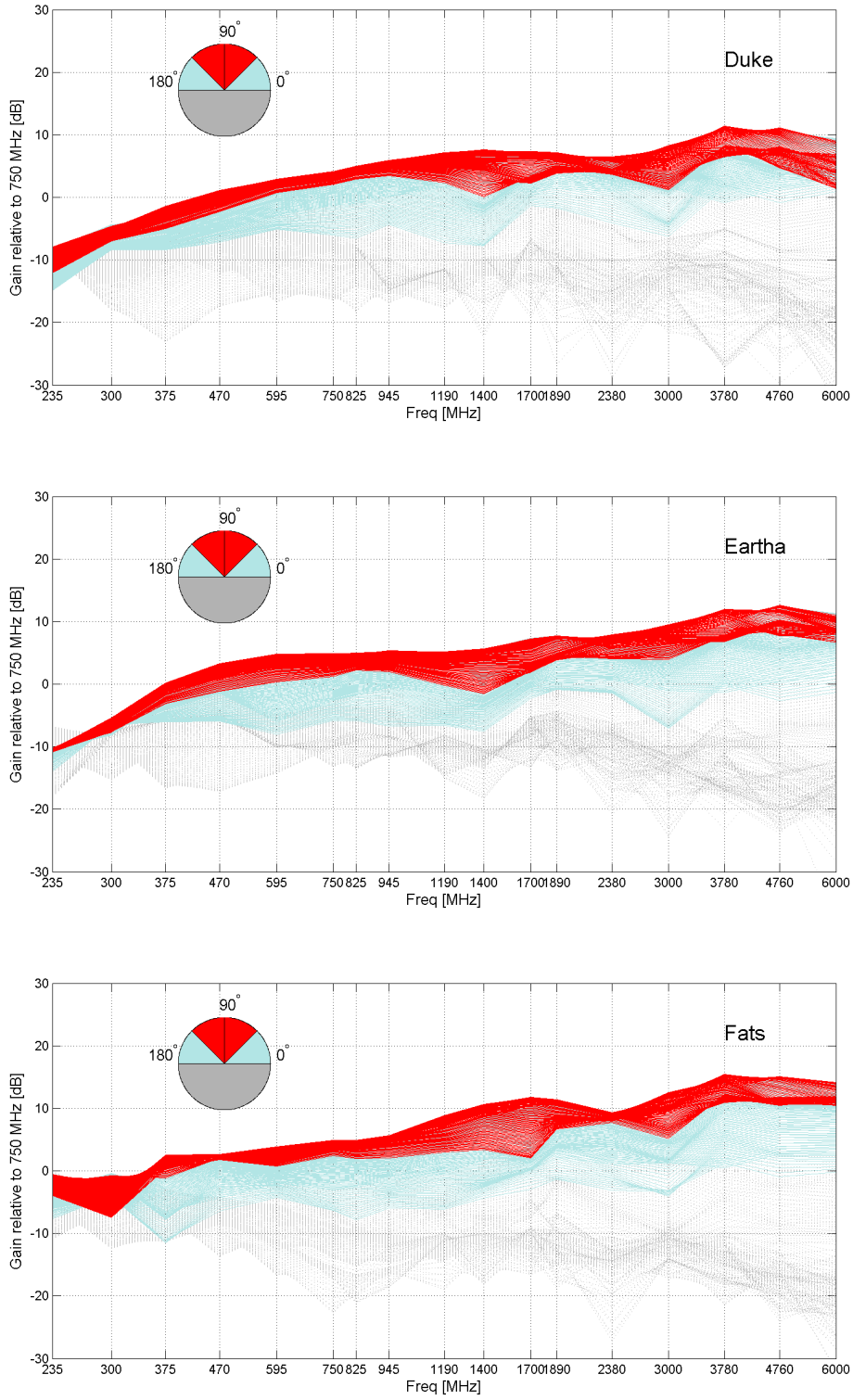

Figure 53: Bodypack Microphone: Gain at all frequencies relative to average in all directions at 750 MHz in the XY plane. The color code indicates to which angular sector do the depicted points belong: Gray for the shadowed region, red and blue for the rest of XY plane, as indicated in the polar sketch on the figure.

5 Conclusions

This project aimed to quantify the degradation in the wireless microphone transmission performances due to shadowing at higher frequencies as compared to the performances in the UHF band. To reach this goal, the assessment of the changes of the radiation pattern of wireless microphones (in the presence of a human body) as the transmission frequency increases was performed. The interaction of the microphone system with the human body is of course highly dependent on the working frequency, and this fact is very clearly reflected on the results obtained throughout the study, which was performed for a large frequency span. At lower frequencies (Band 1 to mid Band 2) the body acts like an absorber: The radiation in favorable directions is worse than free space due to the power absorbed in the body. For bodypack the gain is up to 15 dB lower in the favorable directions, and for the handheld case 5 dB less than free space. At the same time, the shadowing from the body at low frequencies is less substantial. As the frequency increases the body acts more like a reflector, there is less power absorbed in the body, and the gain may even increase with respect to the free space case in the non-shadowed region. In the shadowed region side lobes and deep nulls appear in the radiation pattern, and this degradation is correlated with the body size.

For higher frequencies the antennas become better radiators, the radiating power increasing due to the decrease of the power absorbed in the body. For frequencies higher than 3 GHz the radiated power for the bodypack is around 70% of the input power, whereas for the handheld microphone 90% of the input power is radiated. However, it must be taken into account that the ratio of the radiated versus the absorbed power in the body is very sensitive to the body to microphone spacing. In this sense, the results obtained for the bodypack microphone show stronger absorption and shadowing than the handheld microphone. The big influence that the distance microphone – body has on the antenna gain is well reflected on the results obtained when the antenna of the bodypack system is positioned leaning towards the body such as to reduce the antenna – body distance to 4 mm. For this smaller distance, the gain decreases by 10 dB with respect to the original distance, for frequencies belonging to Band 2.

The performance of the microphone systems with respect to its own performance at one of the frequencies currently assigned to broadcast (750 MHz in this case) has been assessed. For the handheld the shadowing increases when the wavelength becomes commensurate with the head size. For the bodypack microphones the gain in the most favorable directions can increase at high frequencies with respect to 750 MHz due to reflections in the body, while shadowing becomes more pronounced.

As a general conclusion, all the scenarios have shown shadowing increases as the frequency increases. In non-shadowed regions, however, the gain is not necessarily lower than reference; on the contrary, gain increase with respect to reference has been observed, due to the reflections coming from the body, that is acting more as a reflector rather than an absorber at higher frequencies.

Further work is needed to complete the transmission equation for the selected scenarios. However, it can be said that, all other things being equal, the path loss will increase by 20 dB with a 10 fold increase in frequency.

A Handheld Microphone - Complete Set of Results

A.1 Reference free space radiation patterns for microphone tilted at 45

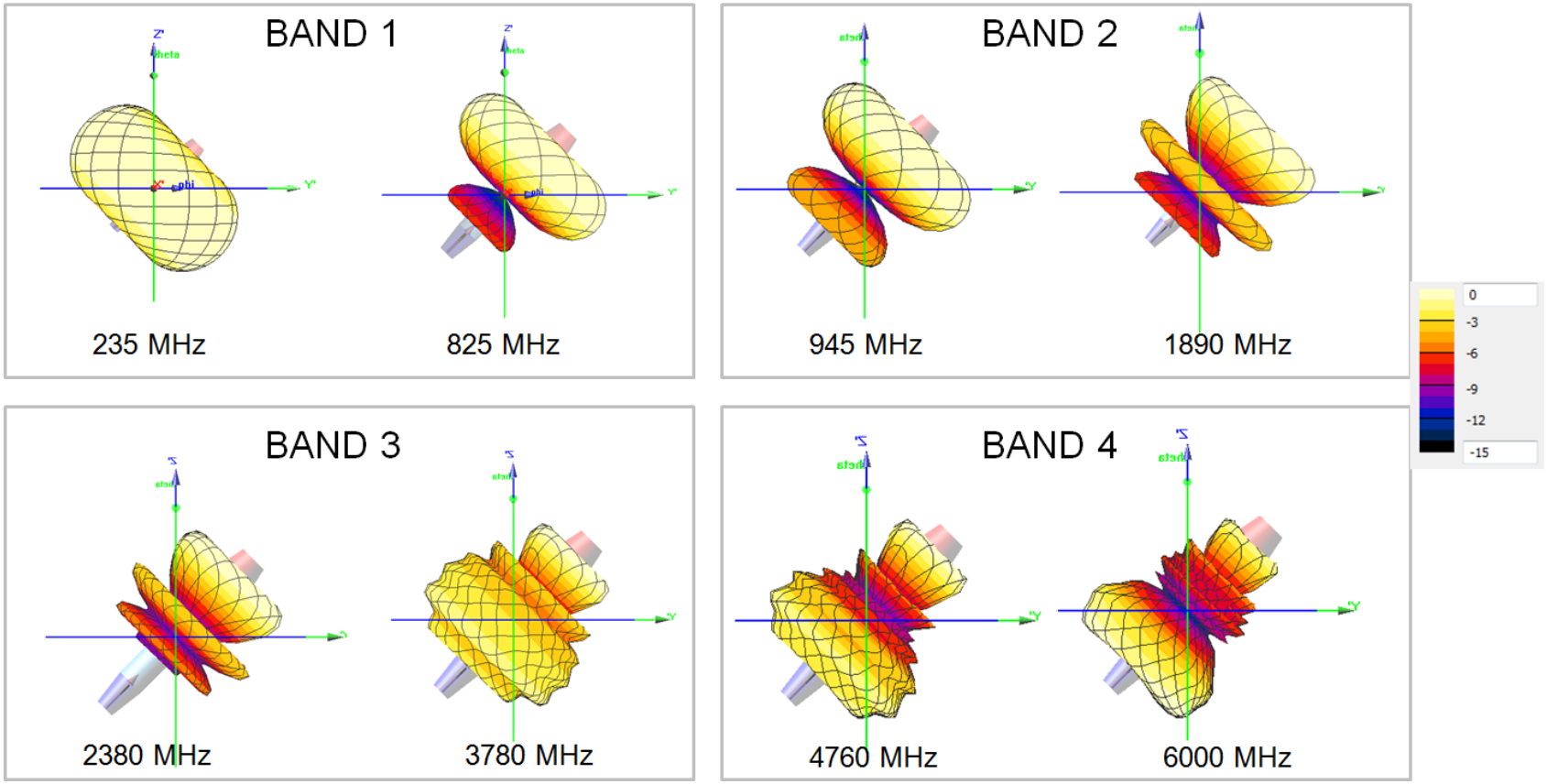

Figure 54: Free space radiation patterns for microphone tilted at 45 for a range of frequencies. Scale referenced to peak gain.

A.2 Radiation patterns for a small user 1.35 m and 31 kg Eartha Virtual Population Model

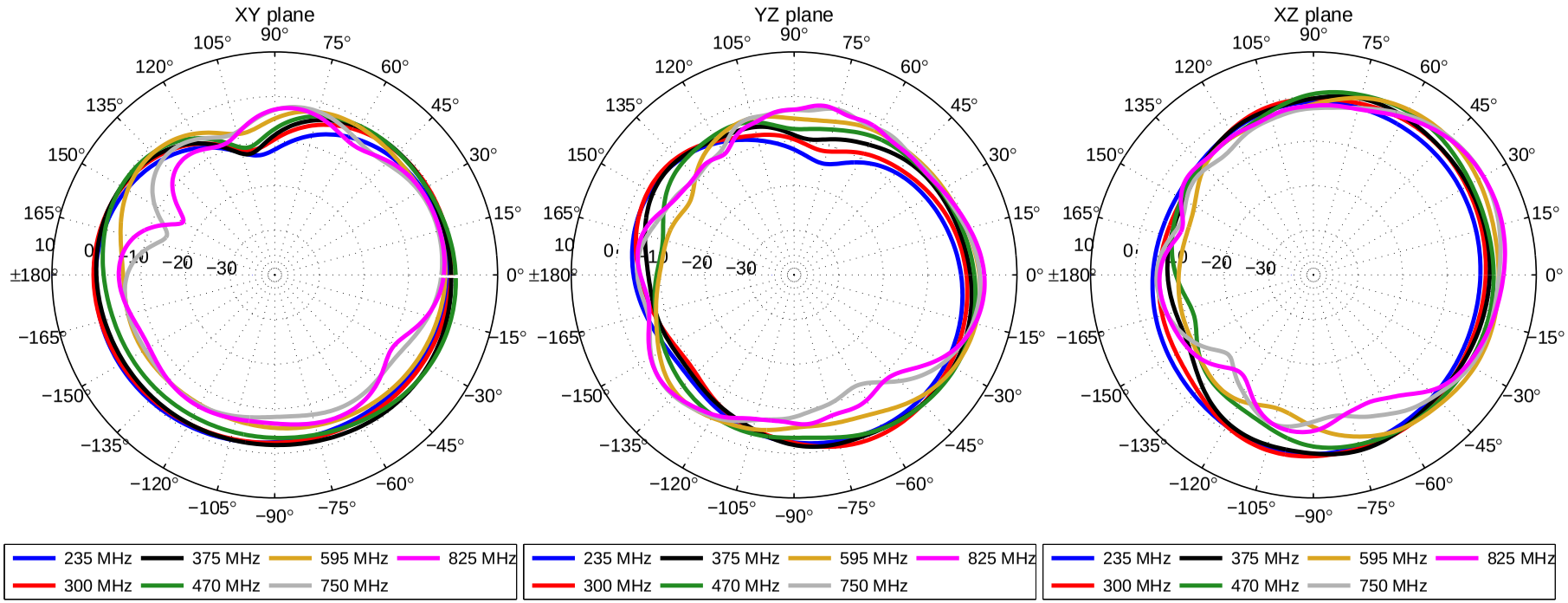

Figure 55: Eartha. Radiation patterns Band 1: 235 MHz - 825 MHz.

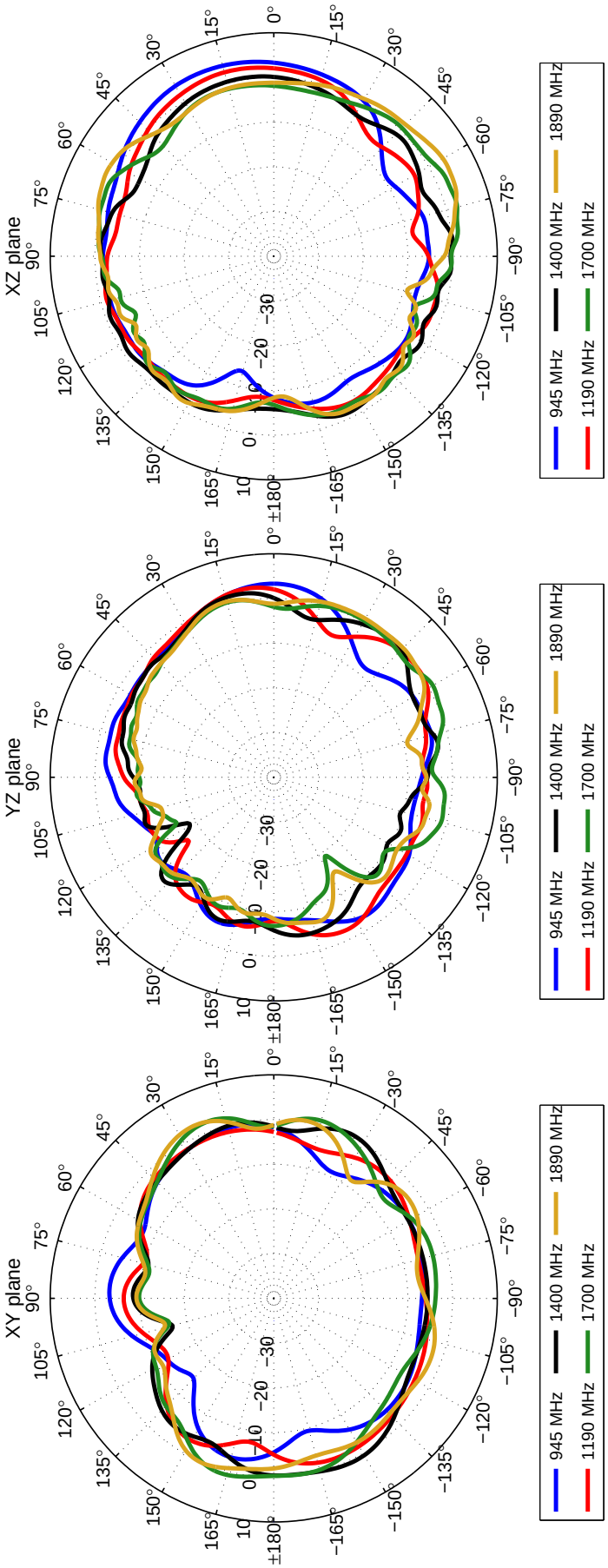

Figure 56: Eartha. Radiation patterns Band 2: 945 MHz - 1890 MHz.

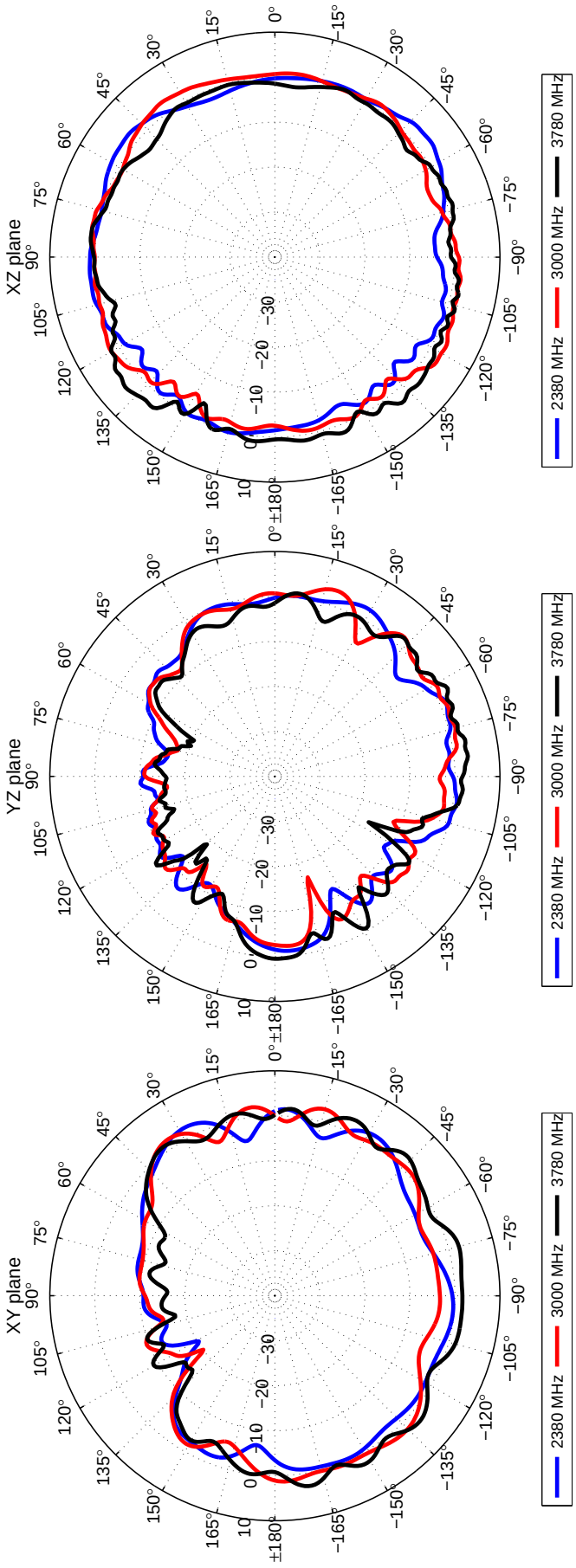

Figure 57: Eartha. Radiation patterns Band 3: 2380 MHz - 3780 MHz.

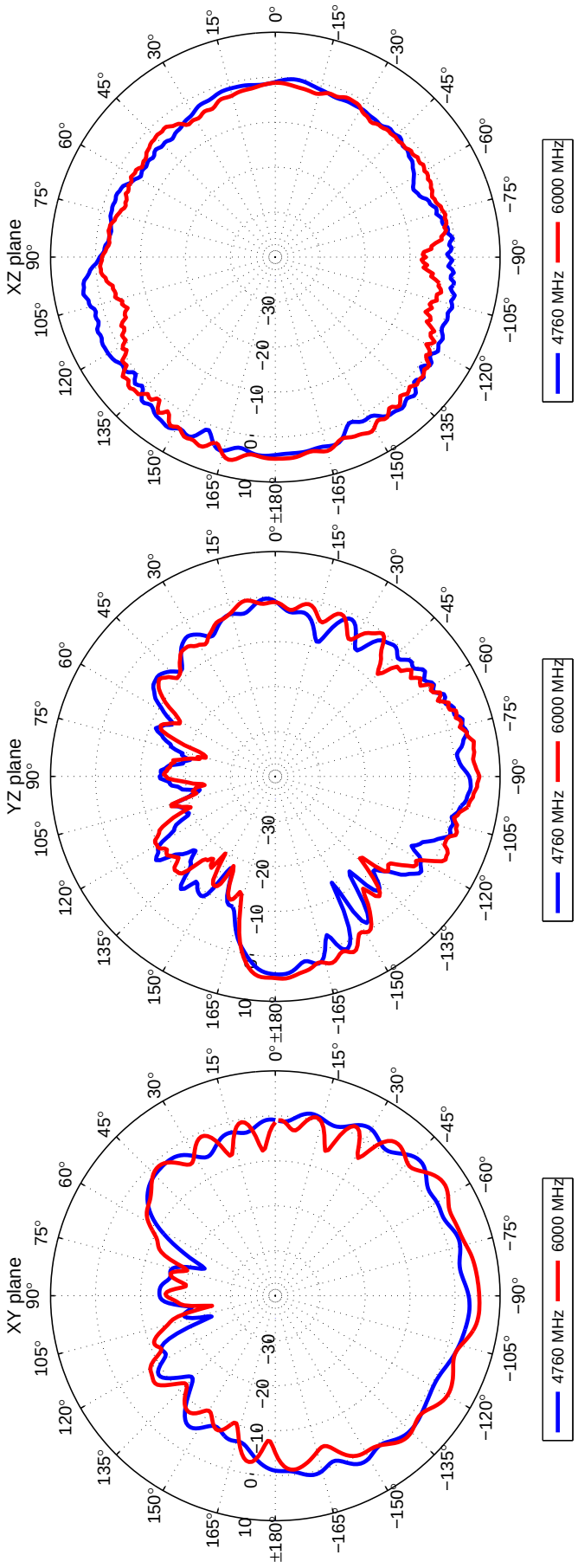

Figure 58: Eartha. Radiation patterns Band 4: 4670 MHz - 6000 MHz.

A.3 Radiation patterns for a medium user 1.75 m and 70 kg Duke Virtual Population Model

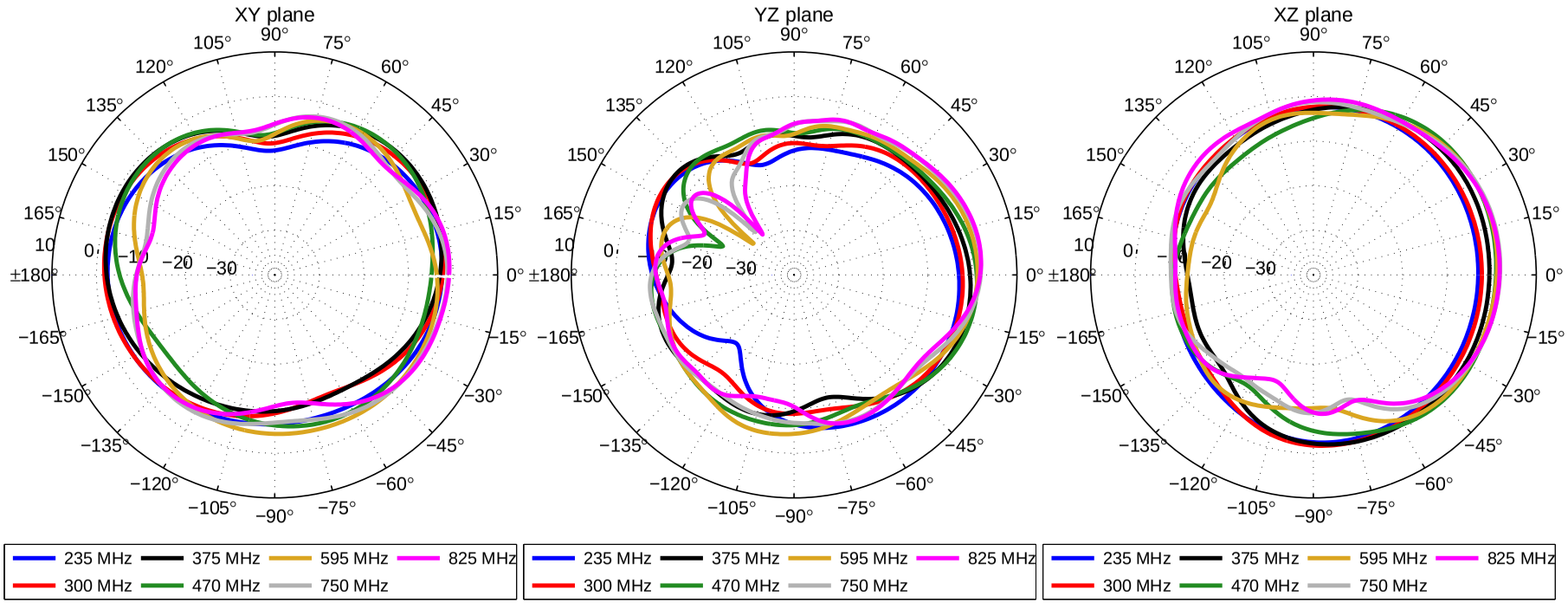

Figure 59: Duke. Radiation patterns Band 1: 235 MHz - 825 MHz.

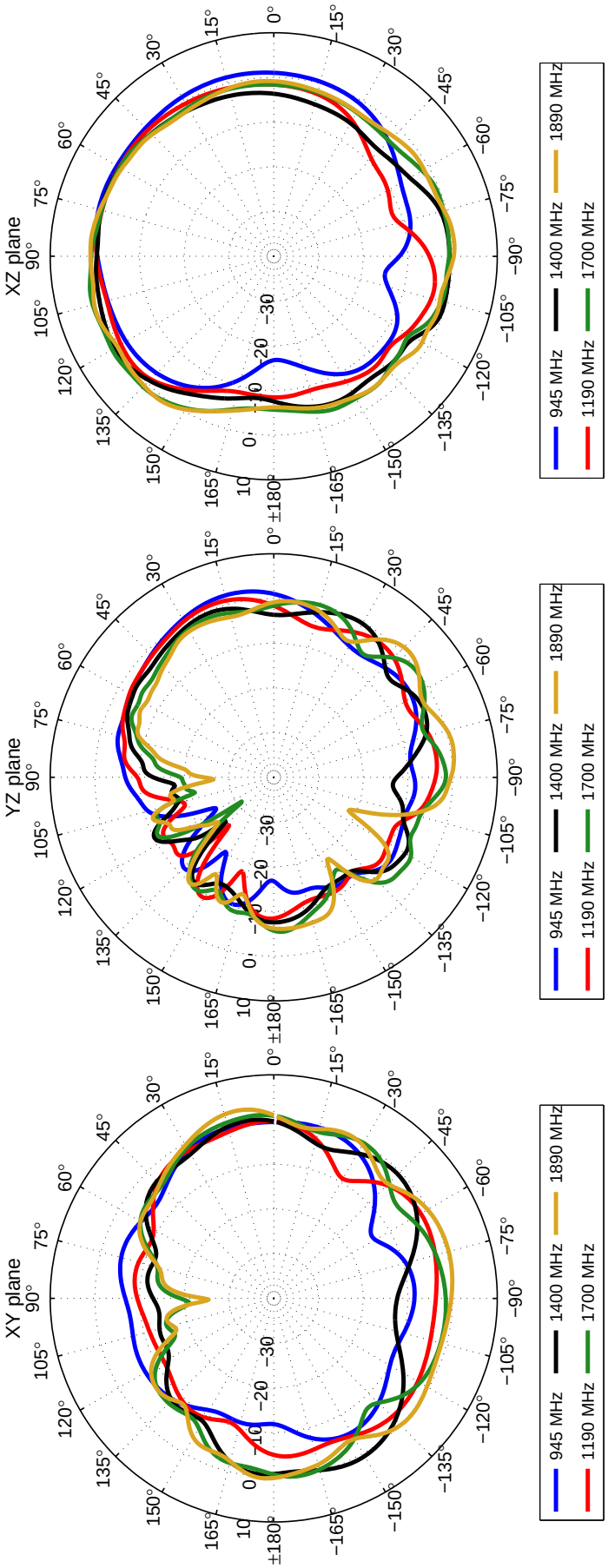

Figure 60: Duke. Radiation patterns Band 2: 945 MHz - 1890 MHz.

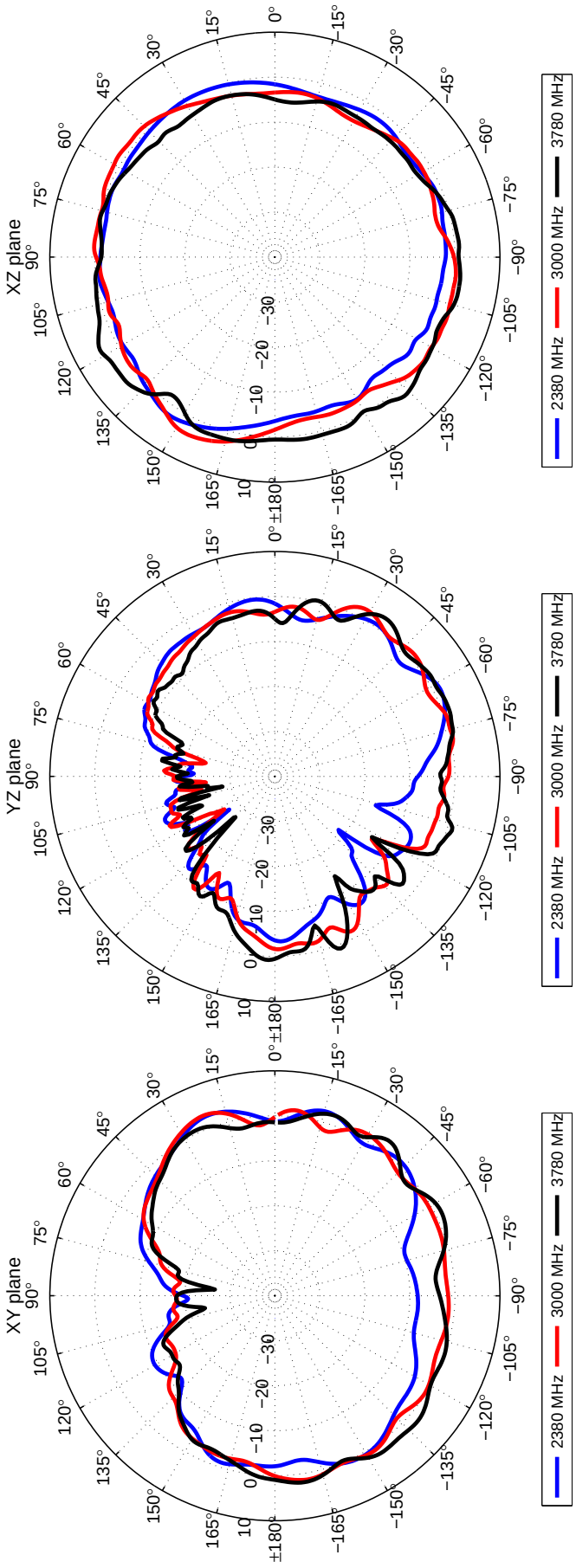

Figure 61: Duke. Radiation patterns Band 3: 2380 MHz - 3780 MHz.

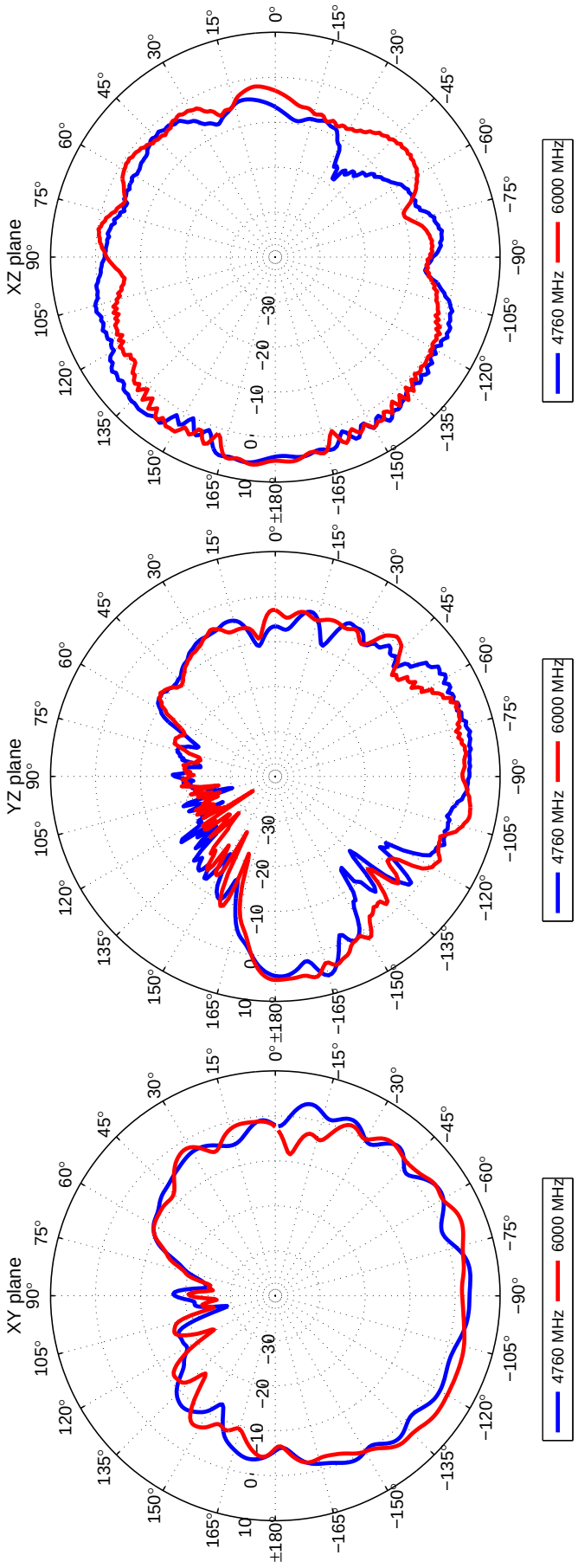

Figure 62: Duke. Radiation patterns Band 4: 4670 MHz - 6000 MHz.

A.4 Radiation patterns for a large user 1.78 m and 120 kg Fats Virtual Population Model

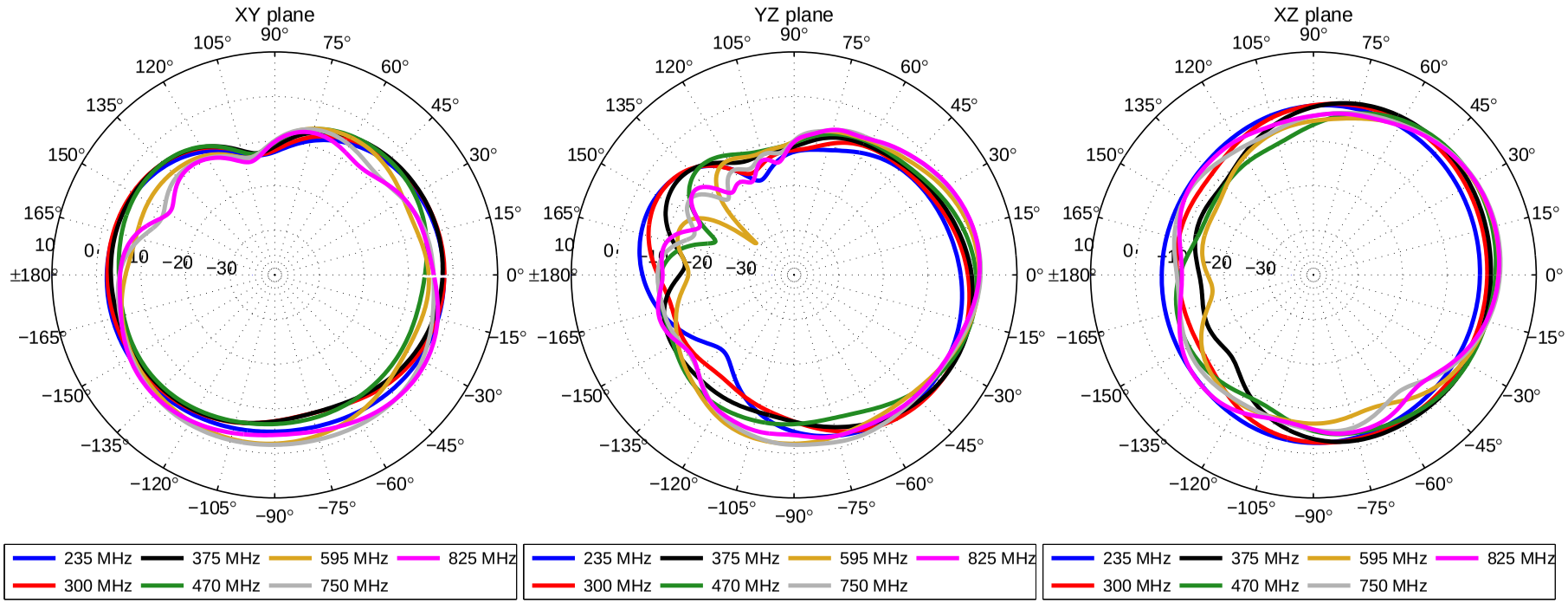

Figure 63: Fats: Radiation patterns Band 1: 235 MHz - 825 MHz.

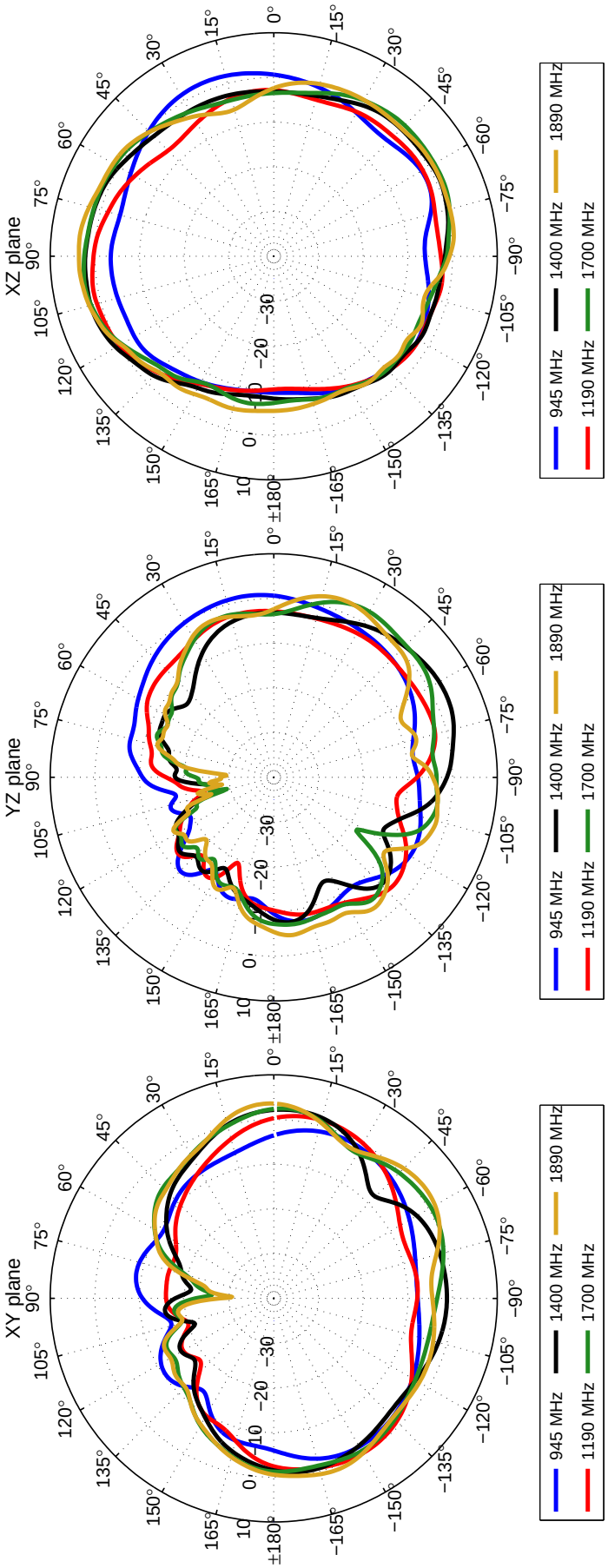

Figure 64: Fats. Radiation patterns Band 2: 945 MHz - 1890 MHz.

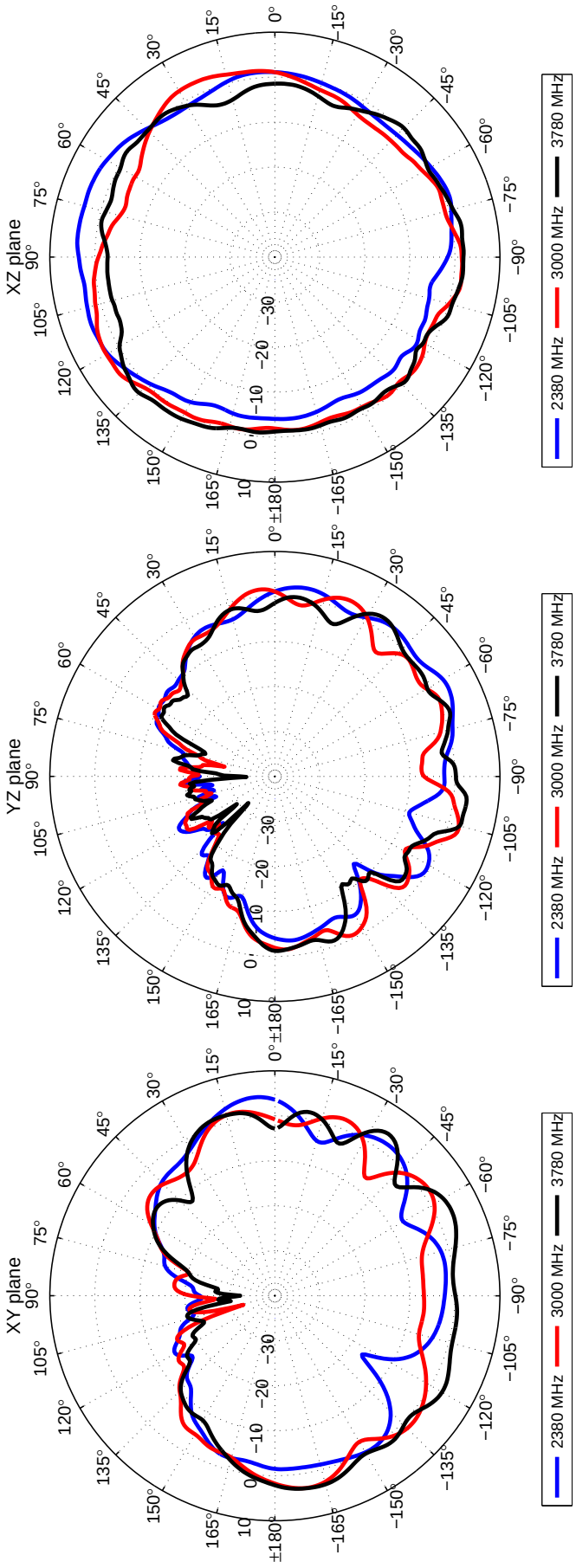

Figure 65: Fats. Radiation patterns Band 3: 2380 MHz - 3780 MHz.

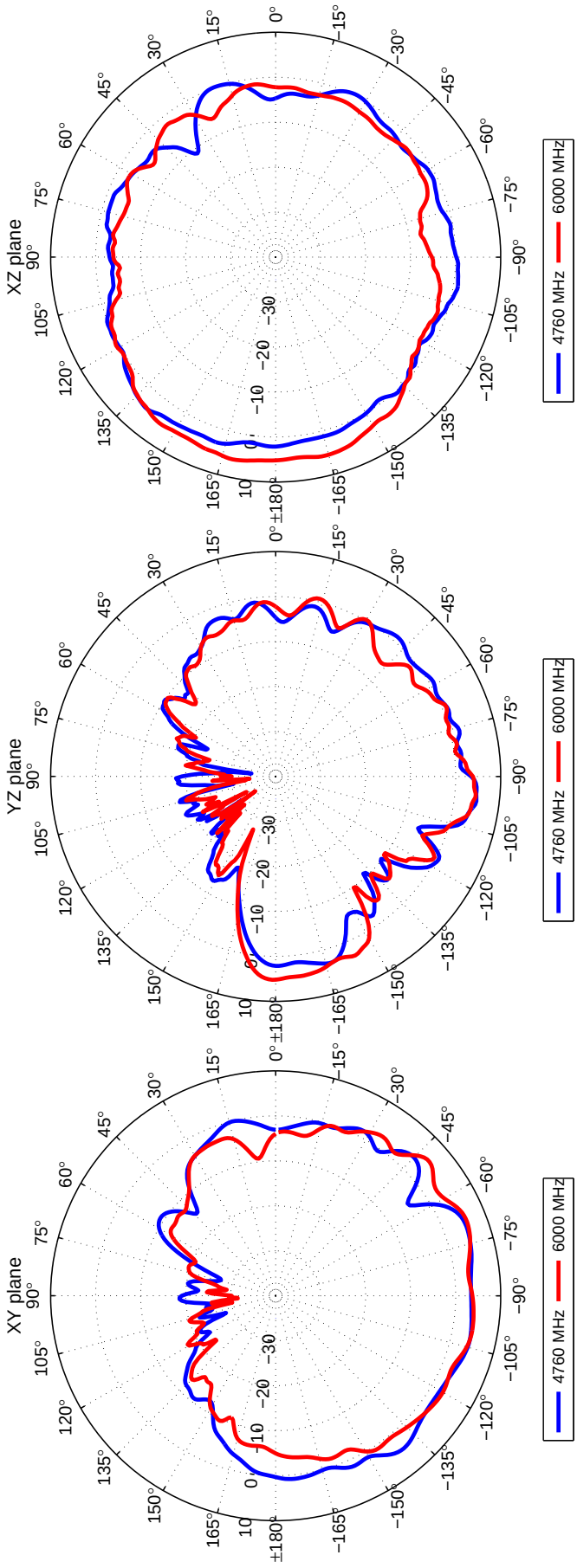

Figure 66: Fats. Radiation patterns Band 4: 4670 MHz - 6000 MHz.

A.5 Radiation patterns per frequency, for all users, compared to the unloaded case (no body, antenna only)

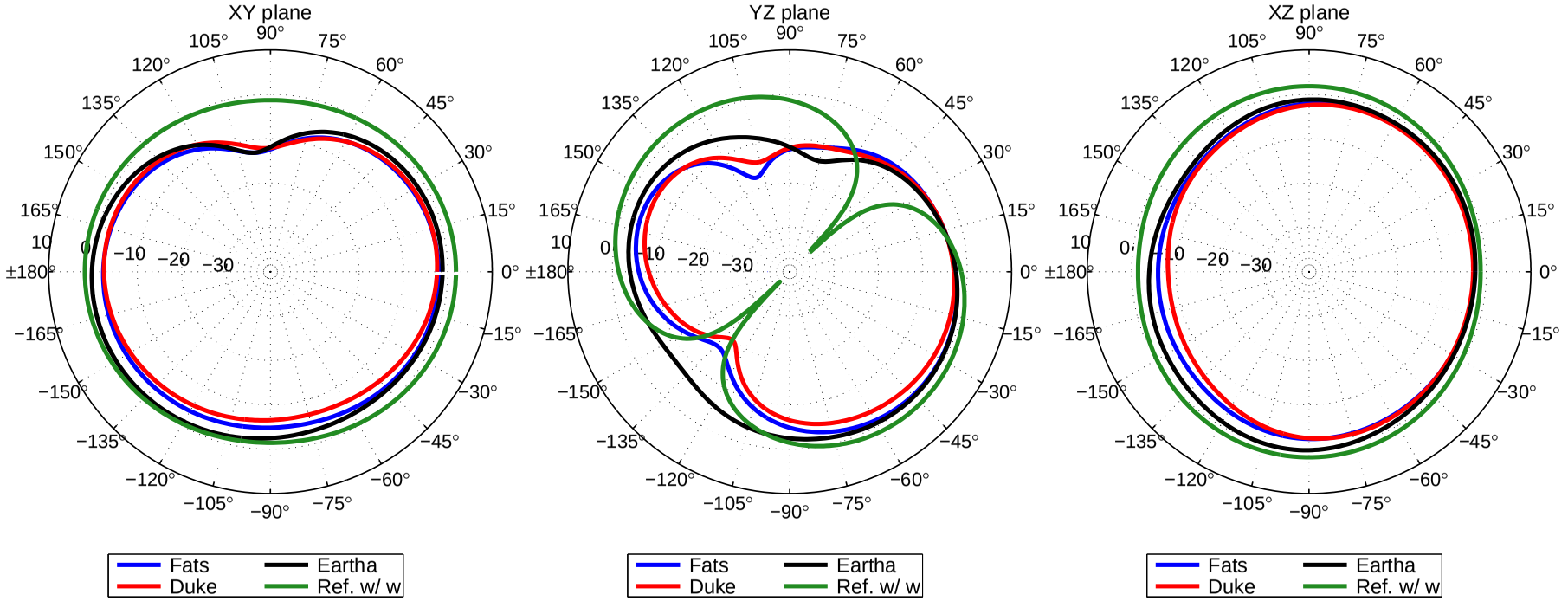

Figure 67: All Models compared to reference – microphone only – at 235 MHz.

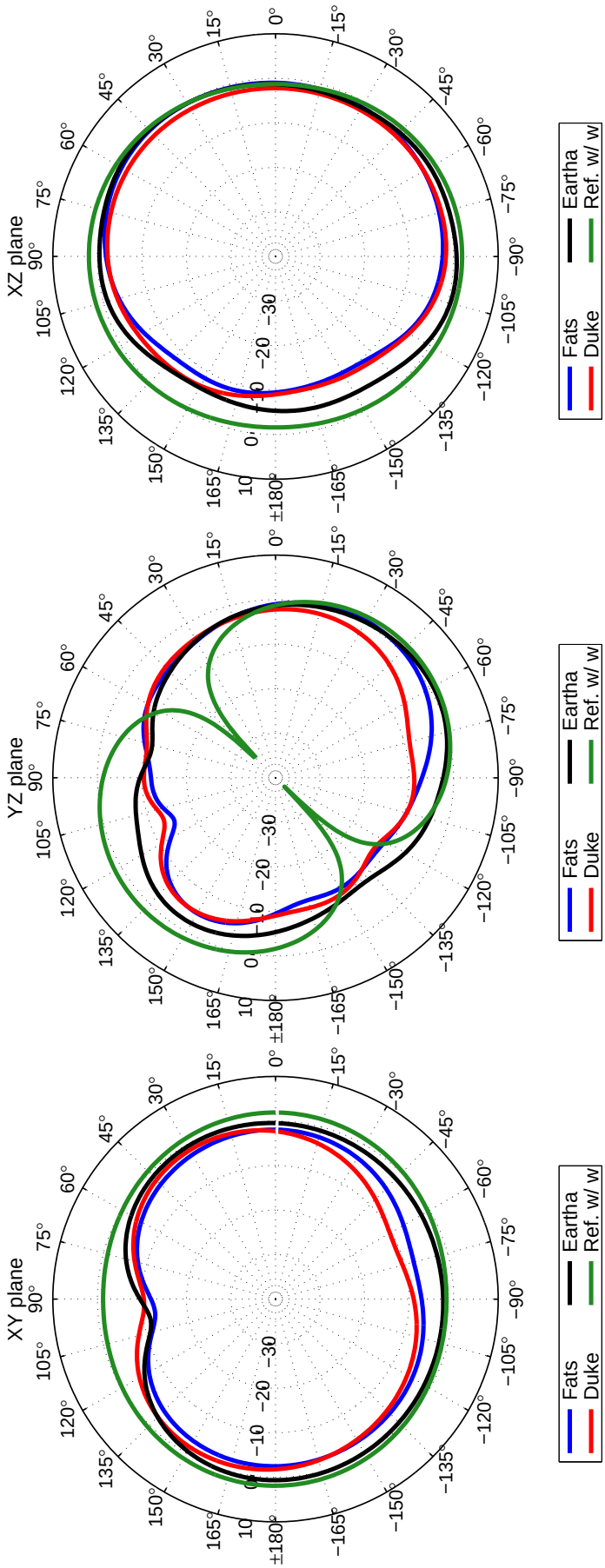

Figure 68: All Models compared to reference – microphone only – at 300 MHz.

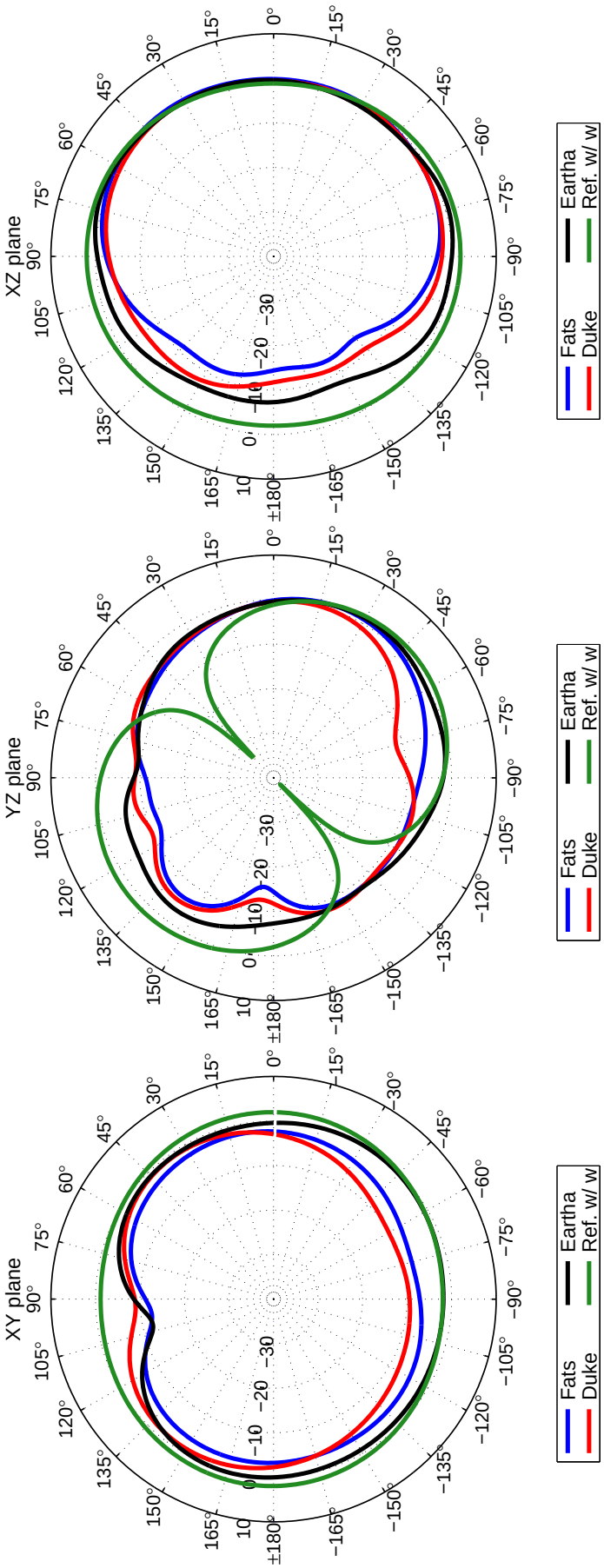

Figure 69: All Models compared to reference – microphone only – at 375 MHz.

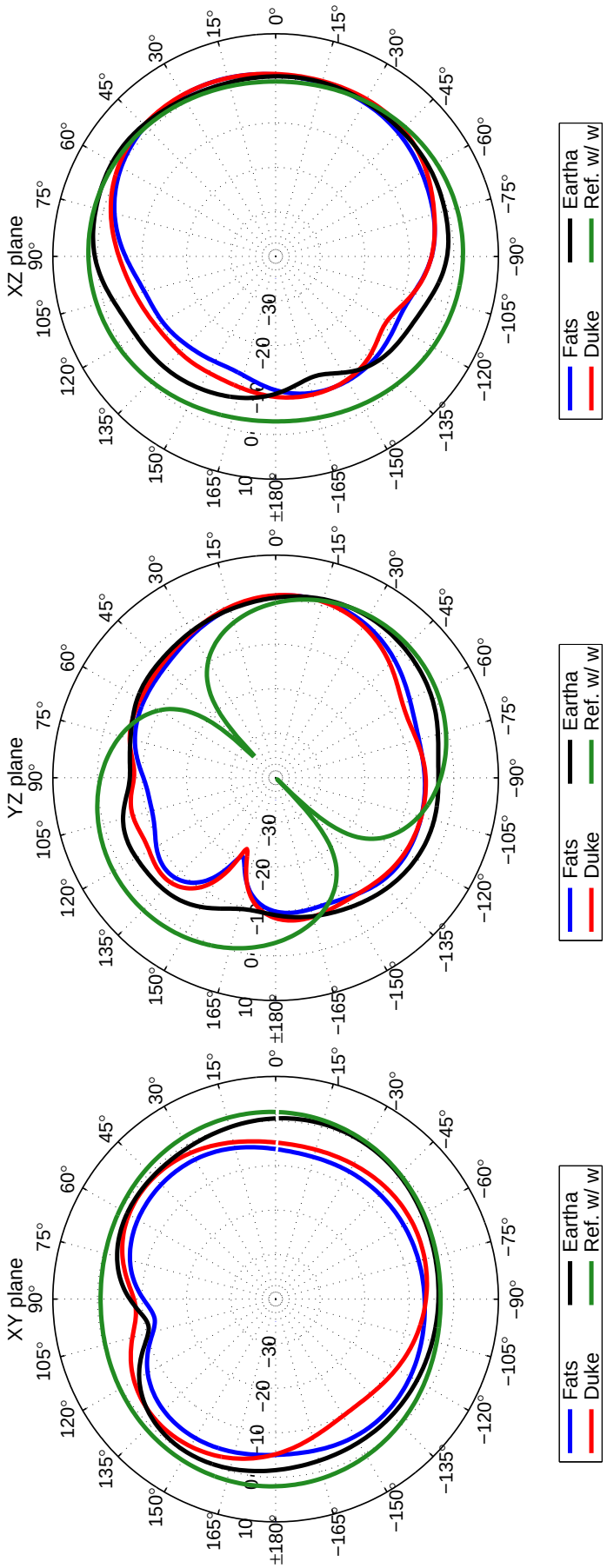

Figure 70: All Models compared to reference – microphone only – at 470 MHz.

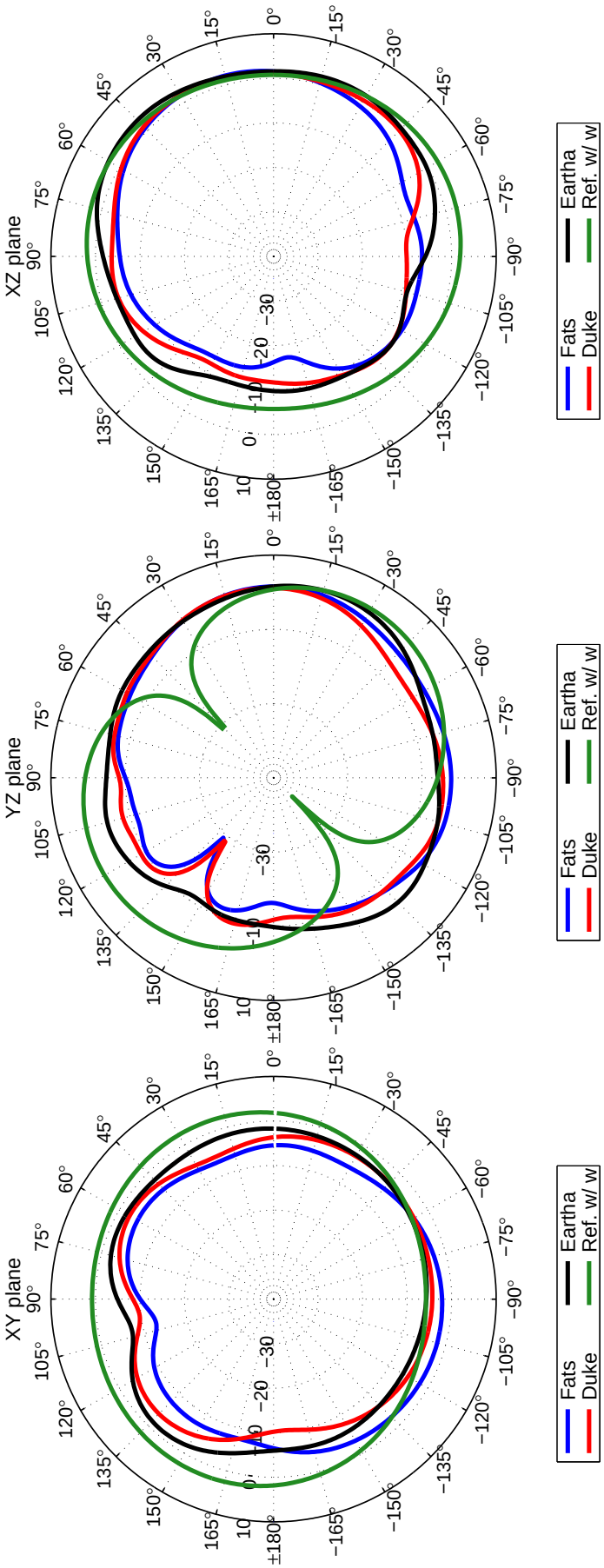

Figure 71: All Models compared to reference – microphone only – at 595 MHz.

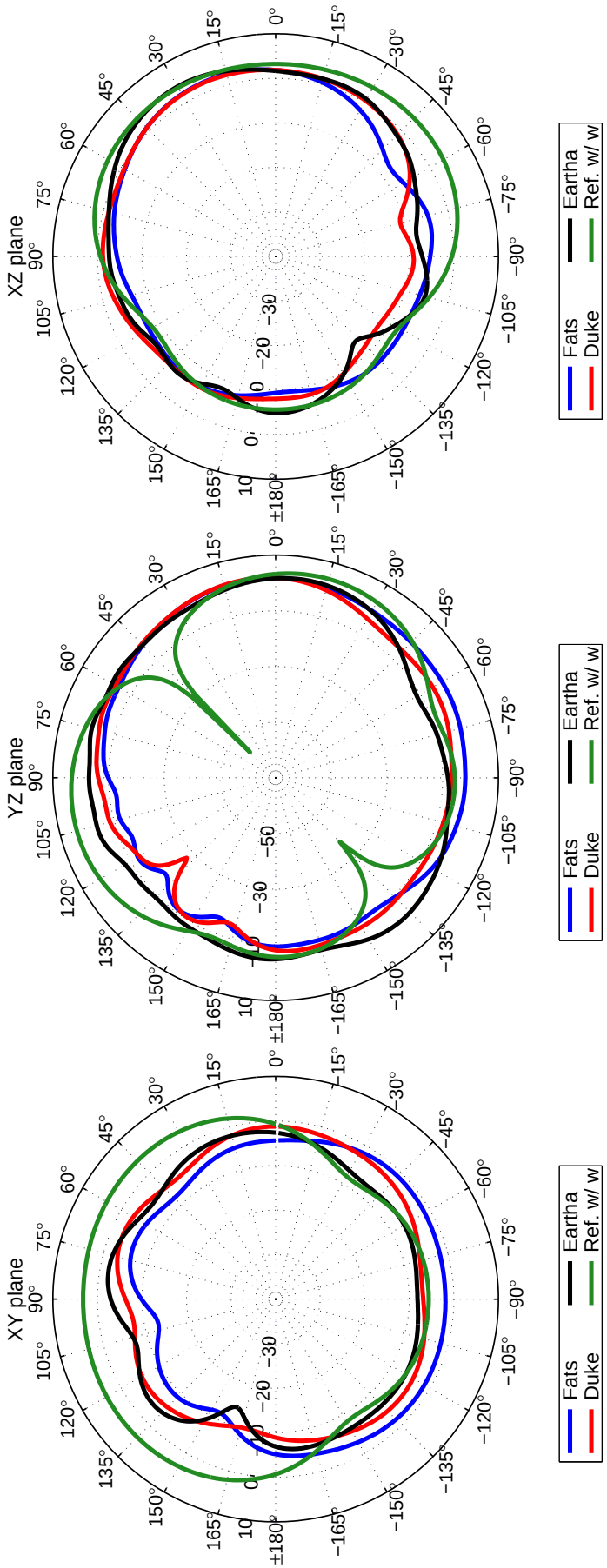

Figure 72: All Models compared to reference – microphone only – at 750 MHz.

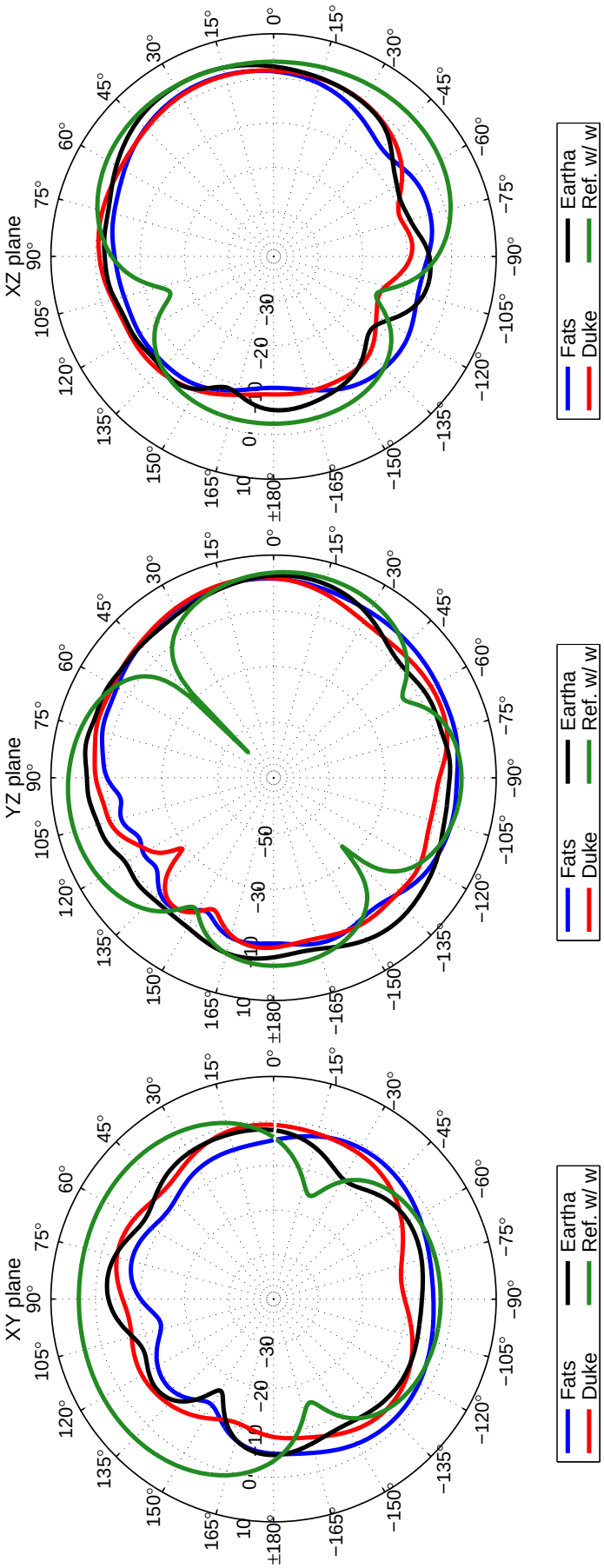

Figure 73: All Models compared to reference – microphone only – at 825 MHz.

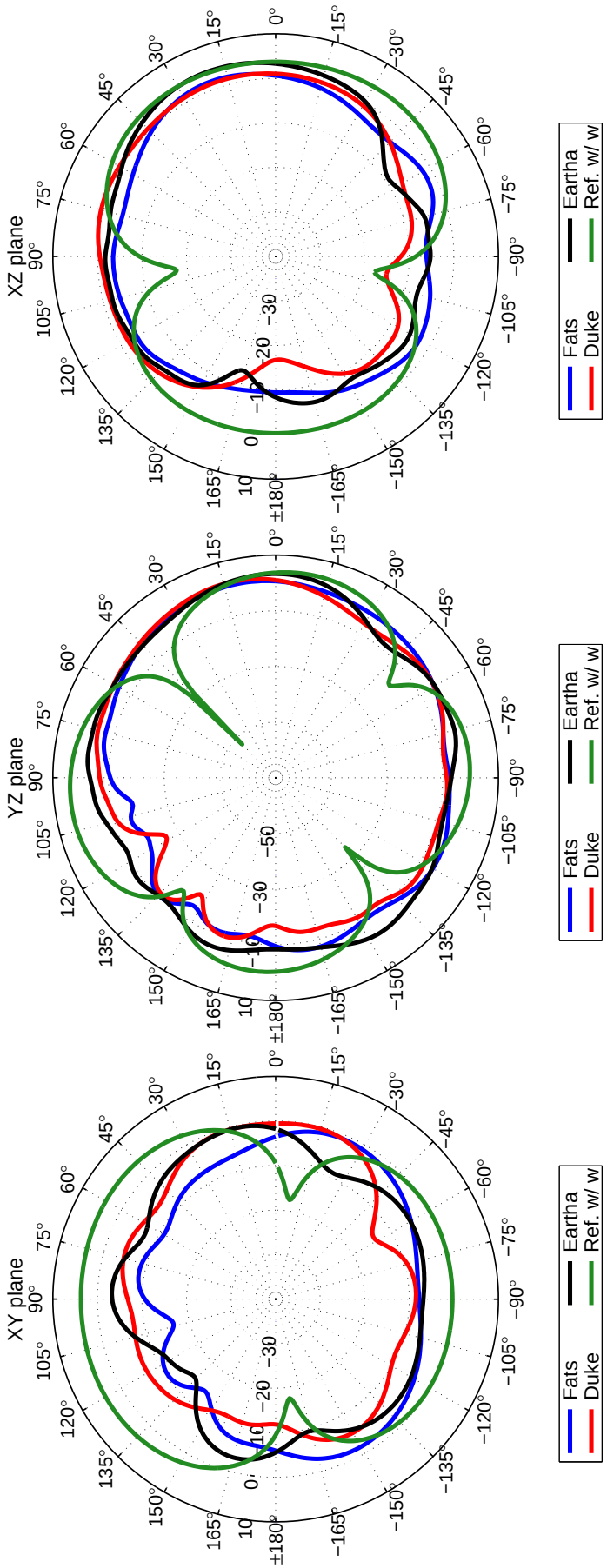

Figure 74: All Models compared to reference – microphone only – at 945 MHz.

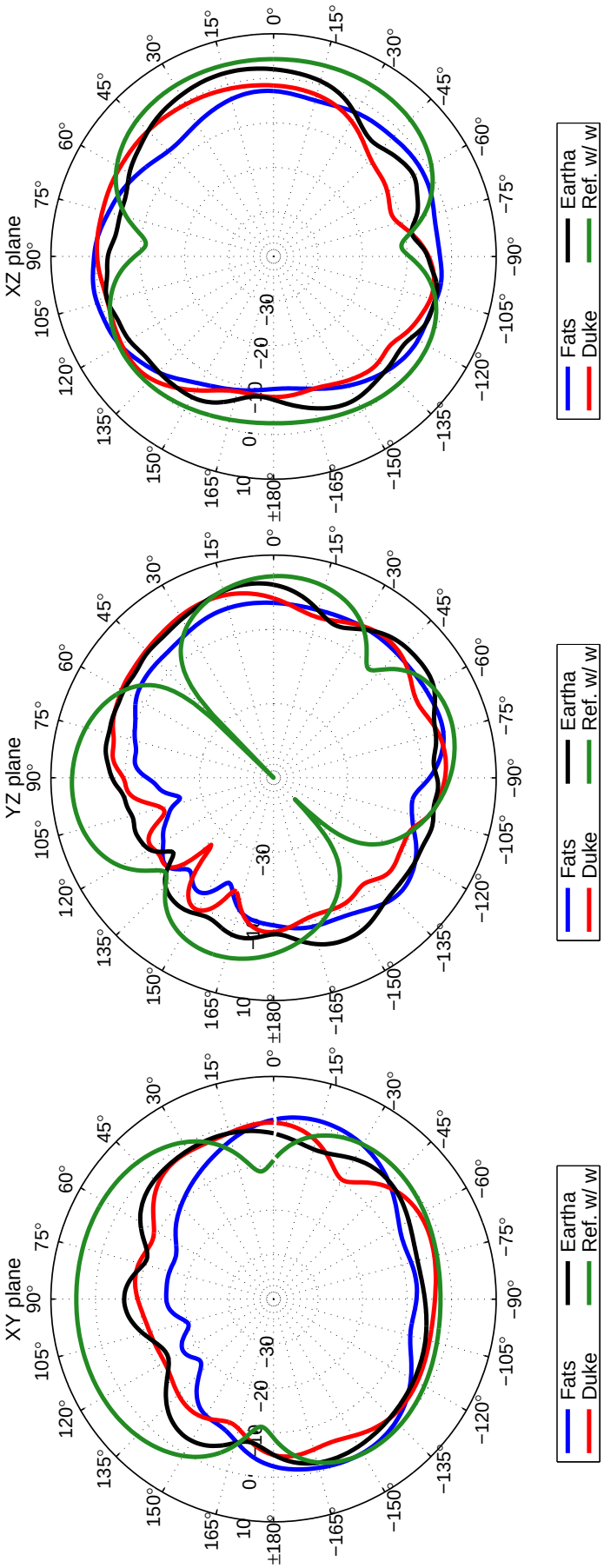

Figure 75: All Models compared to reference – microphone only – at 1190 MHz.

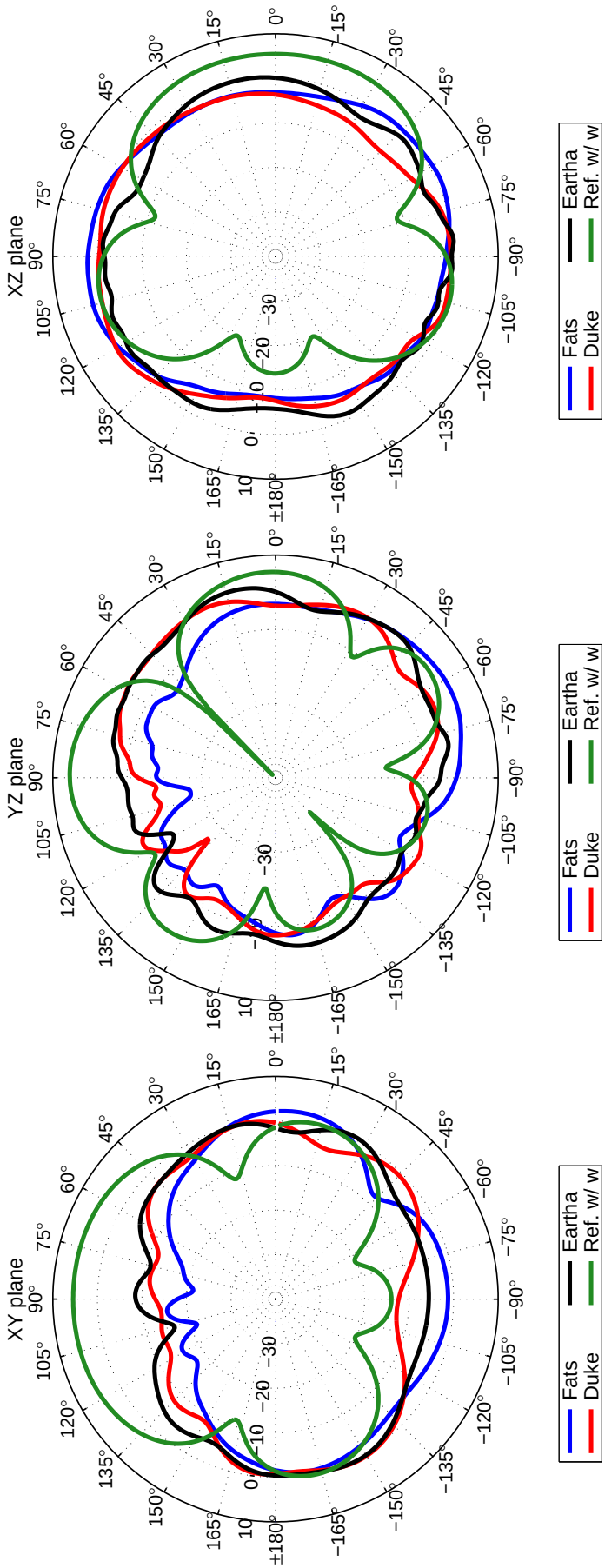

Figure 76: All Models compared to reference – microphone only – at 1400 MHz.

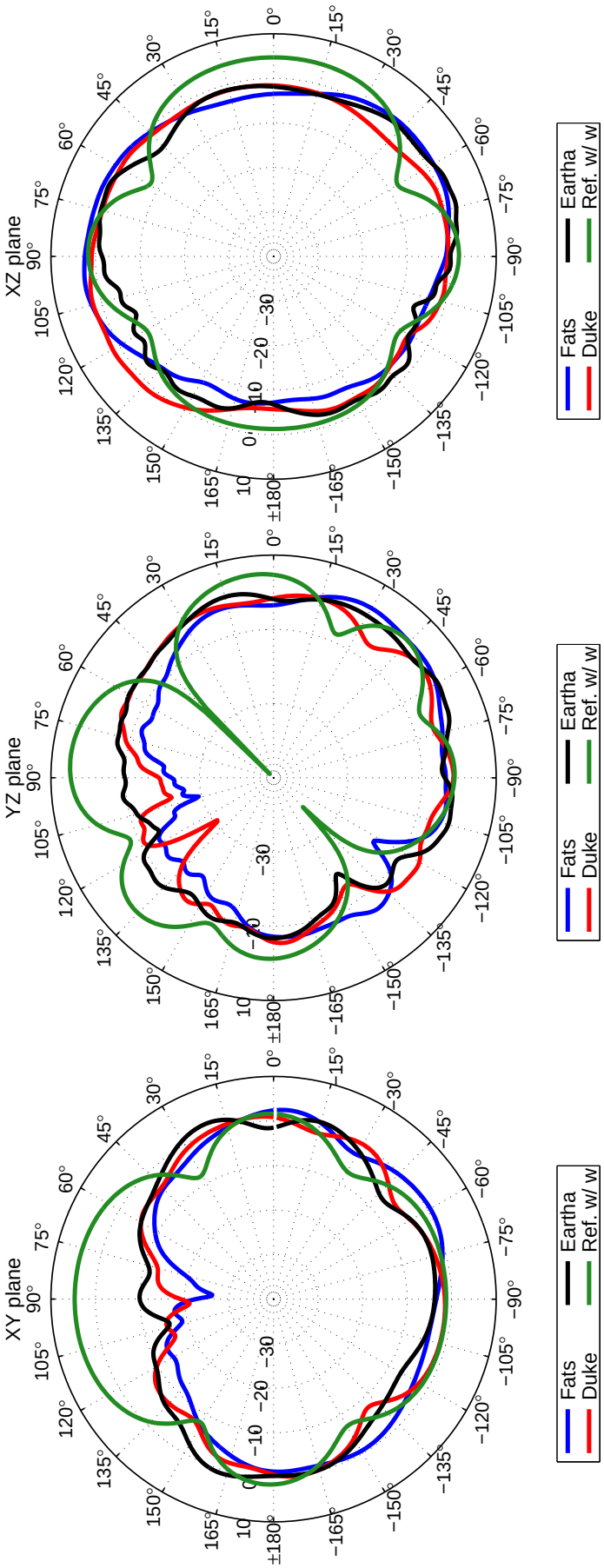

Figure 77: All Models compared to reference – microphone only – at 1700 MHz.

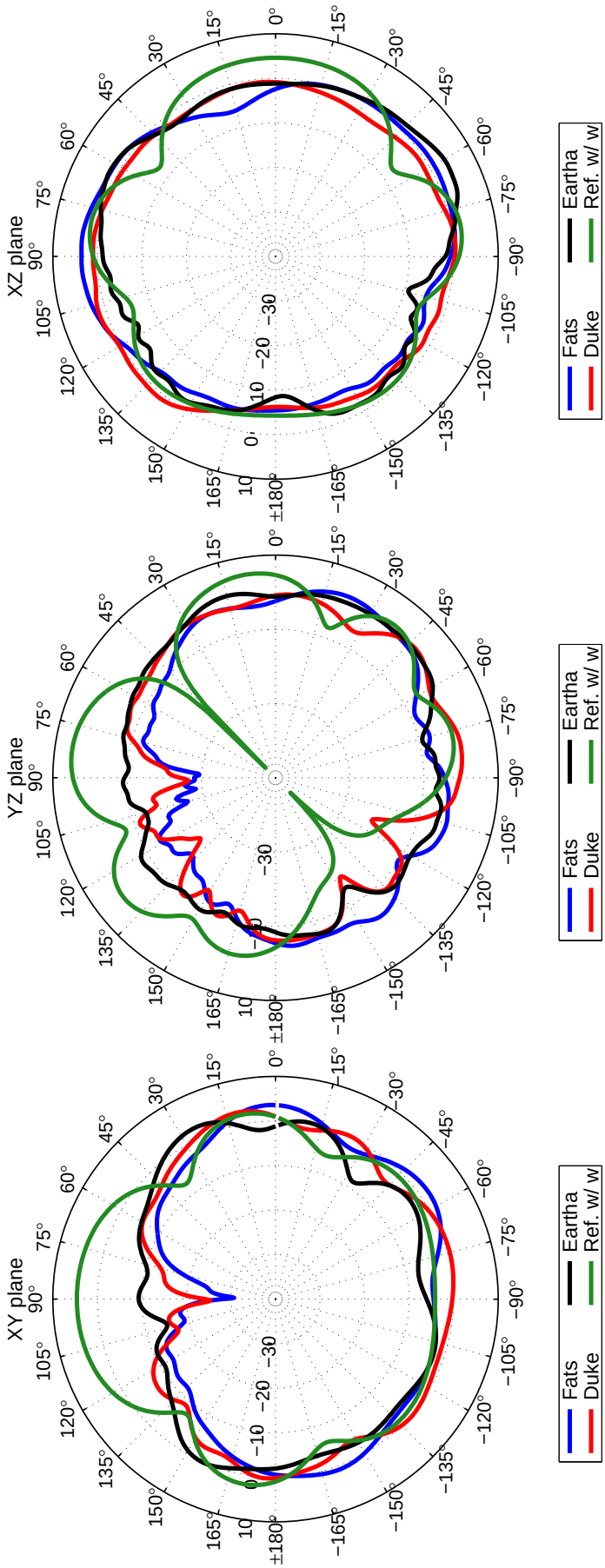

Figure 78: All Models compared to reference – microphone only – at 1890 MHz.

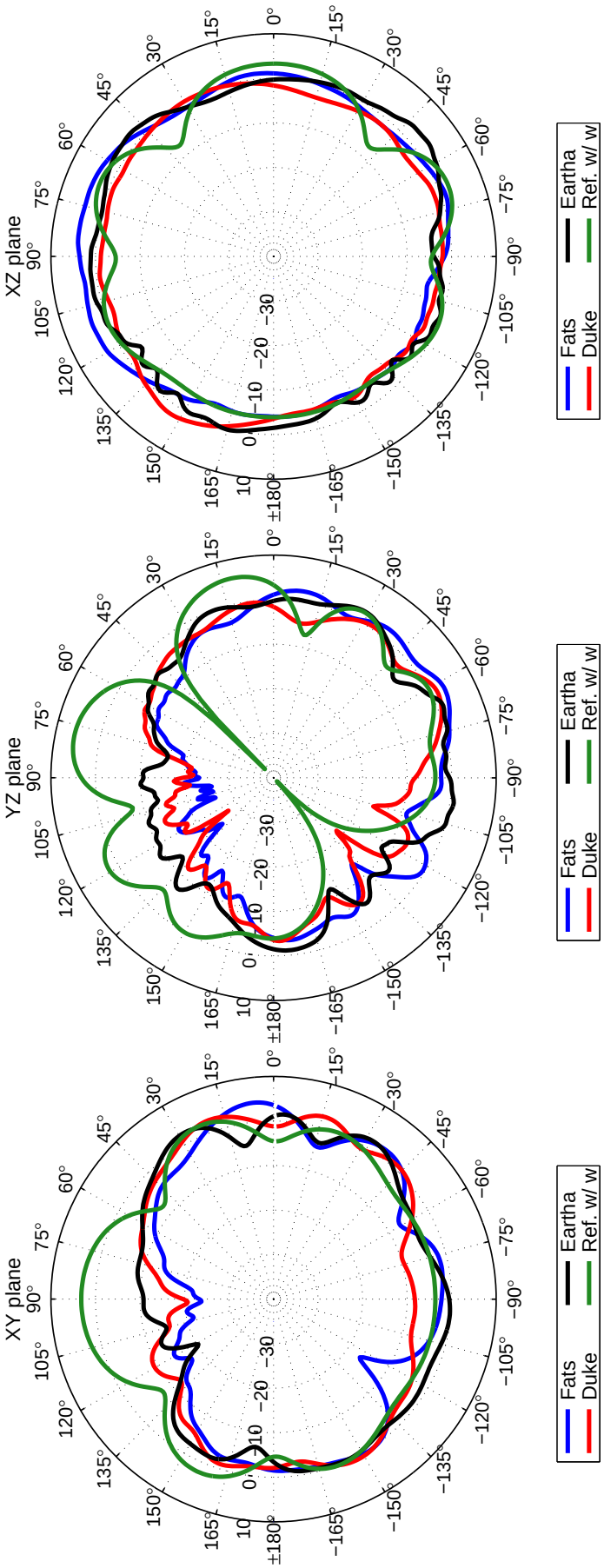

Figure 79: All Models compared to reference – microphone only – at 2380 MHz.

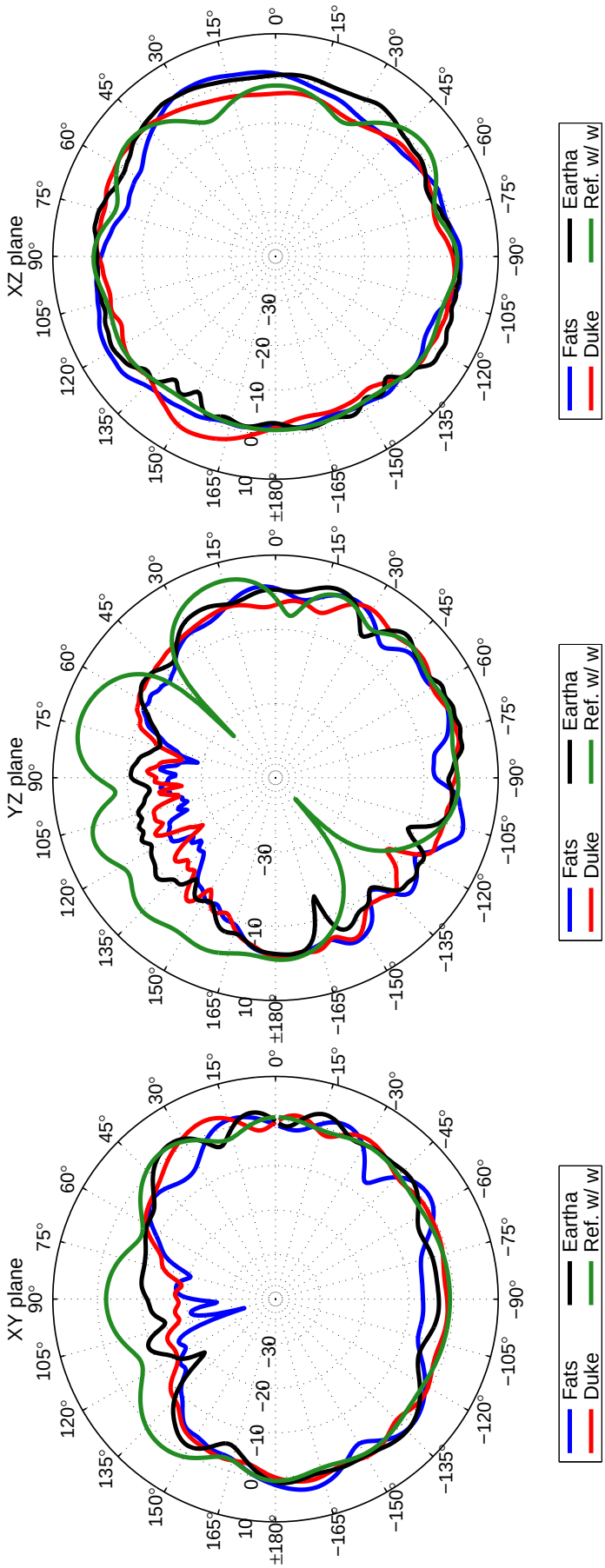

Figure 80: All Models compared to reference – microphone only – at 3000 MHz.

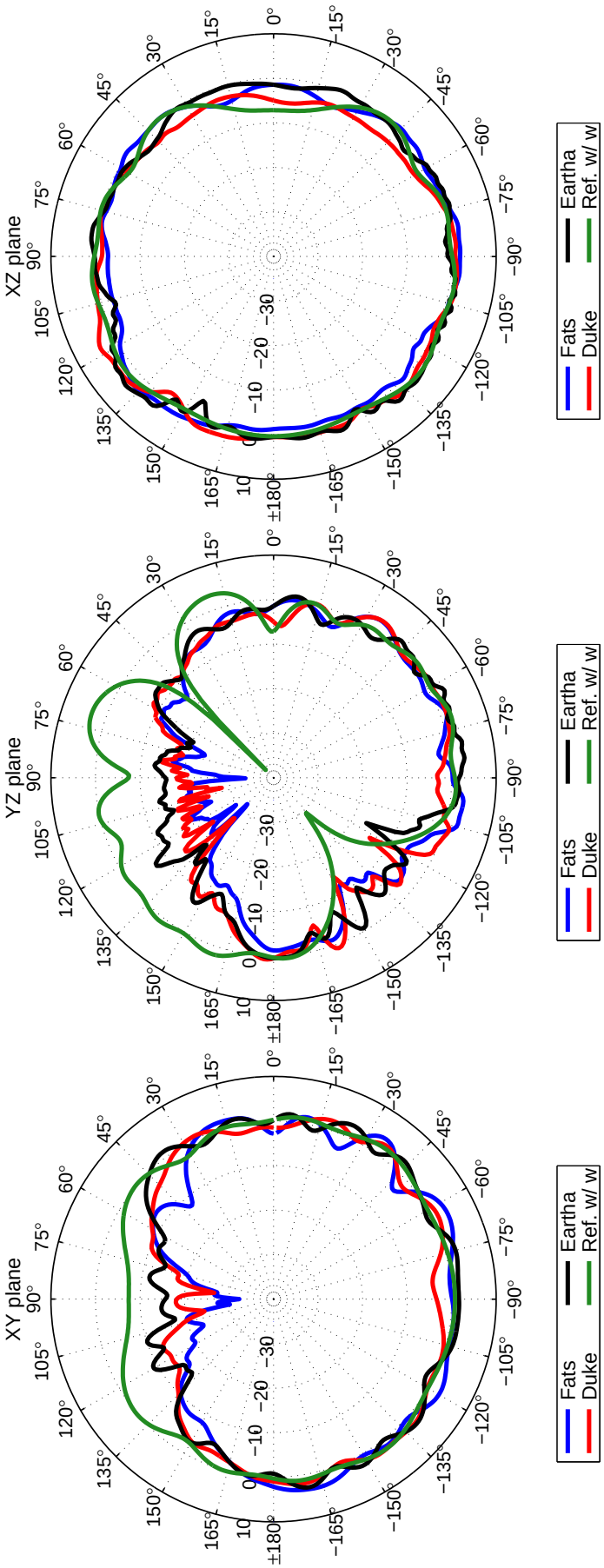

Figure 81: All Models compared to reference – microphone only – at 3780 MHz.

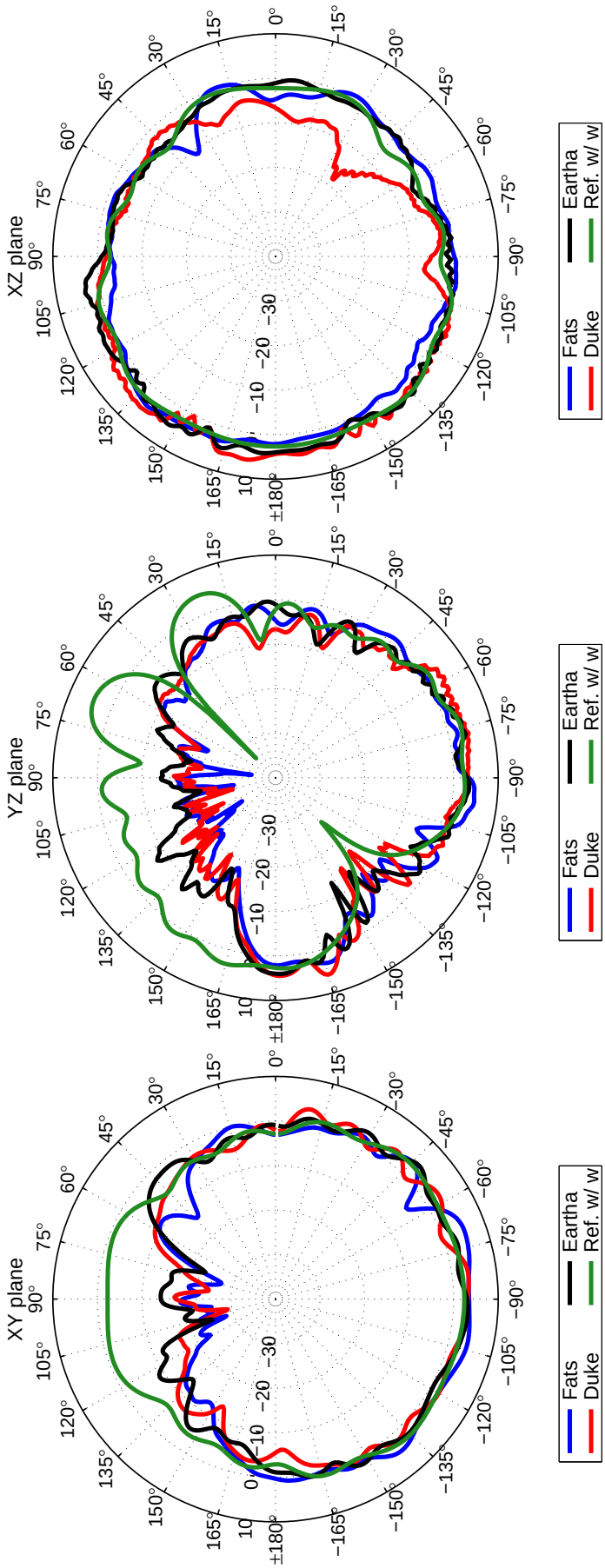

Figure 82: All Models compared to reference – microphone only – at 4760 MHz.

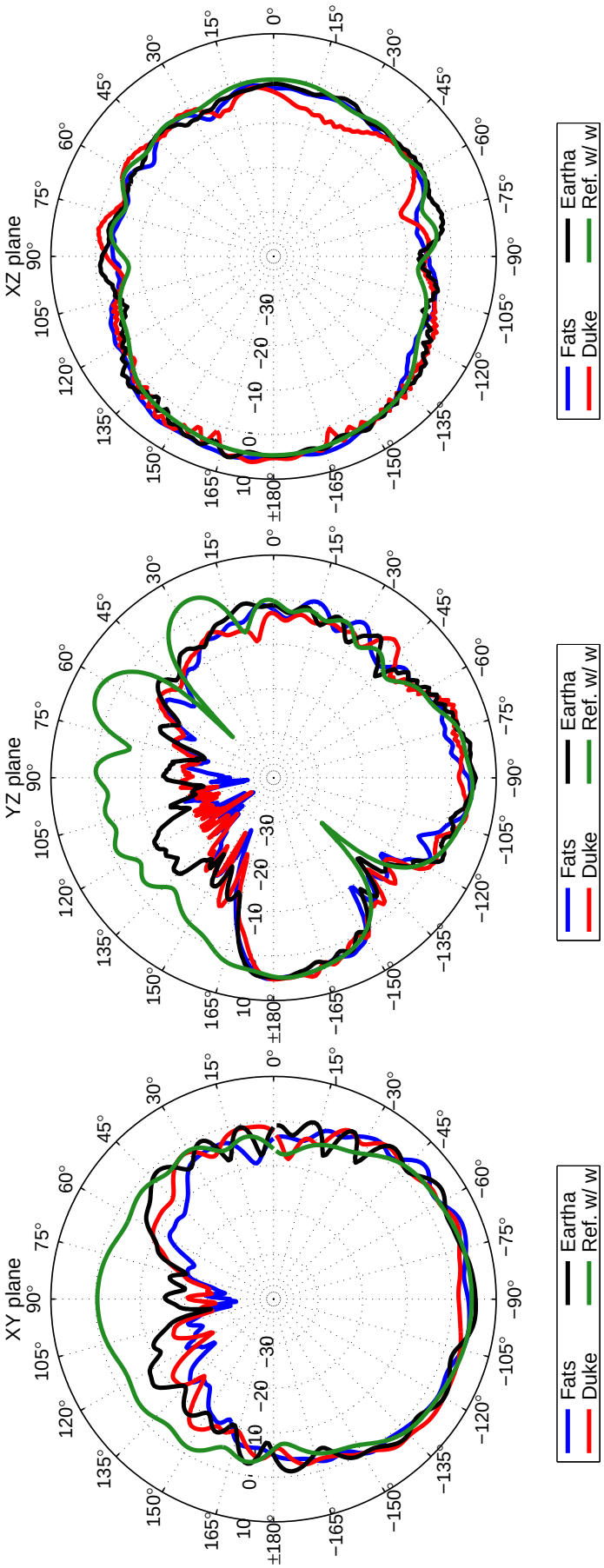

Figure 83: All Models compared to reference – microphone only – at 6000 MHz.

B Bodypack Lavalier Microphone - Complete Set of Results

B.1 Reference free space radiation patterns for the bodypack microphone

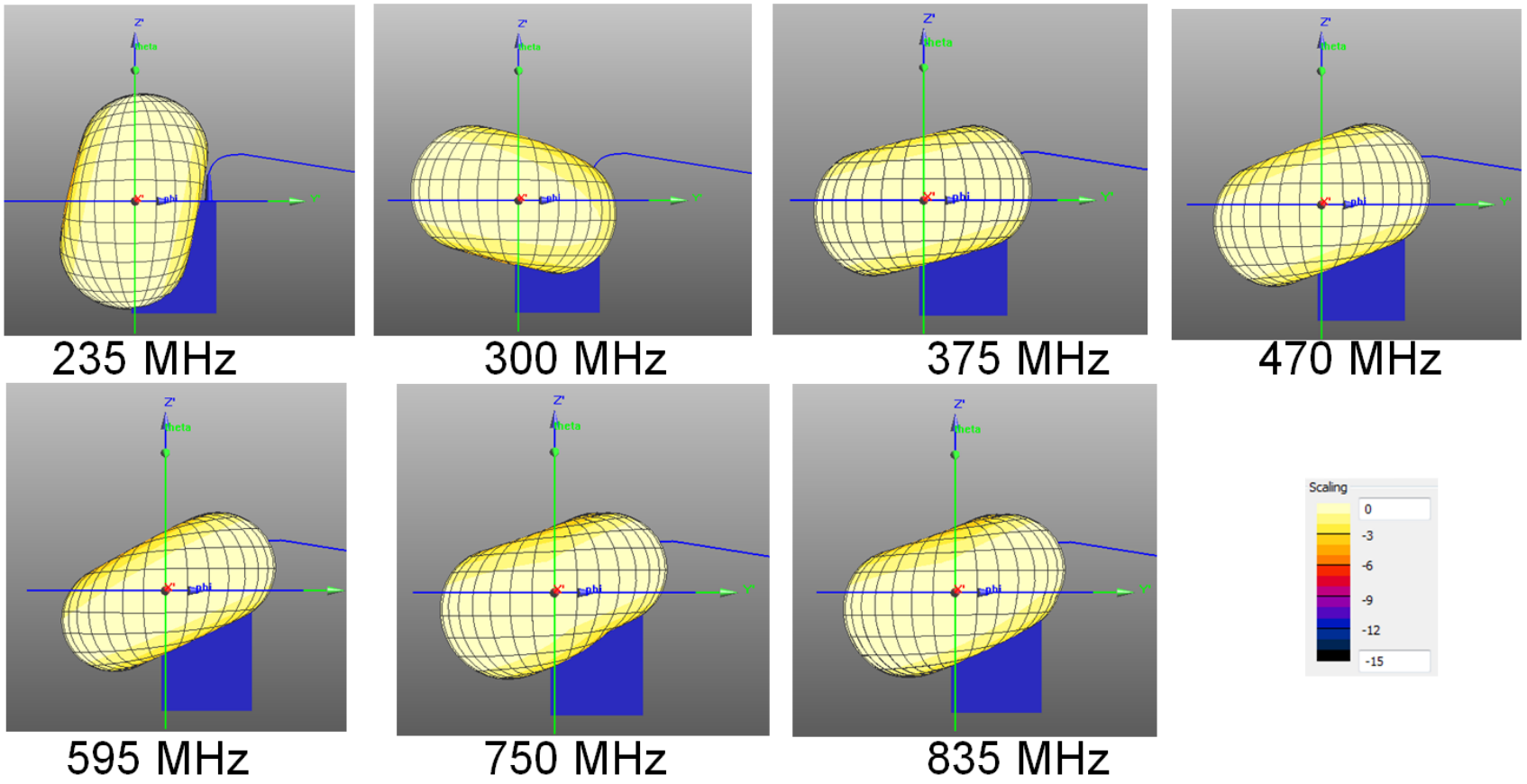

Figure 84: Free space radiation patterns for bodypack microphone for band 1. Scale referenced to peak gain.

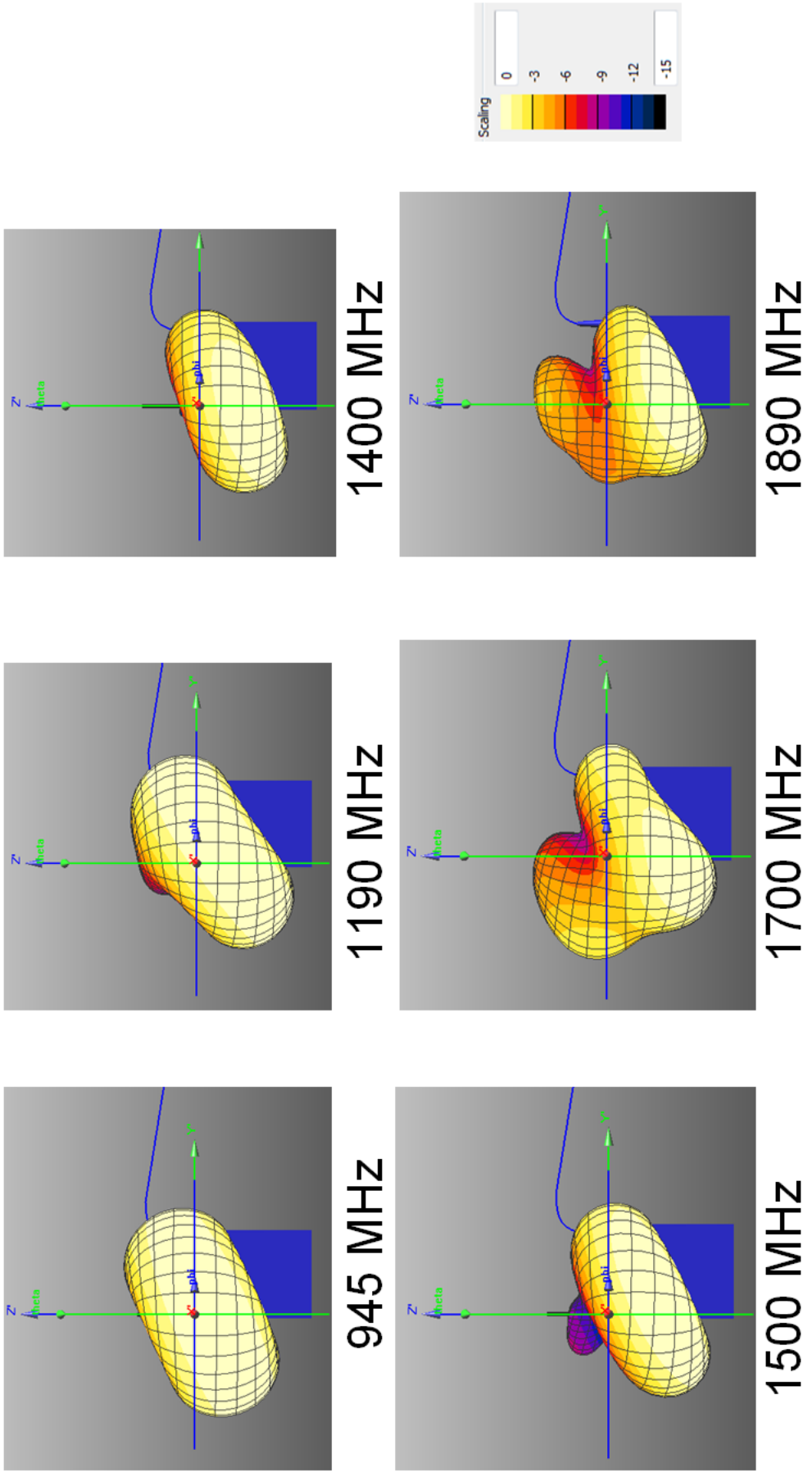

Figure 85: Free space radiation patterns for bodypack microphone for band 2. Scale referenced to peak gain.

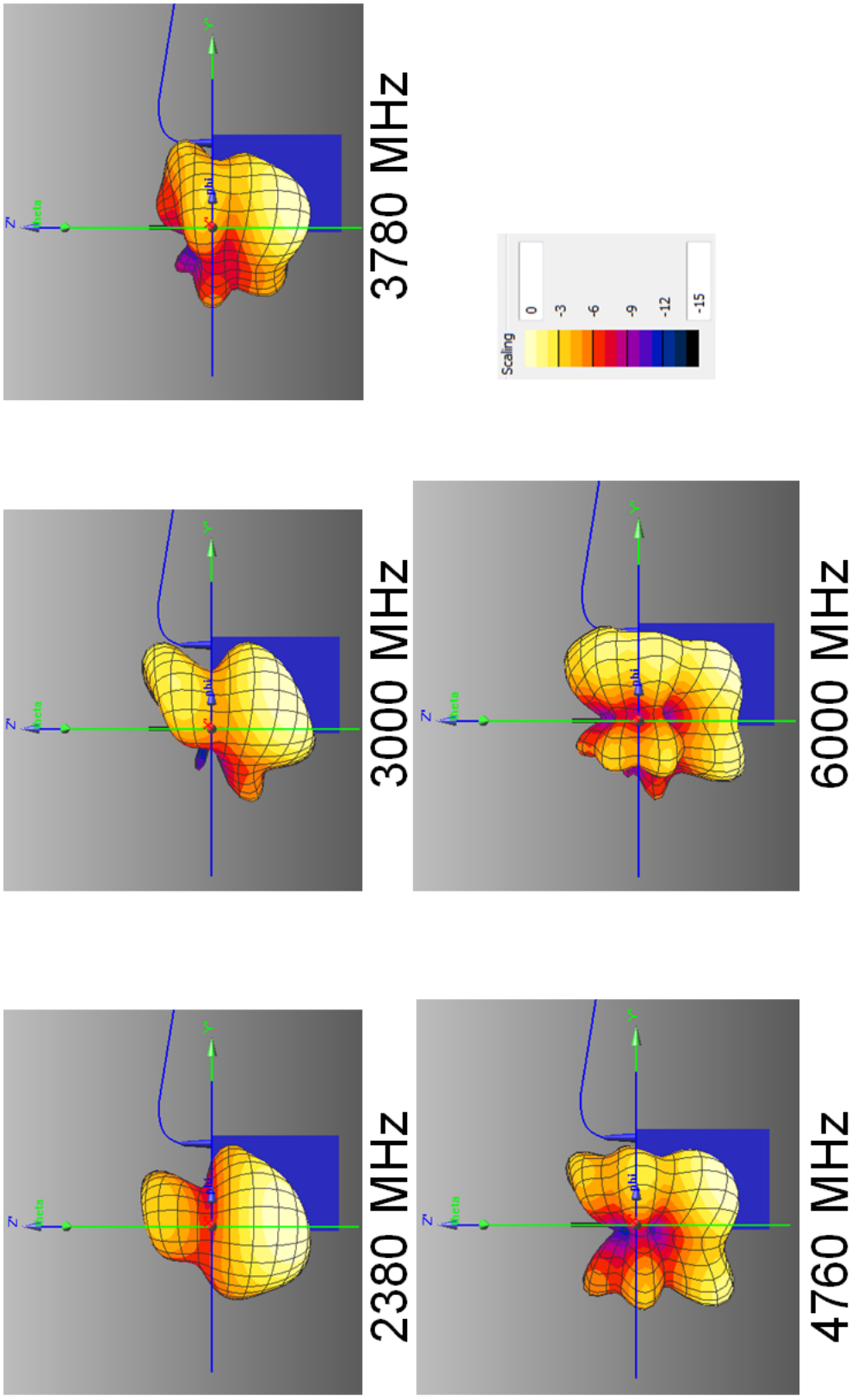

Figure 86: Free space radiation patterns for bodypack microphone for bands 3 and 4. Scale referenced to peak gain.

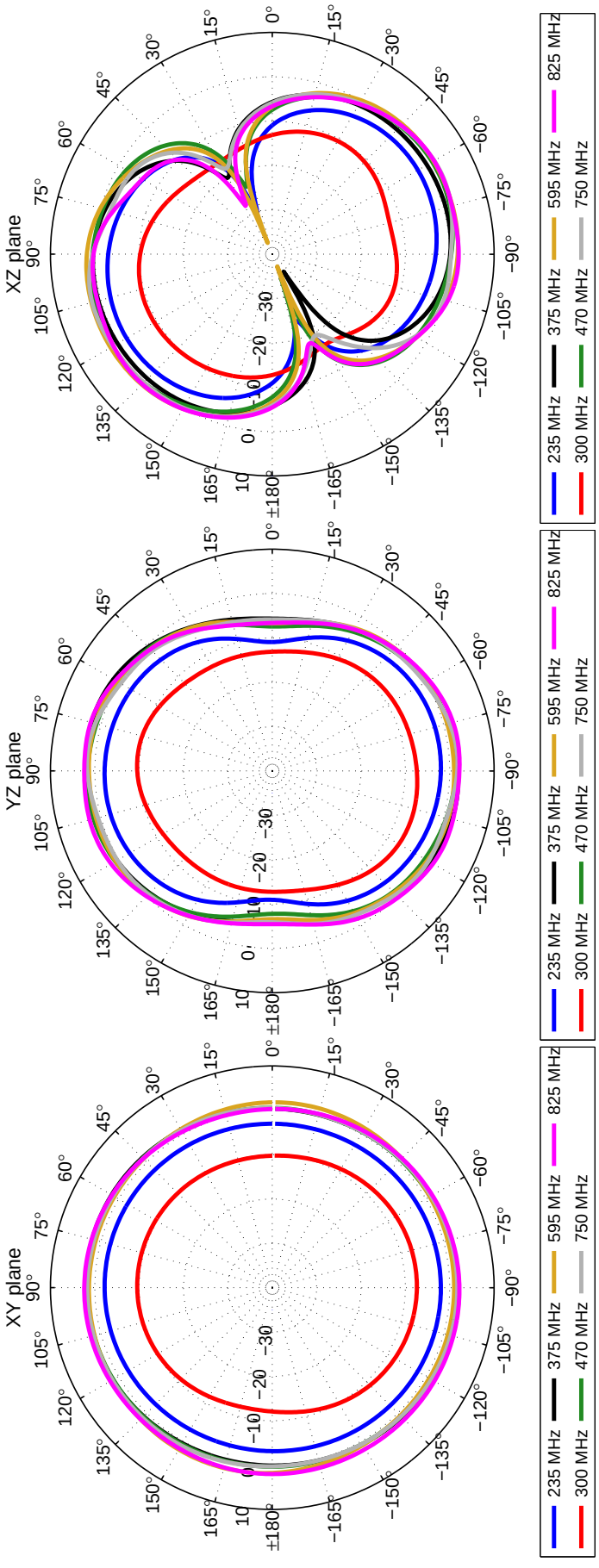

Figure 87: Free space for bodypack with microphone. Radiation patterns Band 1: 235 MHz - 825 MHz.

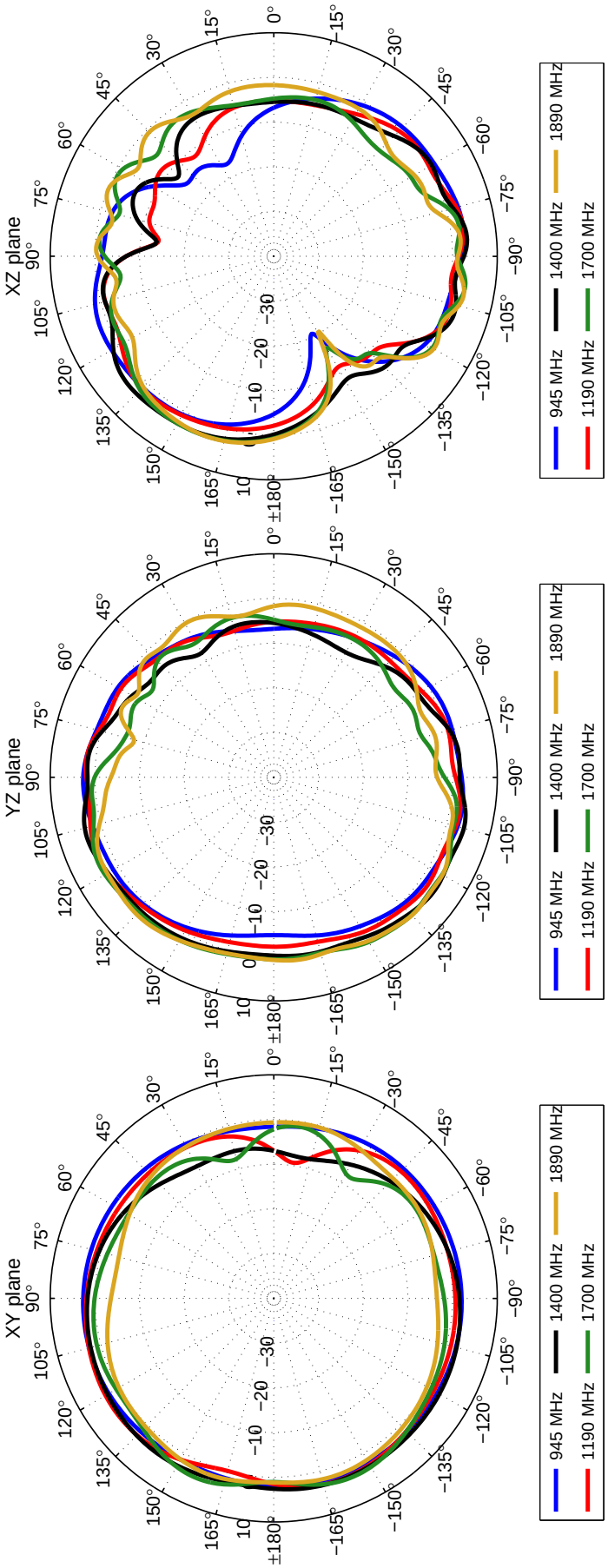

Figure 88: Free space for bodypack with microphone. Radiation patterns Band 2: 945 MHz - 1890 MHz.

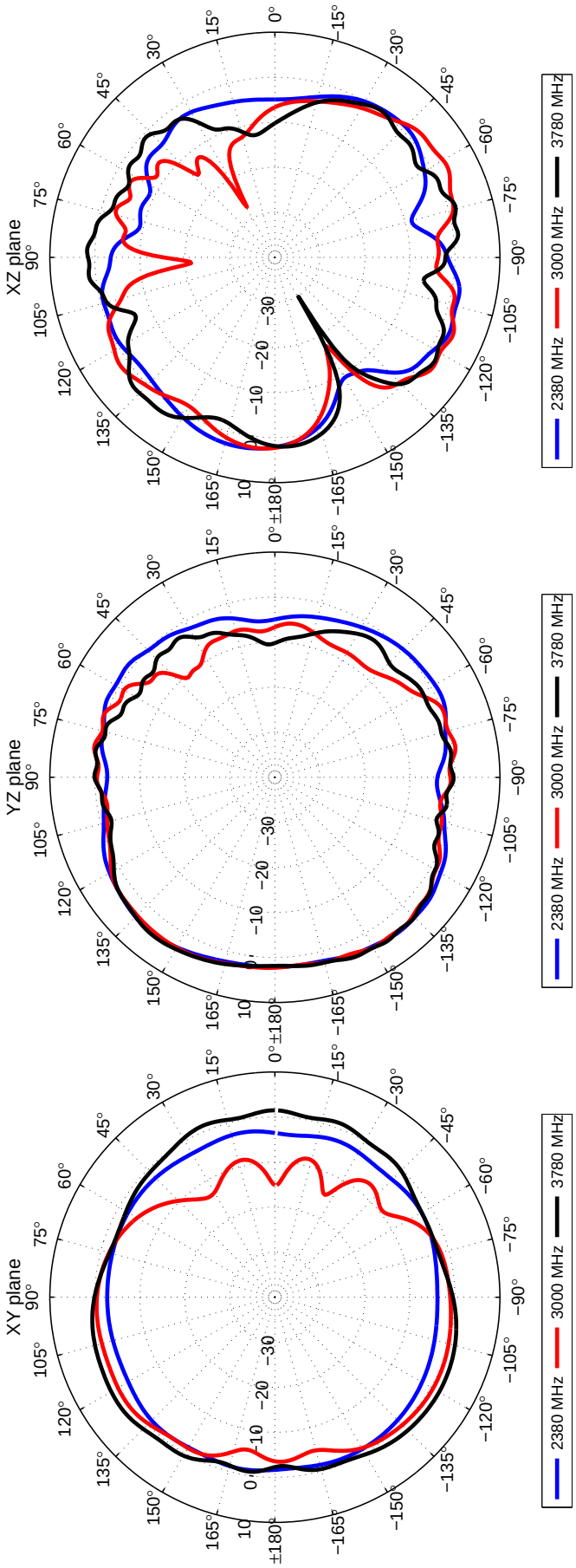

Figure 89: Free space for bodypack with microphone. Radiation patterns Band 3: 2380 MHz - 3780 MHz.

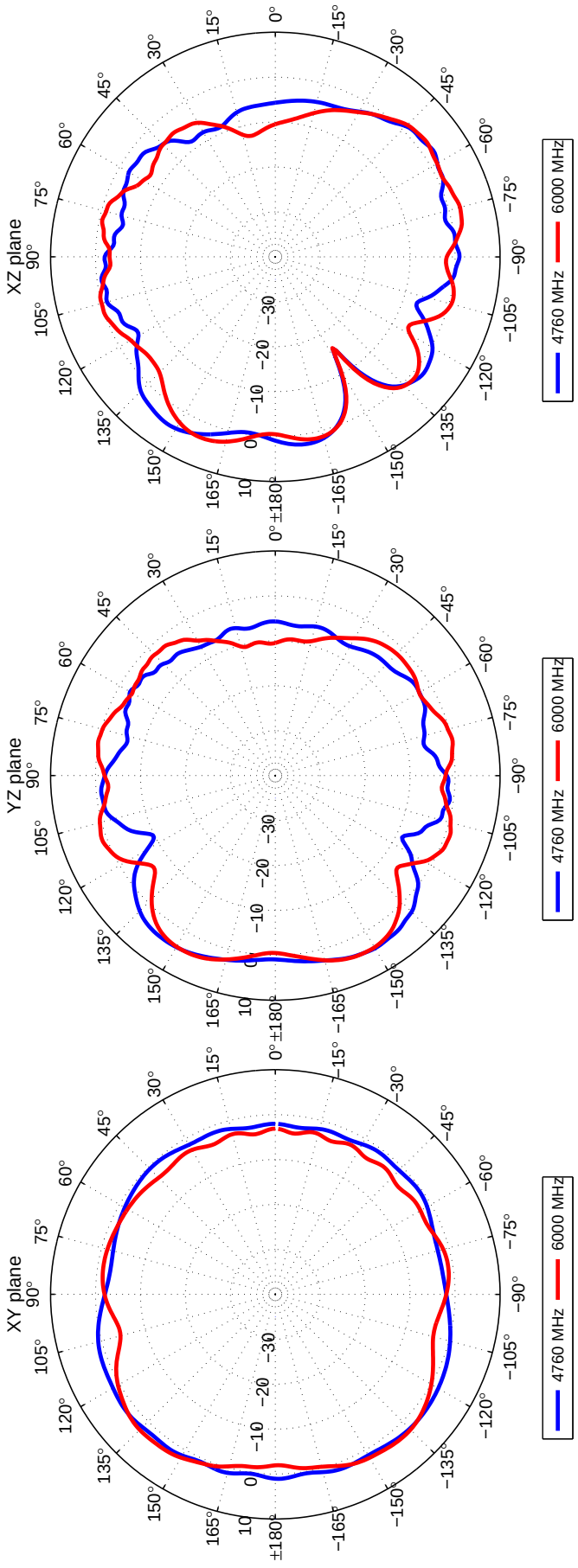

Figure 90: Free space for bodypack with microphone. Radiation patterns Band 4: 4670 MHz - 6000 MHz.

B.2 Radiation patterns for a small user 1.35 m and 31 kg Eartha Virtual Population Model

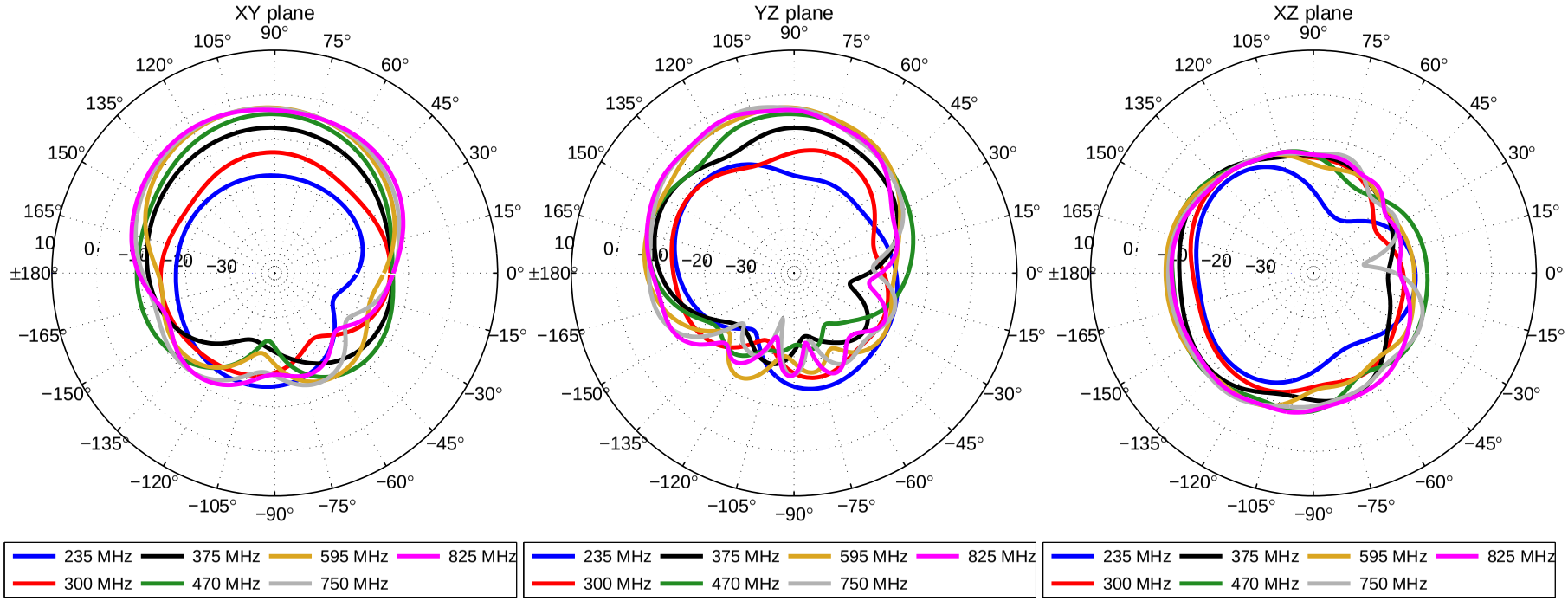

Figure 91: Eartha. Radiation patterns Band 1: 235 MHz - 825 MHz.

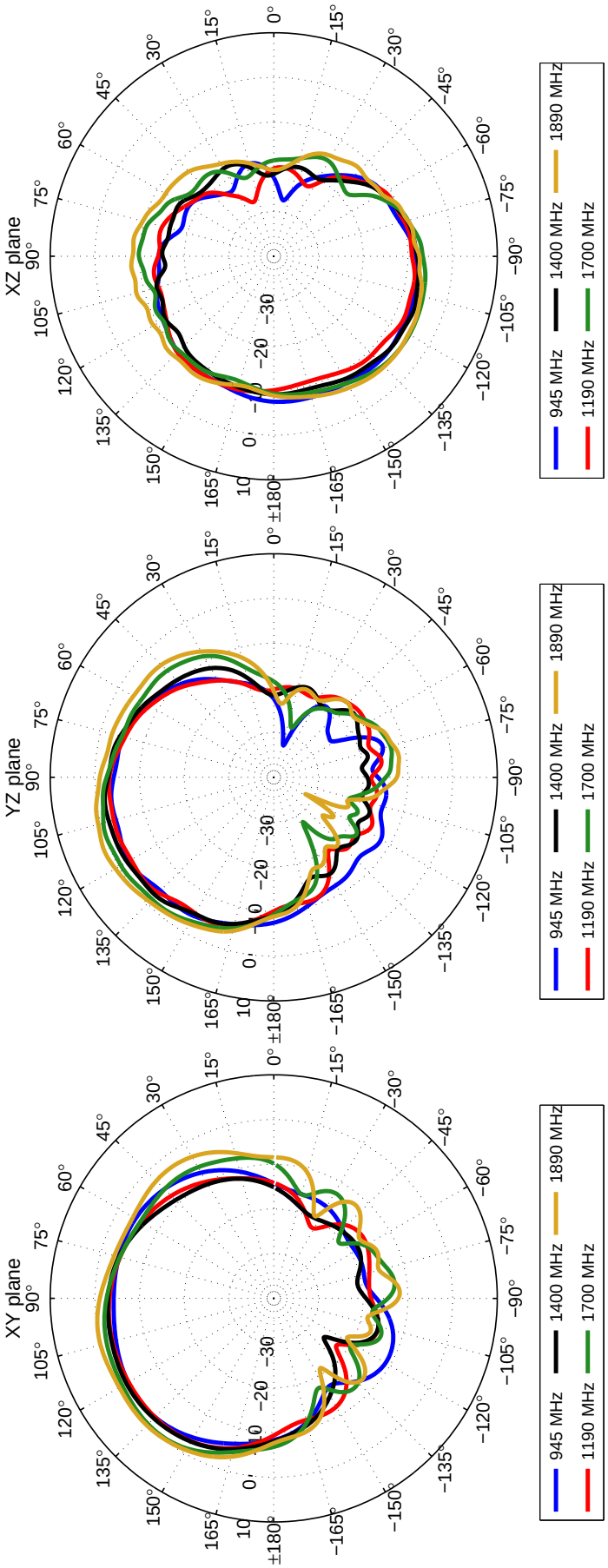

Figure 92: Eartha. Radiation patterns Band 2: 945 MHz - 1890 MHz.

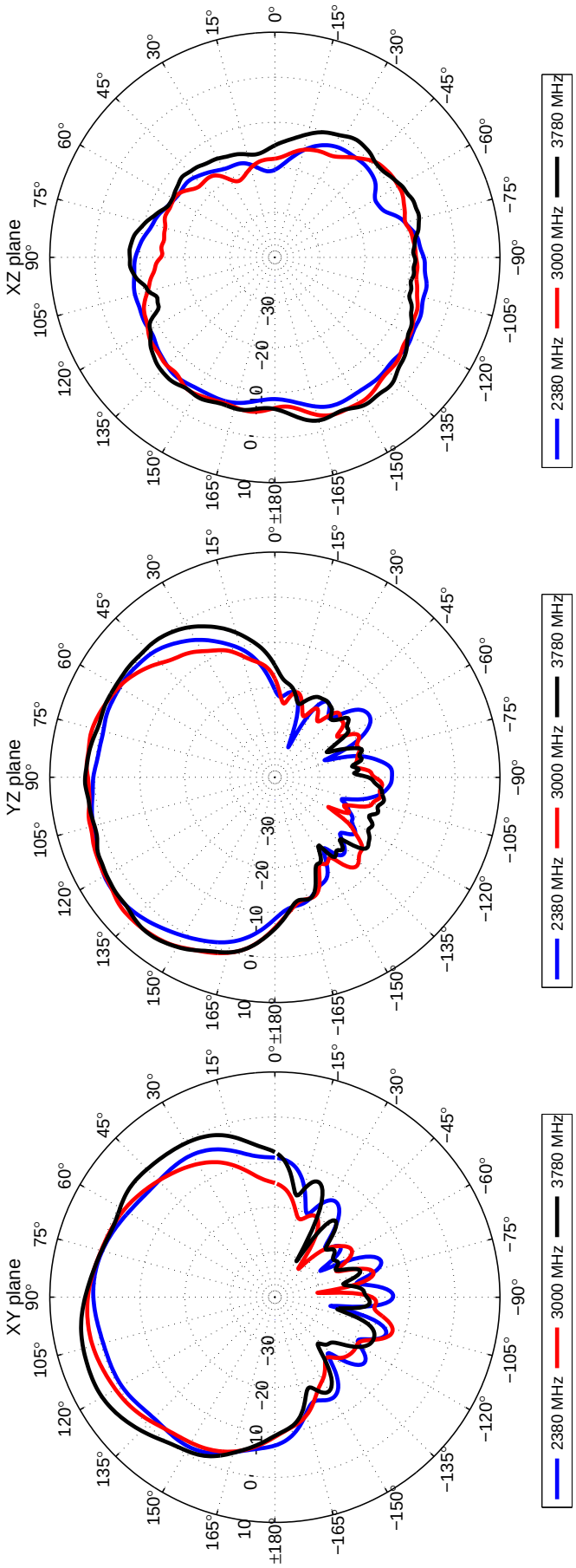

Figure 93: Eartha. Radiation patterns Band 3: 2380 MHz - 3780 MHz.

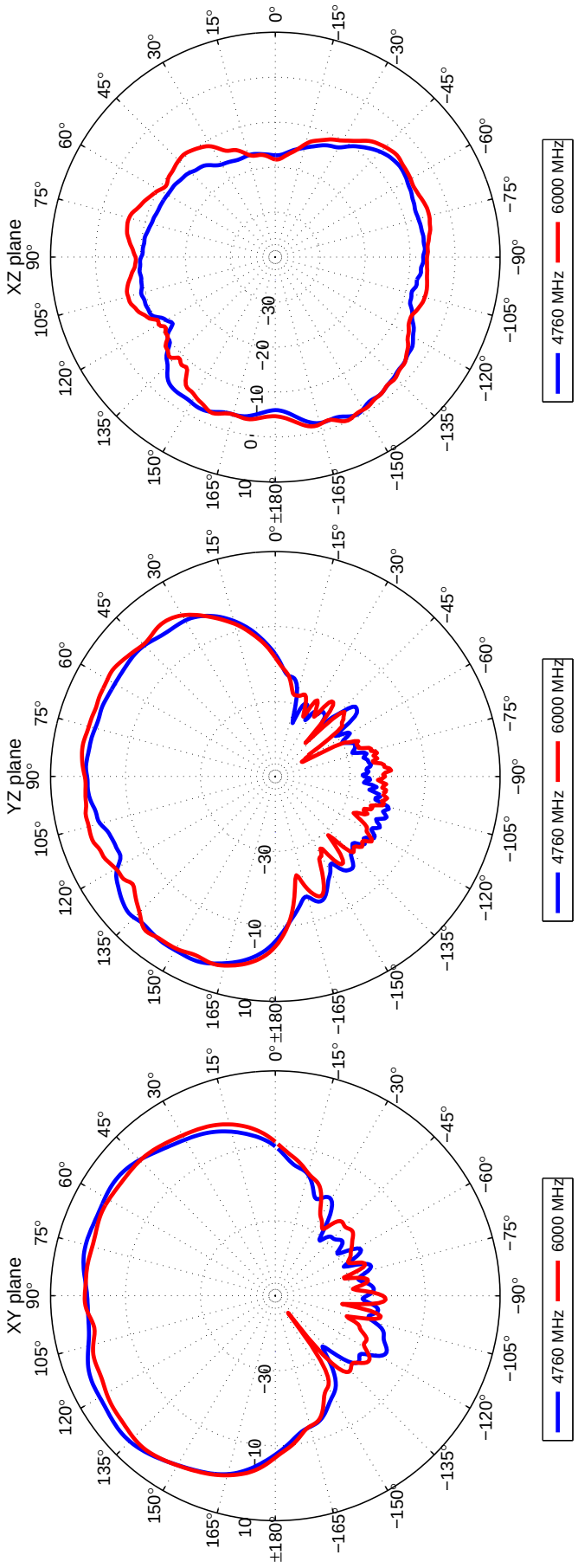

Figure 94: Eartha. Radiation patterns Band 4: 4670 MHz - 6000 MHz.

B.3 Radiation patterns for a medium user 1.75 m and 70 kg Duke Virtual Population Model

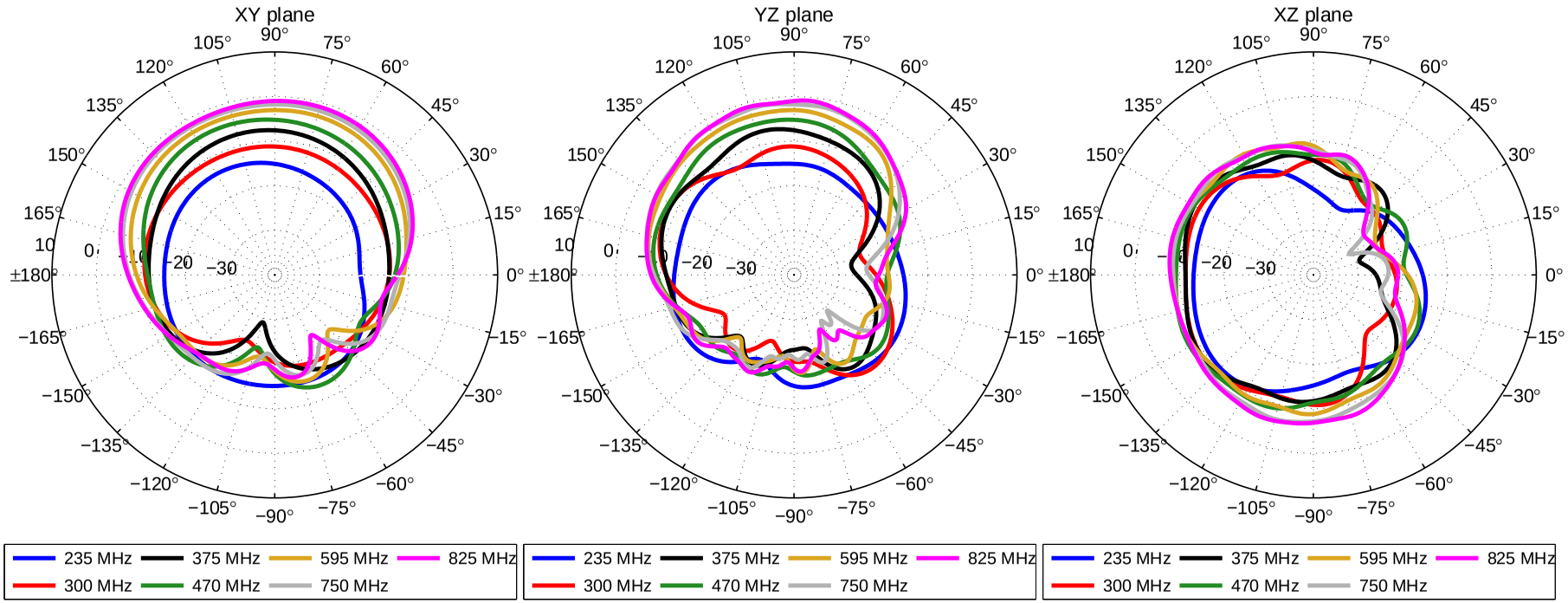

Figure 95: Duke. Radiation patterns Band 1: 235 MHz - 825 MHz.

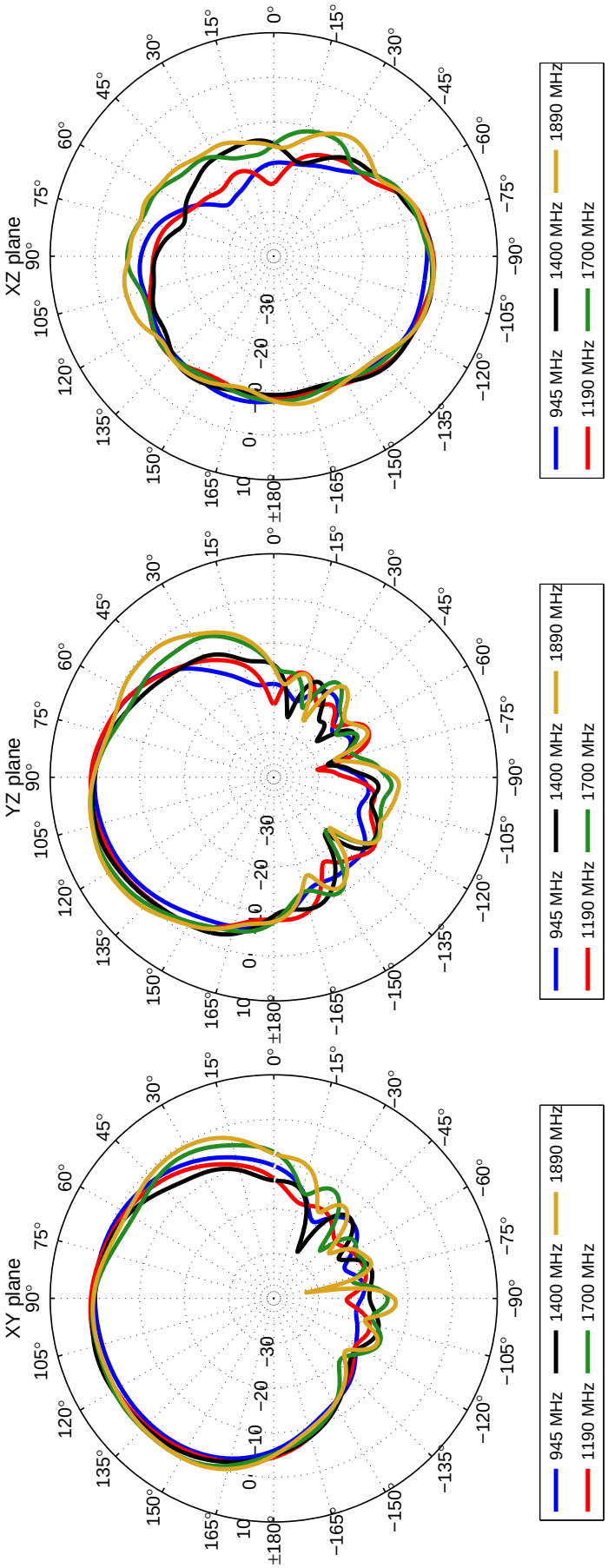

Figure 96: Duke. Radiation patterns Band 2: 945 MHz - 1890 MHz.

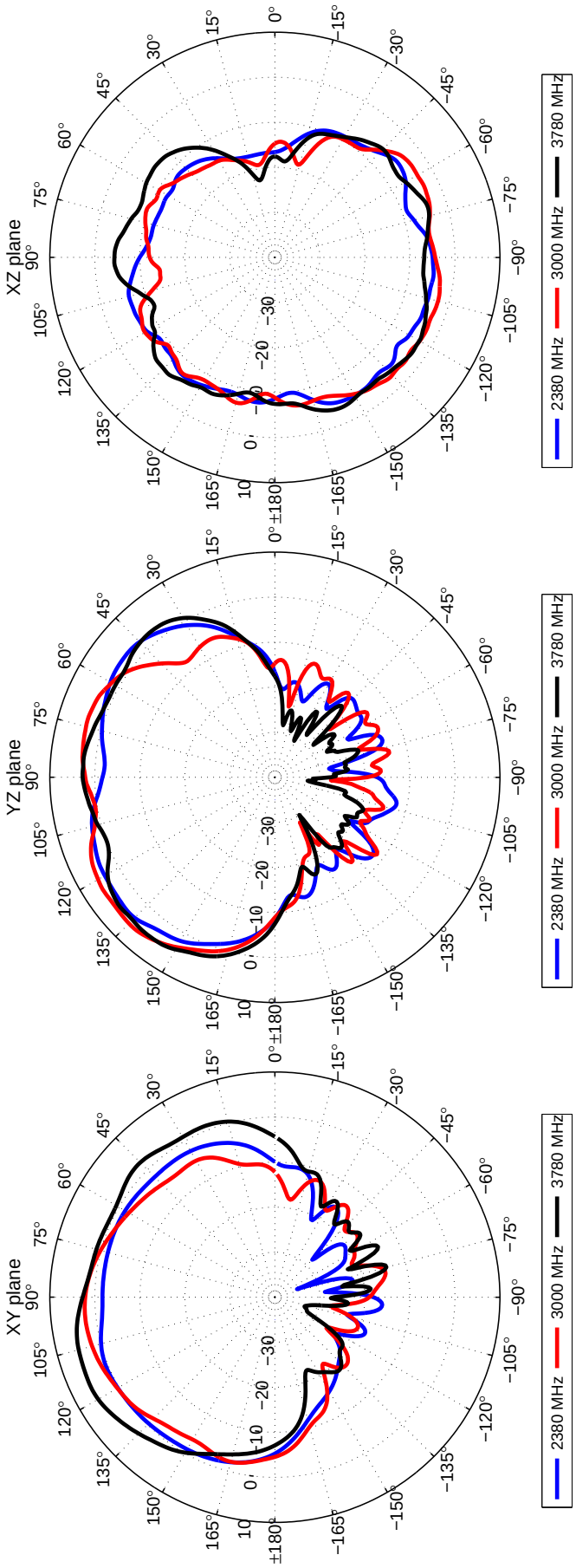

Figure 97: Duke. Radiation patterns Band 3: 2380 MHz - 3780 MHz.

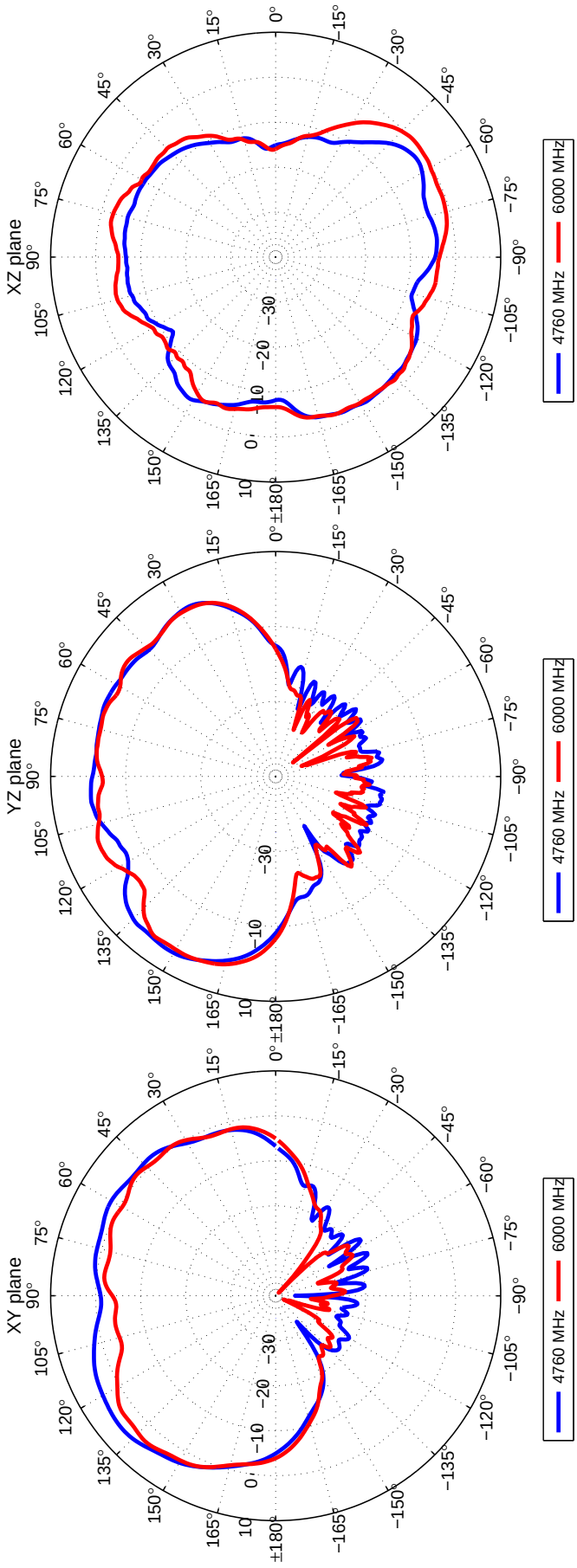

Figure 98: Duke. Radiation patterns Band 4: 4670 MHz - 6000 MHz.

B.4 Radiation patterns for a large user 1.78 m and 120 kg Fats Virtual Population Model

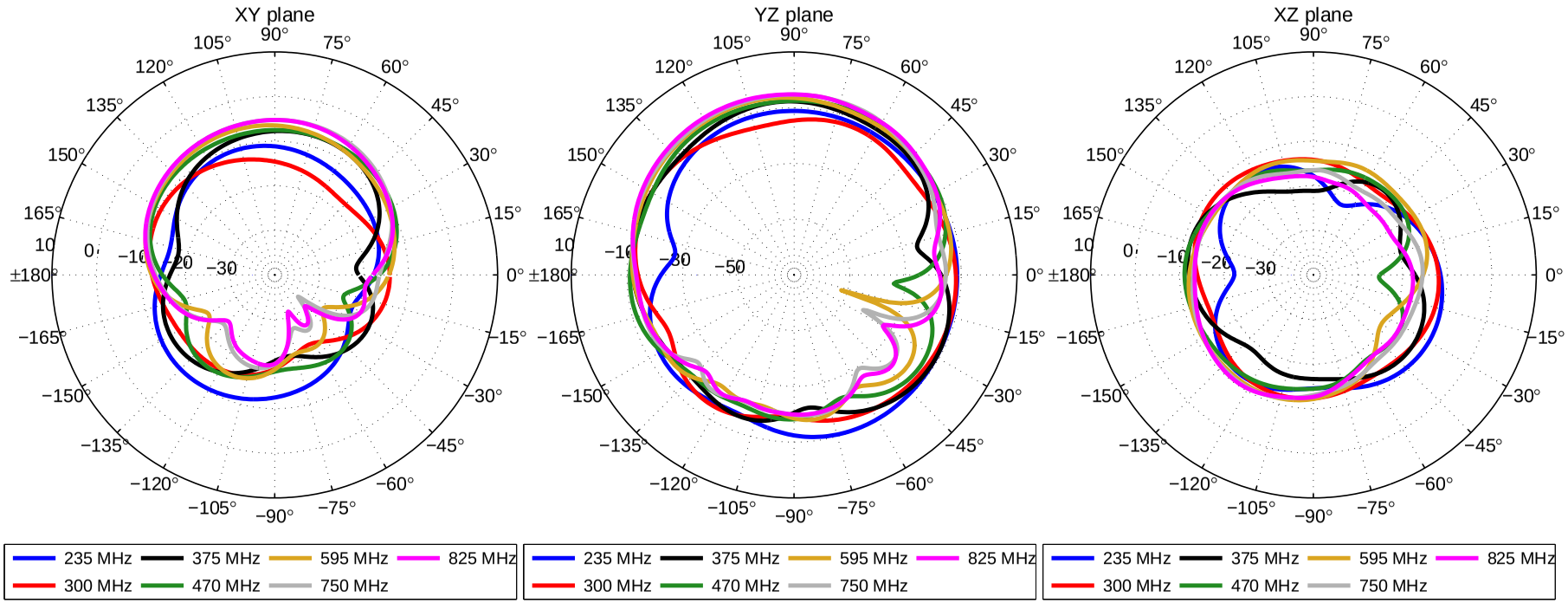

Figure 99: Fats: Radiation patterns Band 1: 235 MHz - 825 MHz.

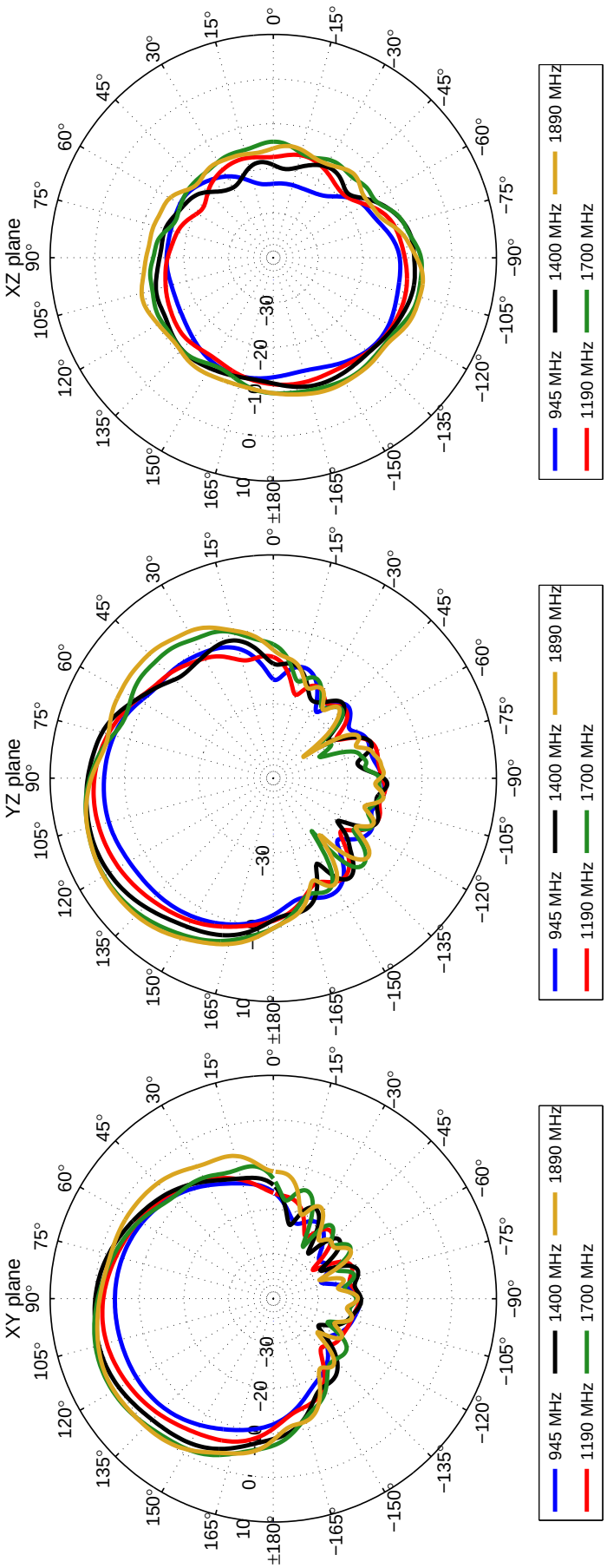

Figure 100: Fats. Radiation patterns Band 2: 945 MHz - 1890 MHz.

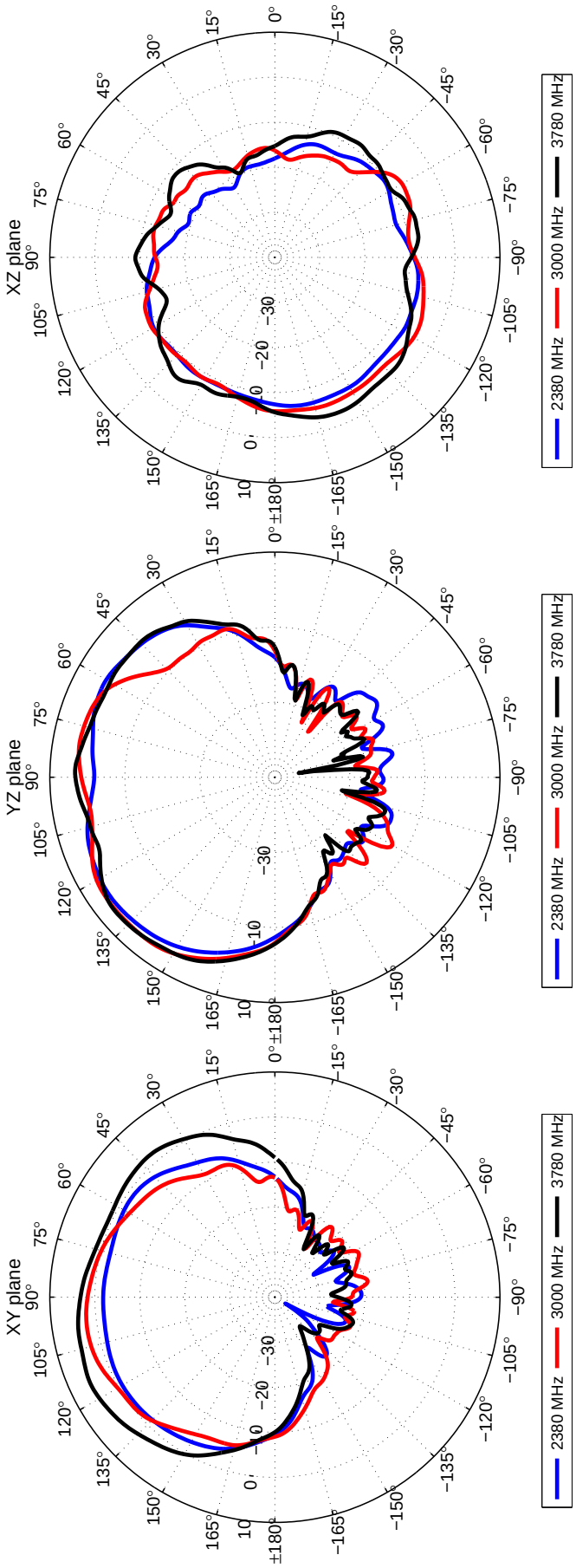

Figure 101: Fats. Radiation patterns Band 3: 2380 MHz - 3780 MHz.

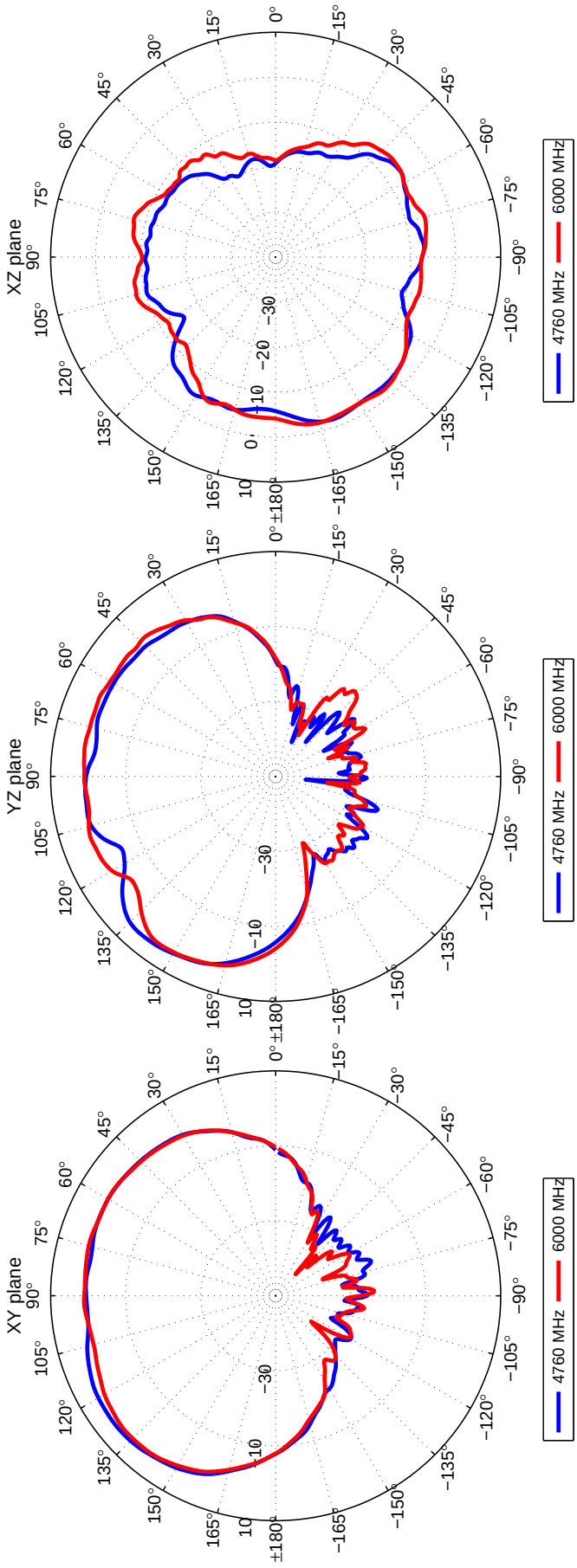

Figure 102: Fats. Radiation patterns Band 4: 4670 MHz - 6000 MHz.

B.5 Radiation patterns per frequency, for all users, compared to device in free space

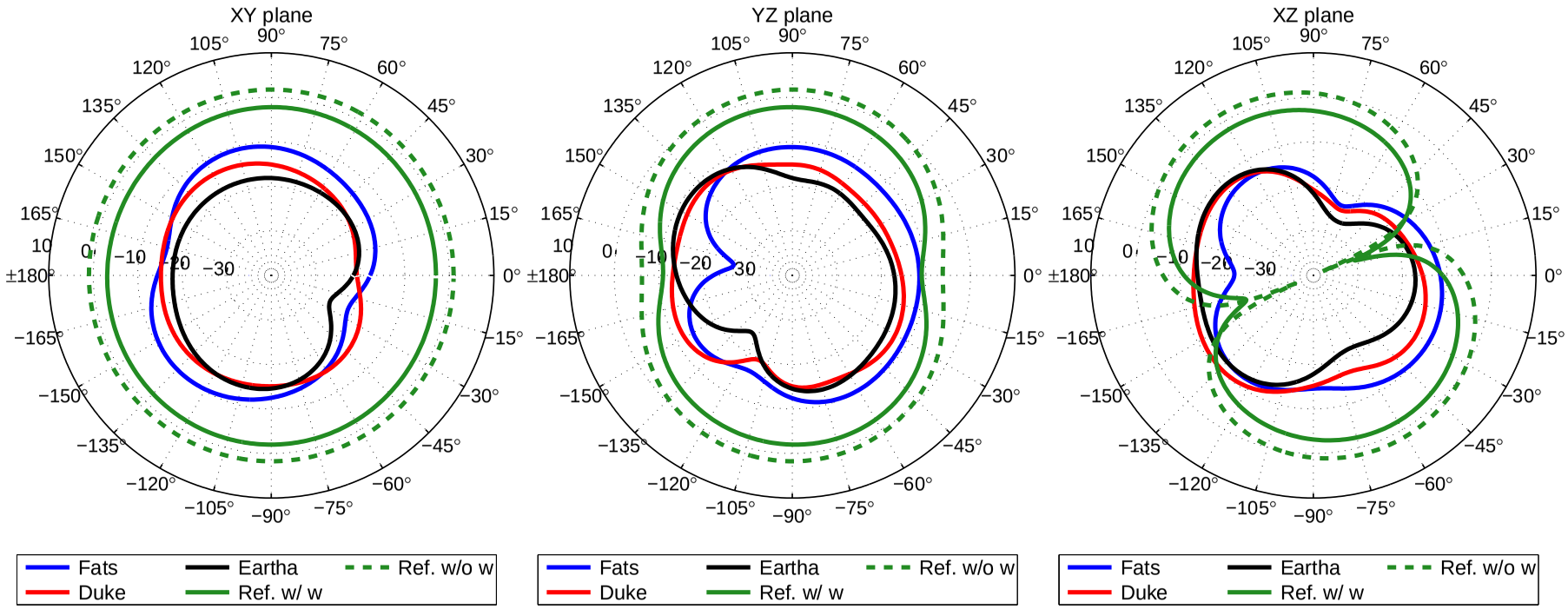

Figure 103: All Models compared to reference – bodypack monopole with wire (Ref. w/ w) and bodypack monopole without wire (Ref. w/o w)– at 235 MHz.

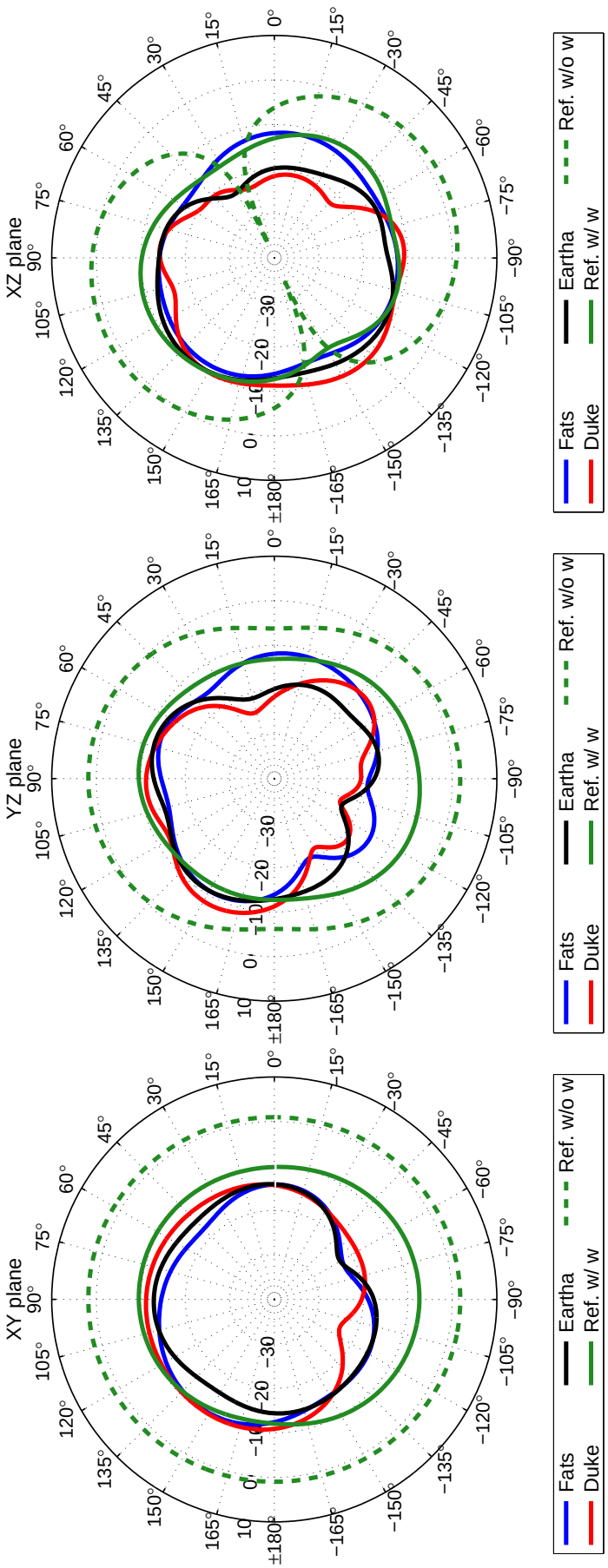

Figure 104: All Models compared to reference – bodypack monopole with wire (Ref. w/ w) and bodypack monopole without wire (Ref. w/o w)– at 300 MHz.

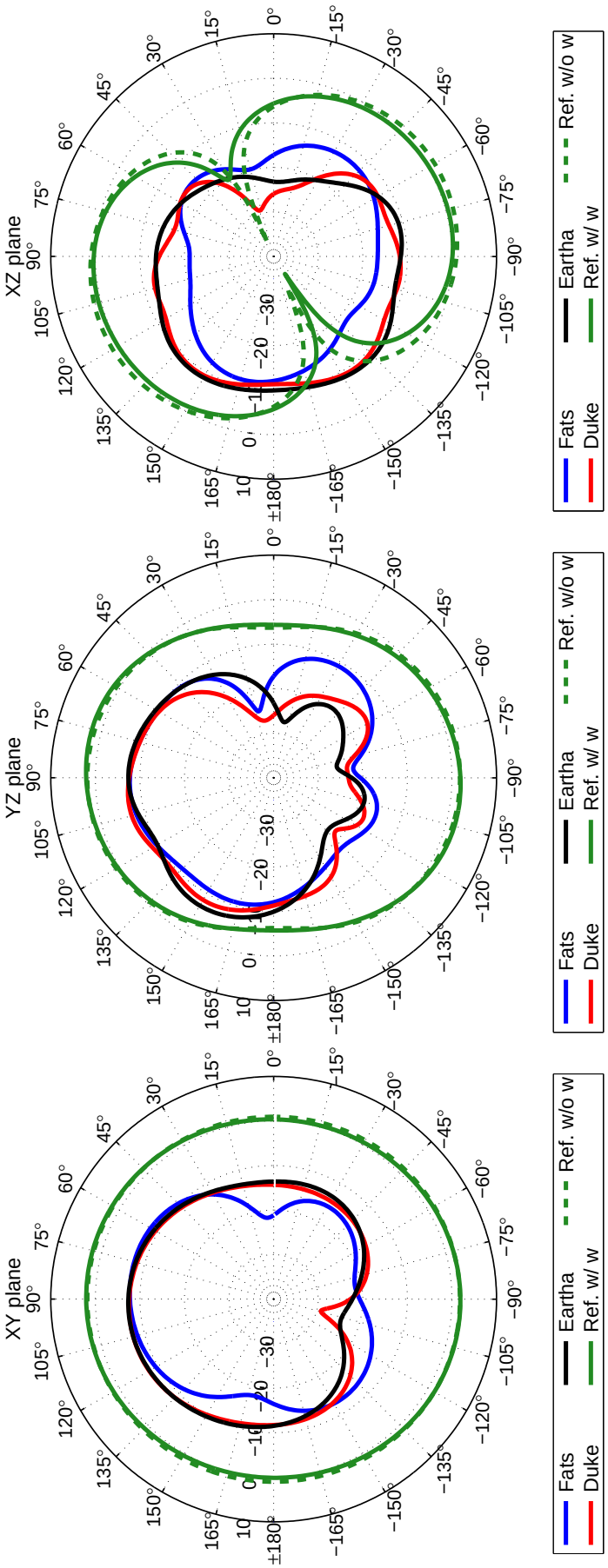

Figure 105: All Models compared to reference – bodypack monopole with wire (Ref. w/ w) and bodypack monopole without wire (Ref. w/o w)– at 375 MHz.

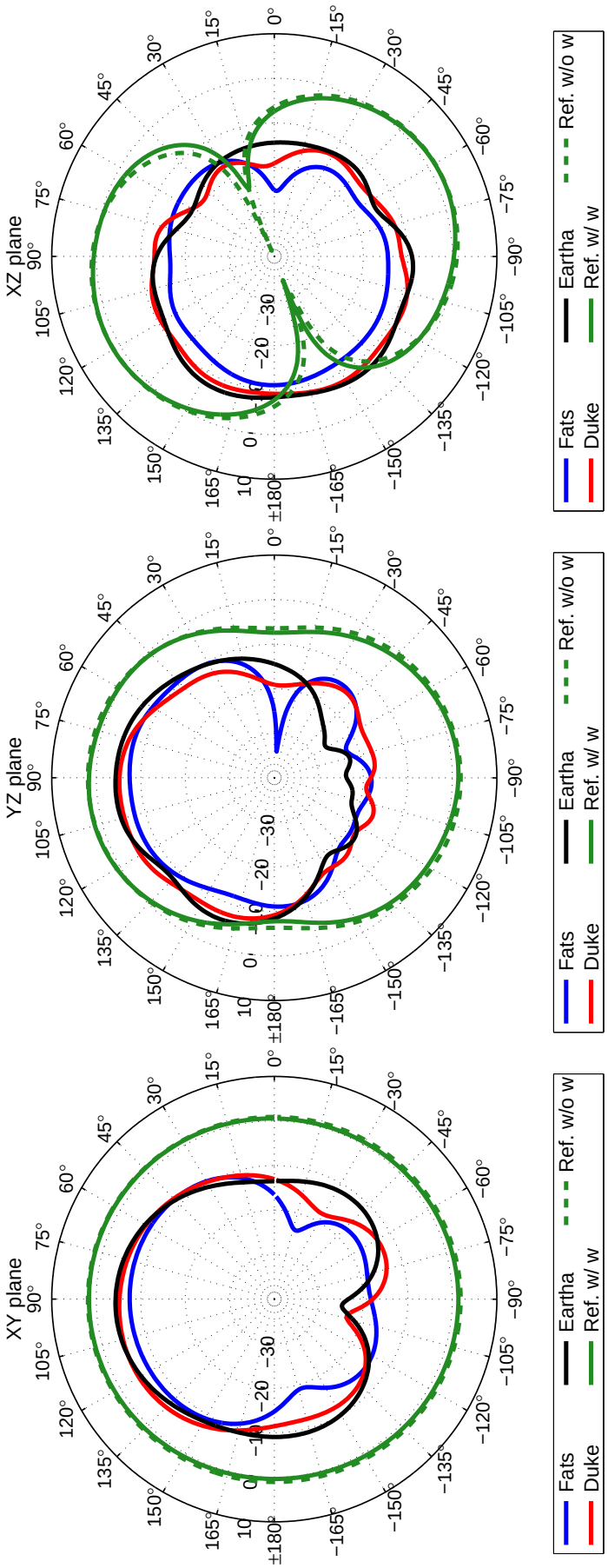

Figure 106: All Models compared to reference – bodypack monopole with wire (Ref. w/ w) and bodypack monopole without wire (Ref. w/o w)– at 470 MHz.

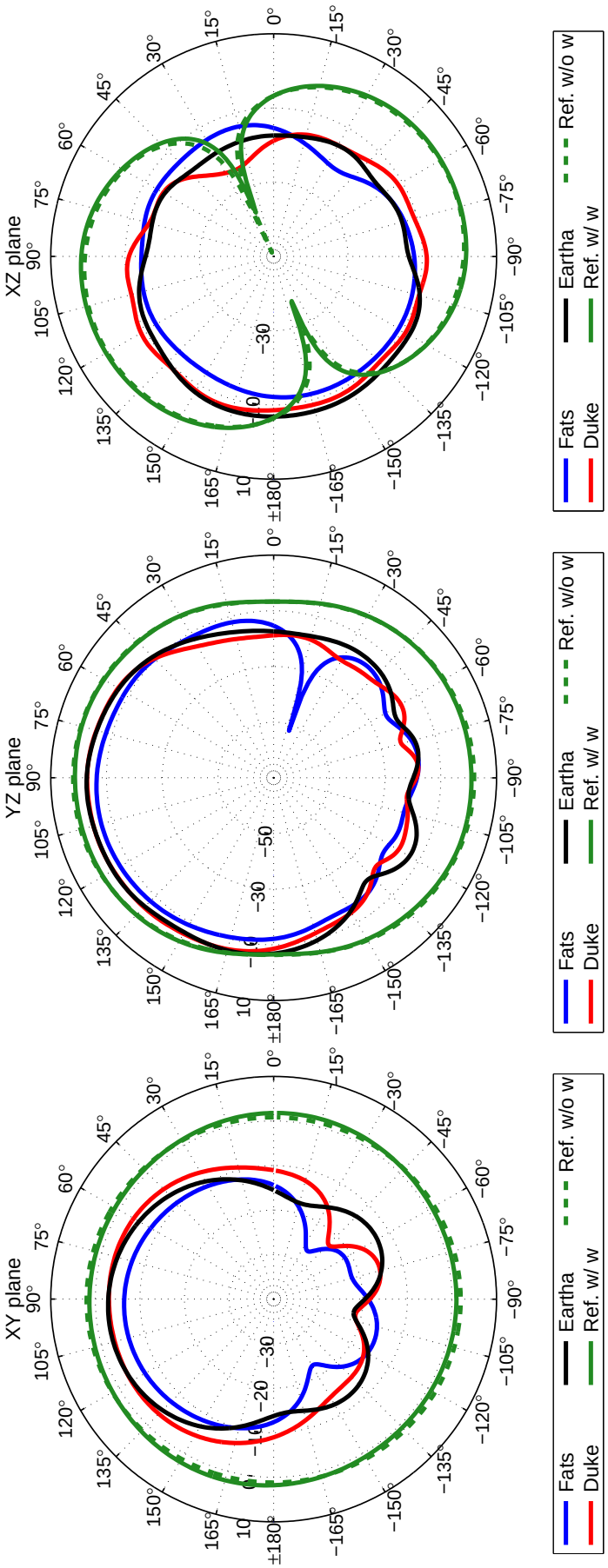

Figure 107: All Models compared to reference – bodypack monopole with wire (Ref. w/ w) and bodypack monopole without wire (Ref. w/o w)– at 595 MHz.

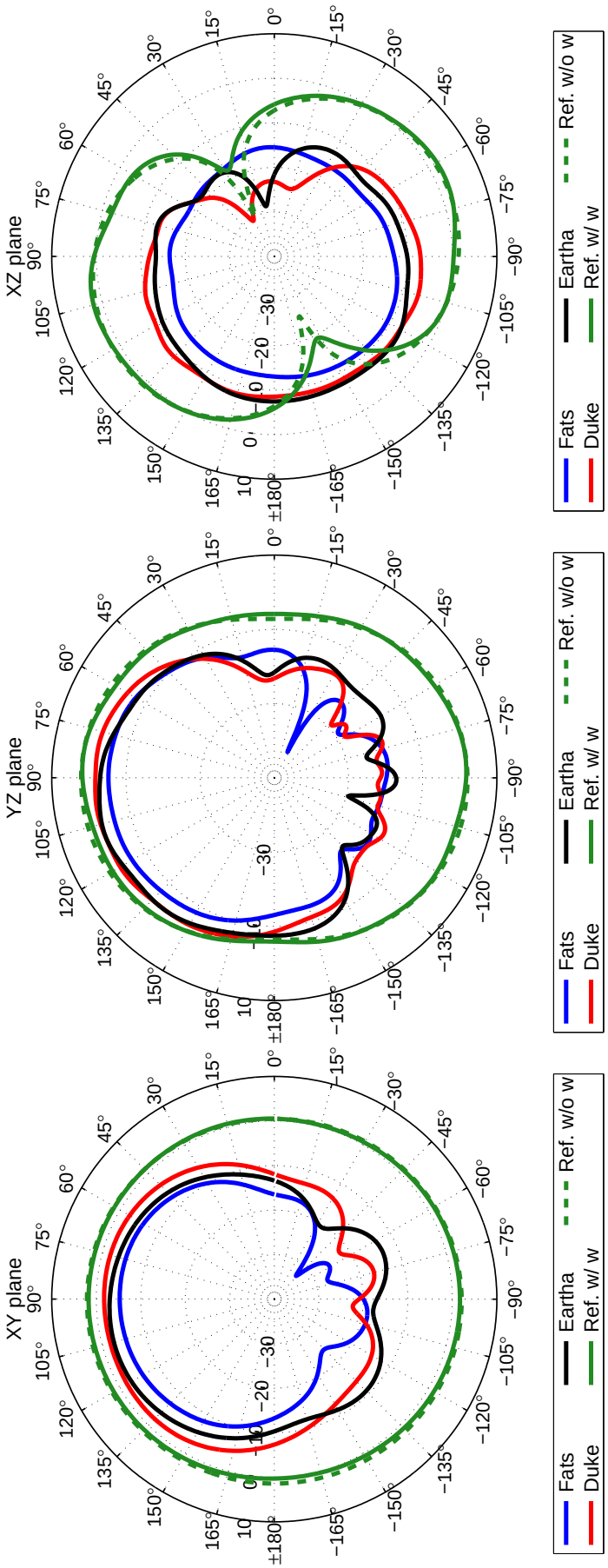

Figure 108: All Models compared to reference – bodypack monopole with wire (Ref. w/ w) and bodypack monopole without wire (Ref. w/o w)– at 750 MHz.

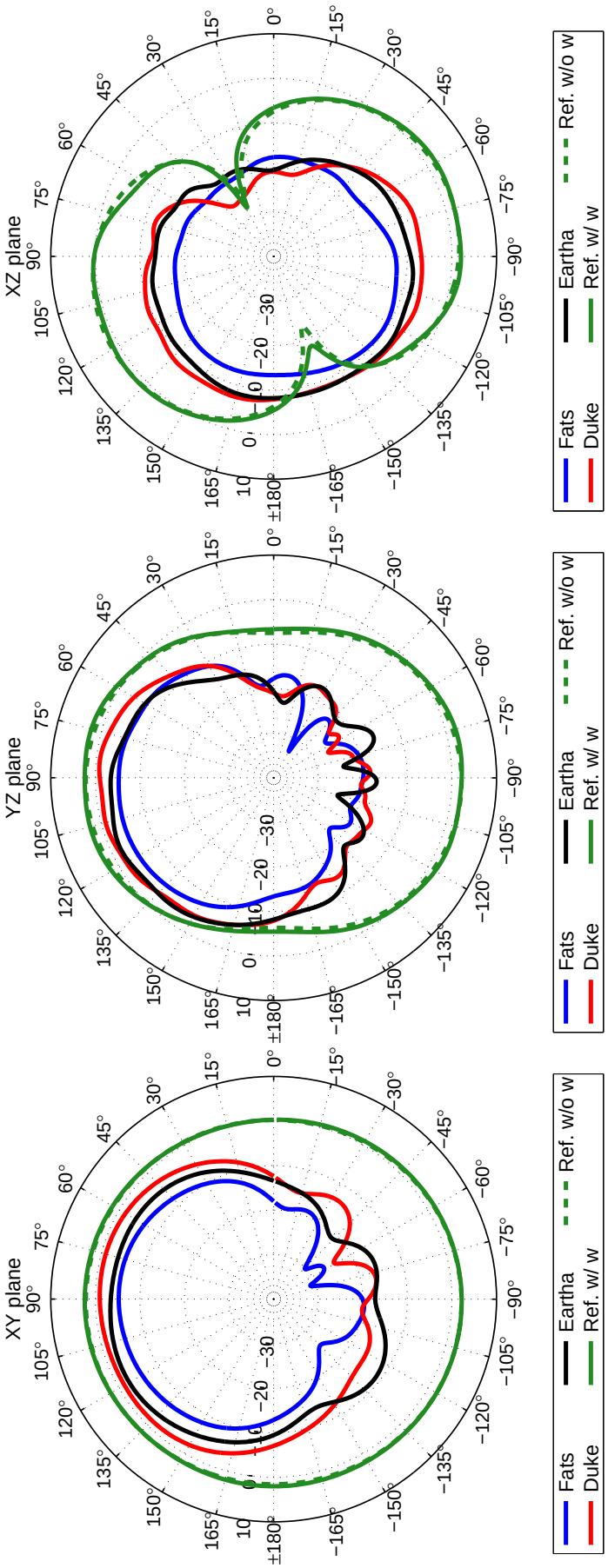

Figure 109: All Models compared to reference – bodypack monopole with wire (Ref. w/ w) and bodypack monopole without wire (Ref. w/o w)– at 825 MHz.

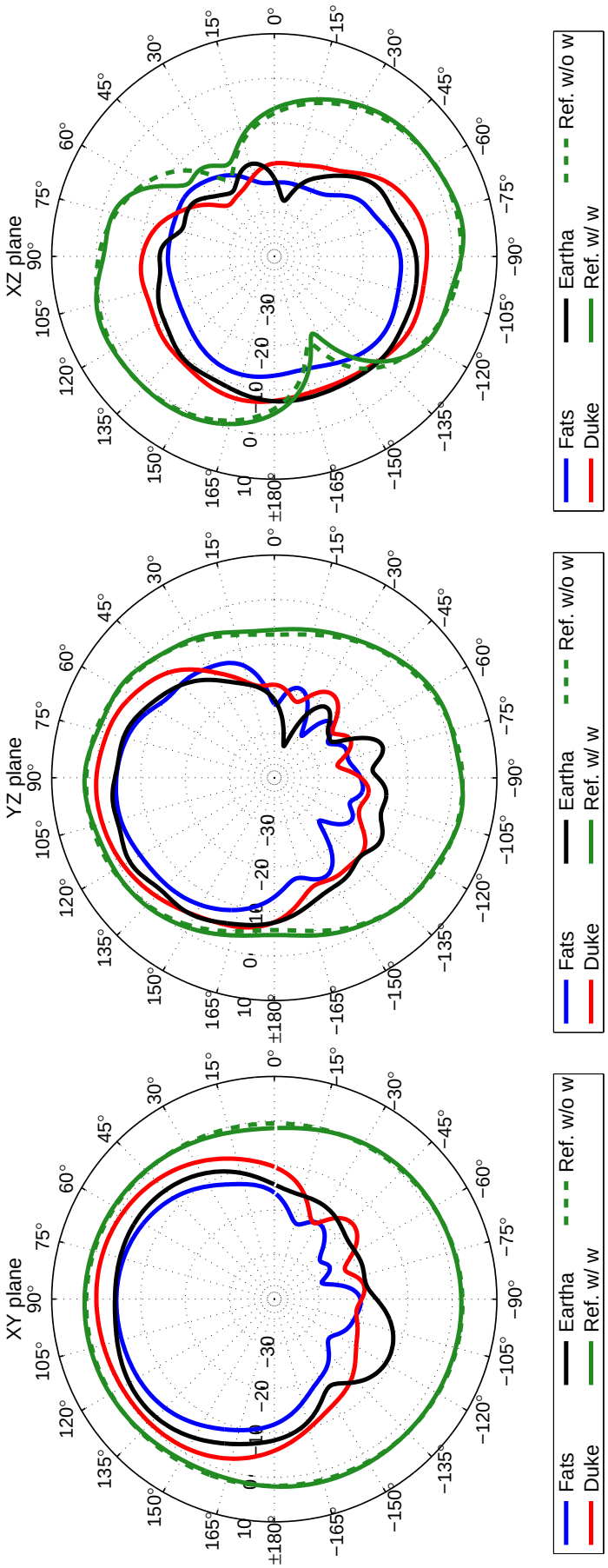

Figure 110: All Models compared to reference – bodypack monopole with wire (Ref. w/ w) and bodypack monopole without wire (Ref. w/o w)– at 945 MHz.

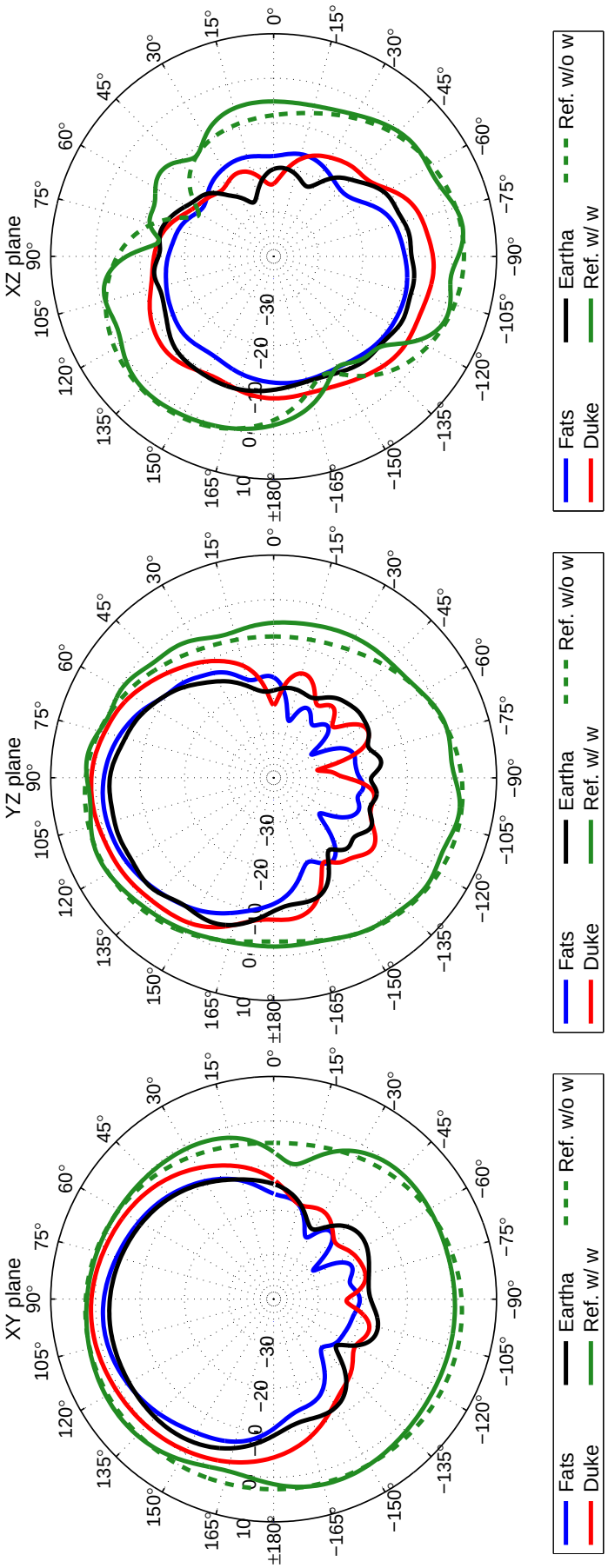

Figure 111: All Models compared to reference – bodypack monopole with wire (Ref. w/ w) and bodypack monopole without wire (Ref. w/o w)– at 1190 MHz.

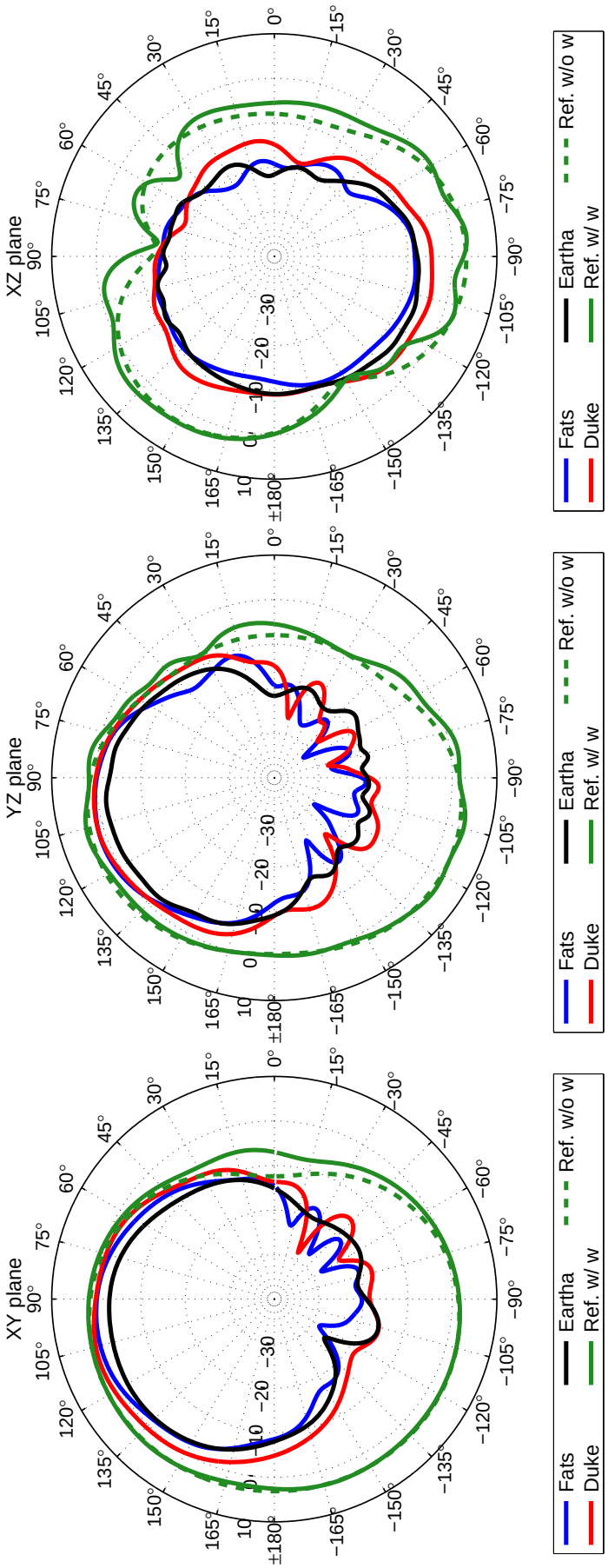

Figure 112: All Models compared to reference – bodypack monopole with wire (Ref. w/ w) and bodypack monopole without wire (Ref. w/o w)– at 1400 MHz.

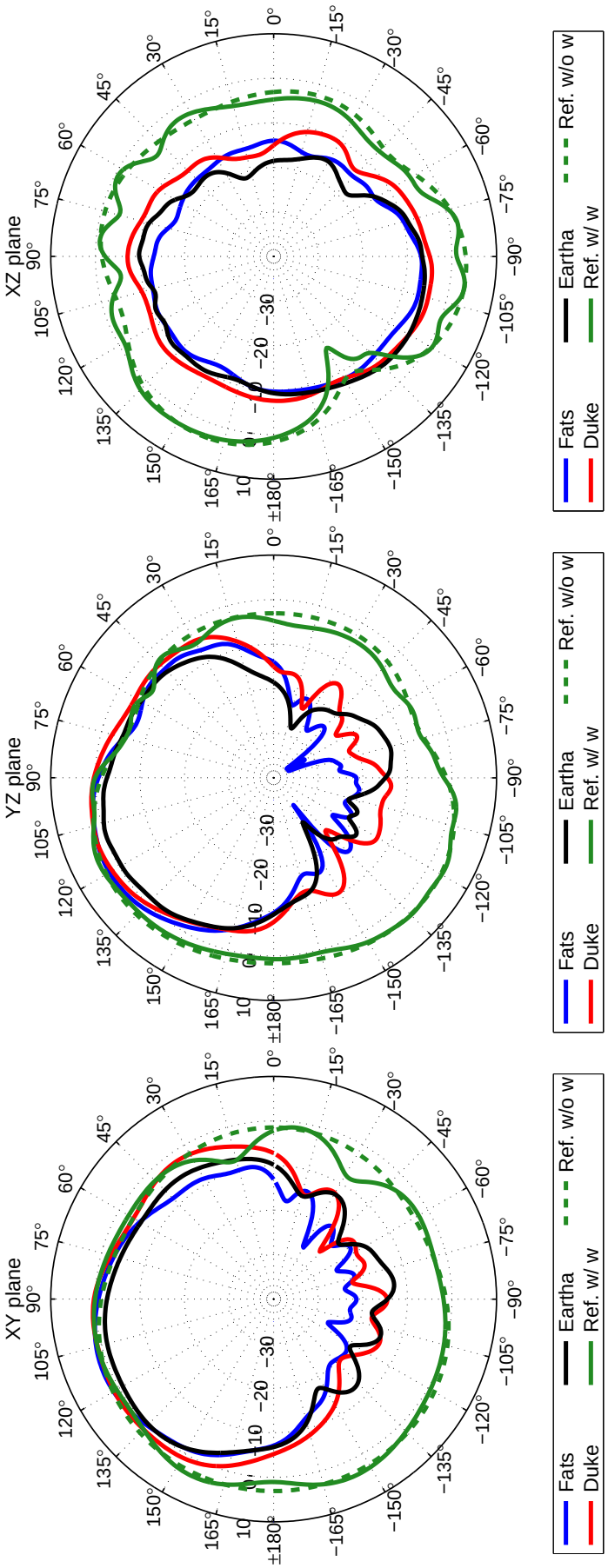

Figure 113: All Models compared to reference – bodypack monopole with wire (Ref. w/ w) and bodypack monopole without wire (Ref. w/o w)– at 1700 MHz.

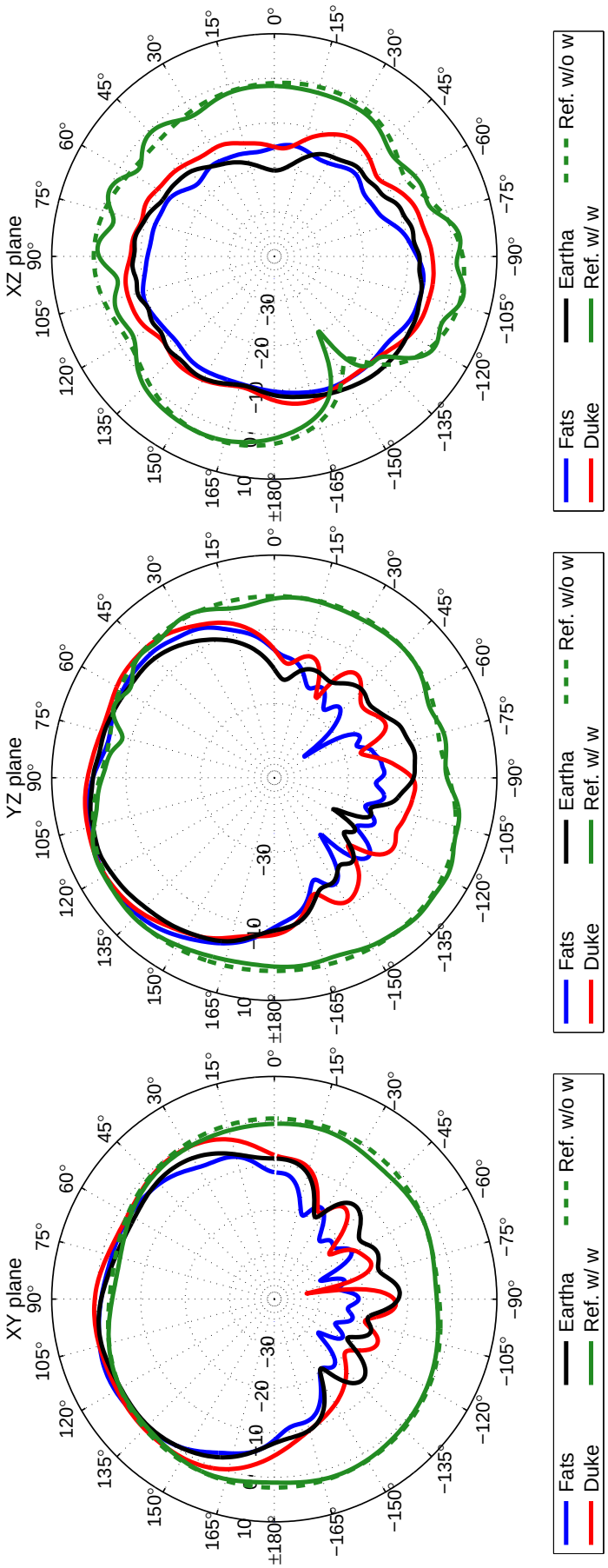

Figure 114: All Models compared to reference – bodypack monopole with wire (Ref. w/ w) and bodypack monopole without wire (Ref. w/o w)– at 1890 MHz.

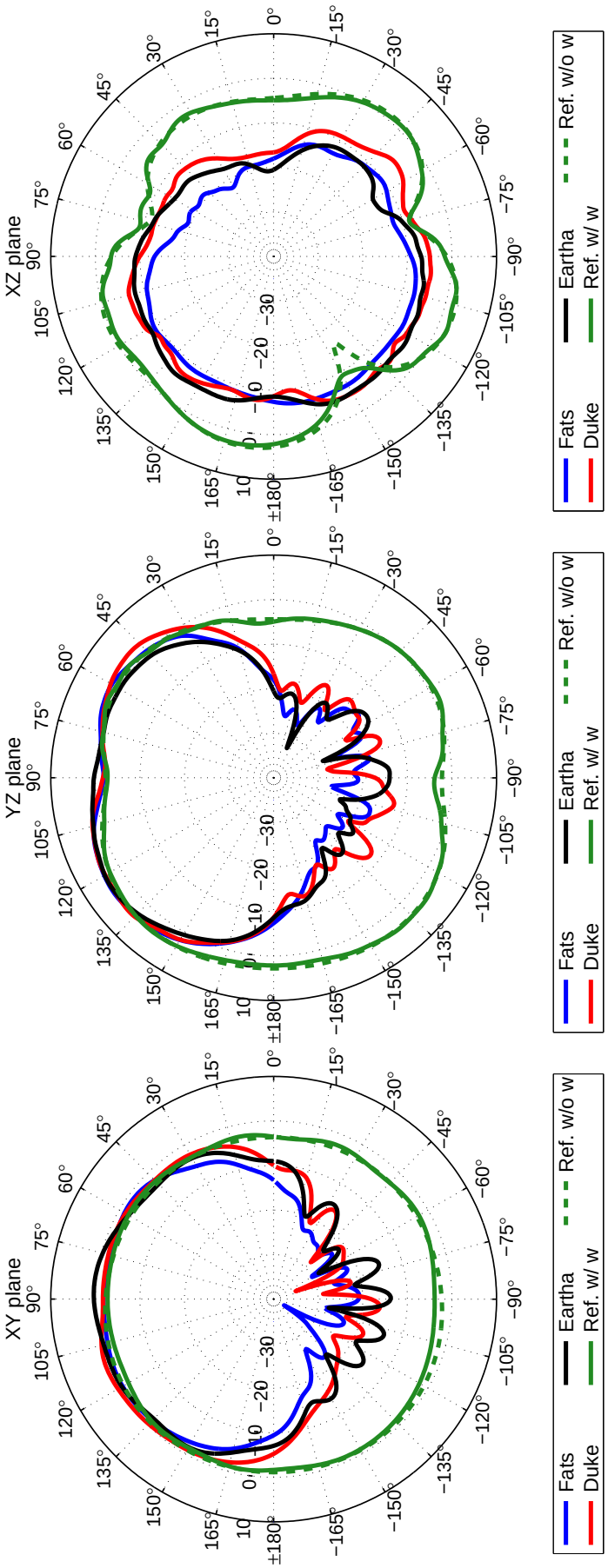

Figure 115: All Models compared to reference – bodypack monopole with wire (Ref. w/ w) and bodypack monopole without wire (Ref. w/o w)– at 2380 MHz.

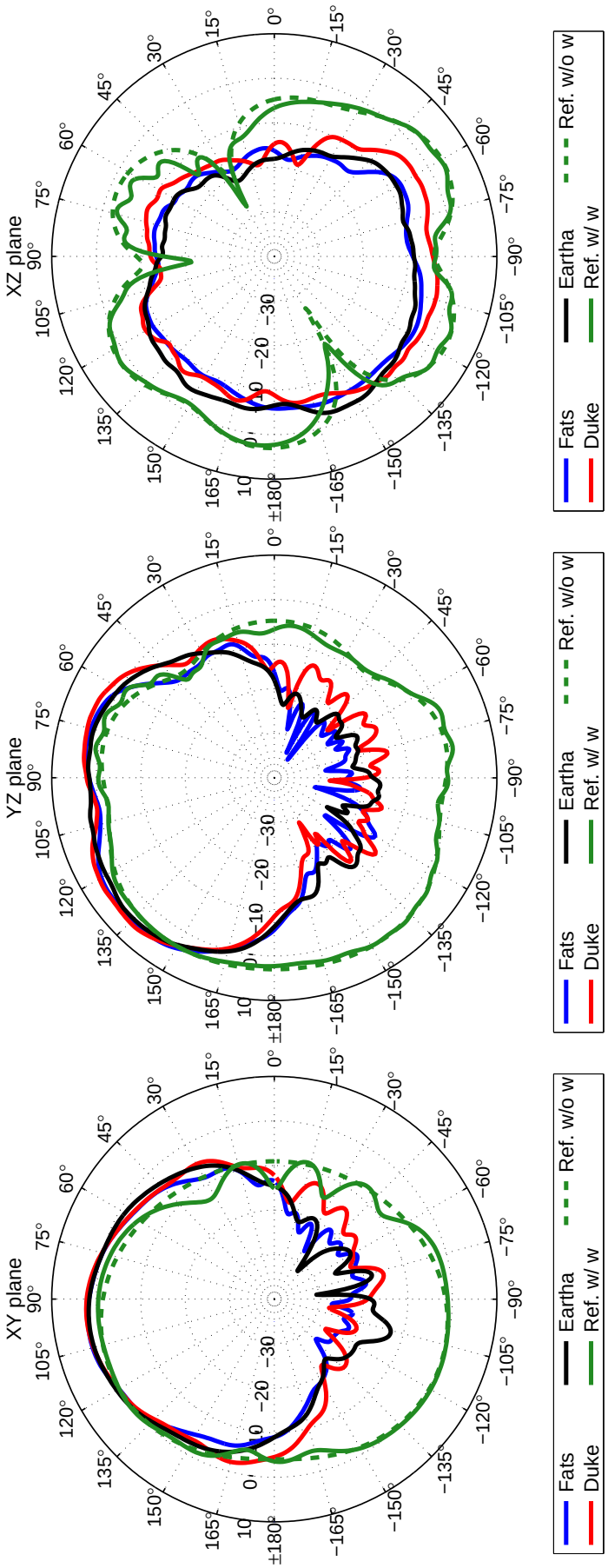

Figure 116: All Models compared to reference – bodypack monopole with wire (Ref. w/ w) and bodypack monopole without wire (Ref. w/o w)– at 3000 MHz.

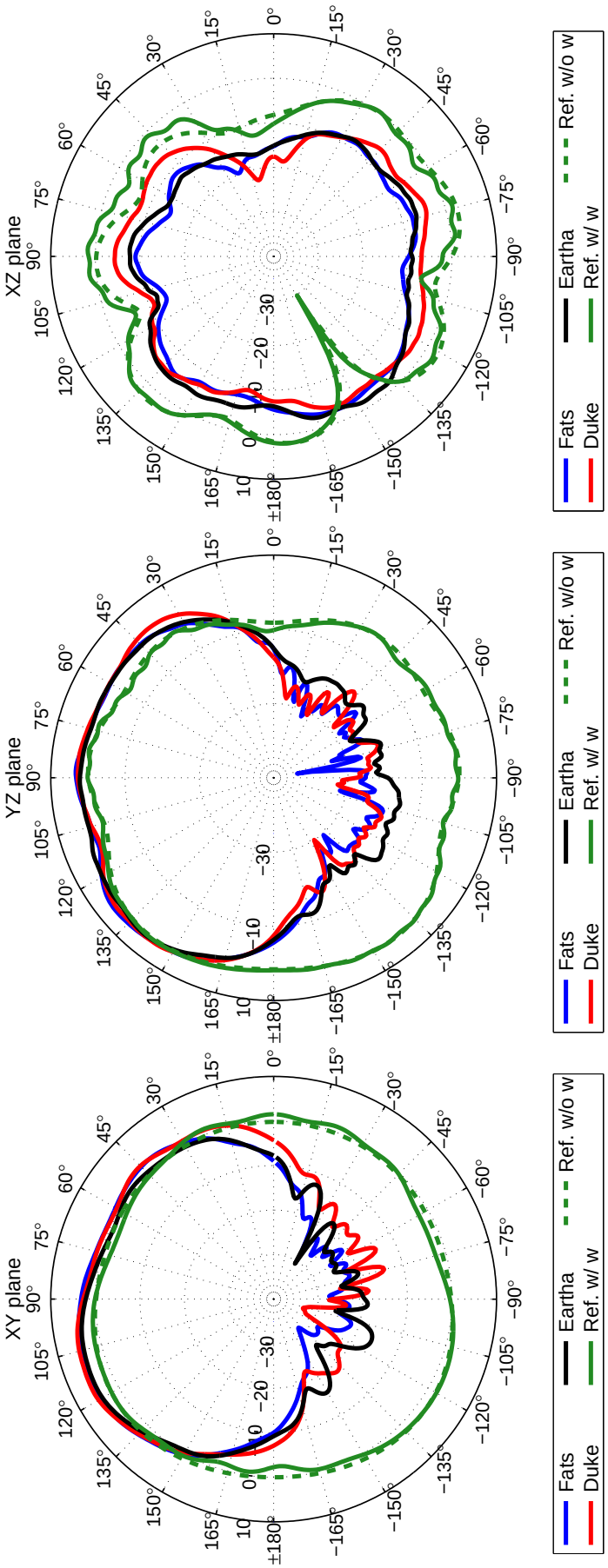

Figure 117: All Models compared to reference – bodypack monopole with wire (Ref. w/ w) and bodypack monopole without wire (Ref. w/o w)– at 3780 MHz.

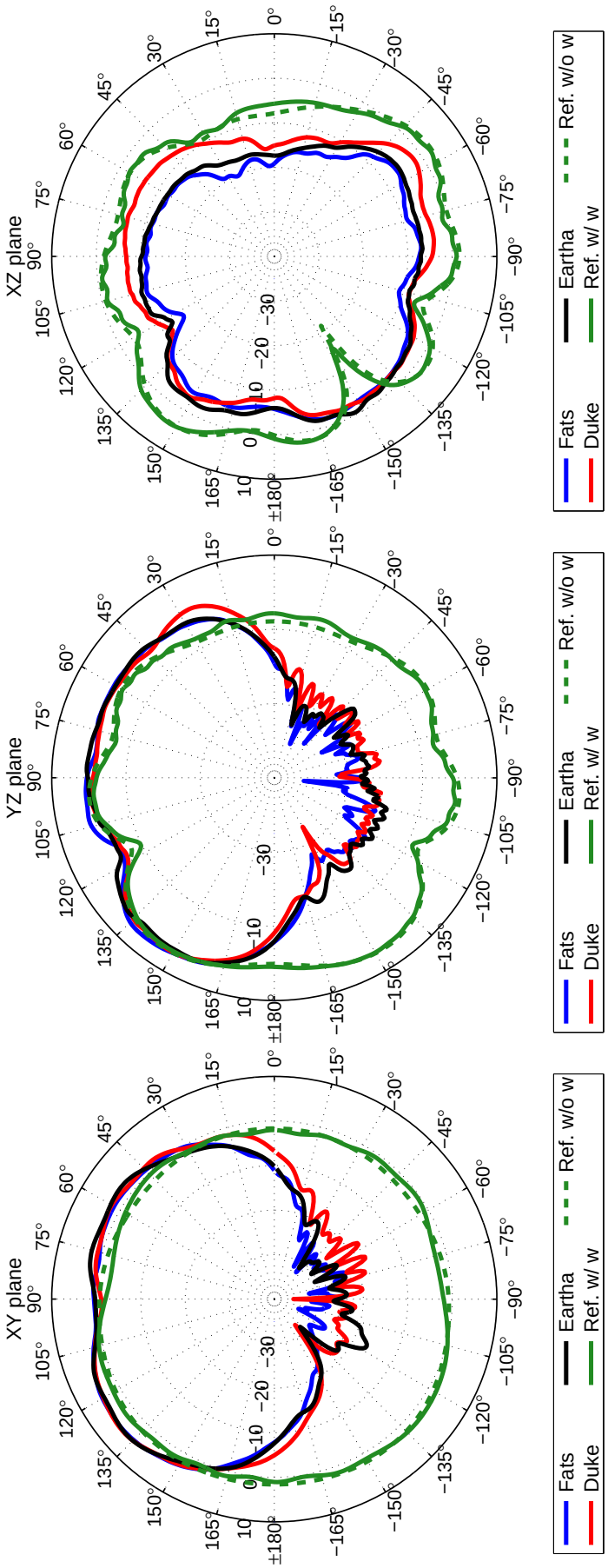

Figure 118: All Models compared to reference – bodypack monopole with wire (Ref. w/ w) and bodypack monopole without wire (Ref. w/o w)– at 4760 MHz.

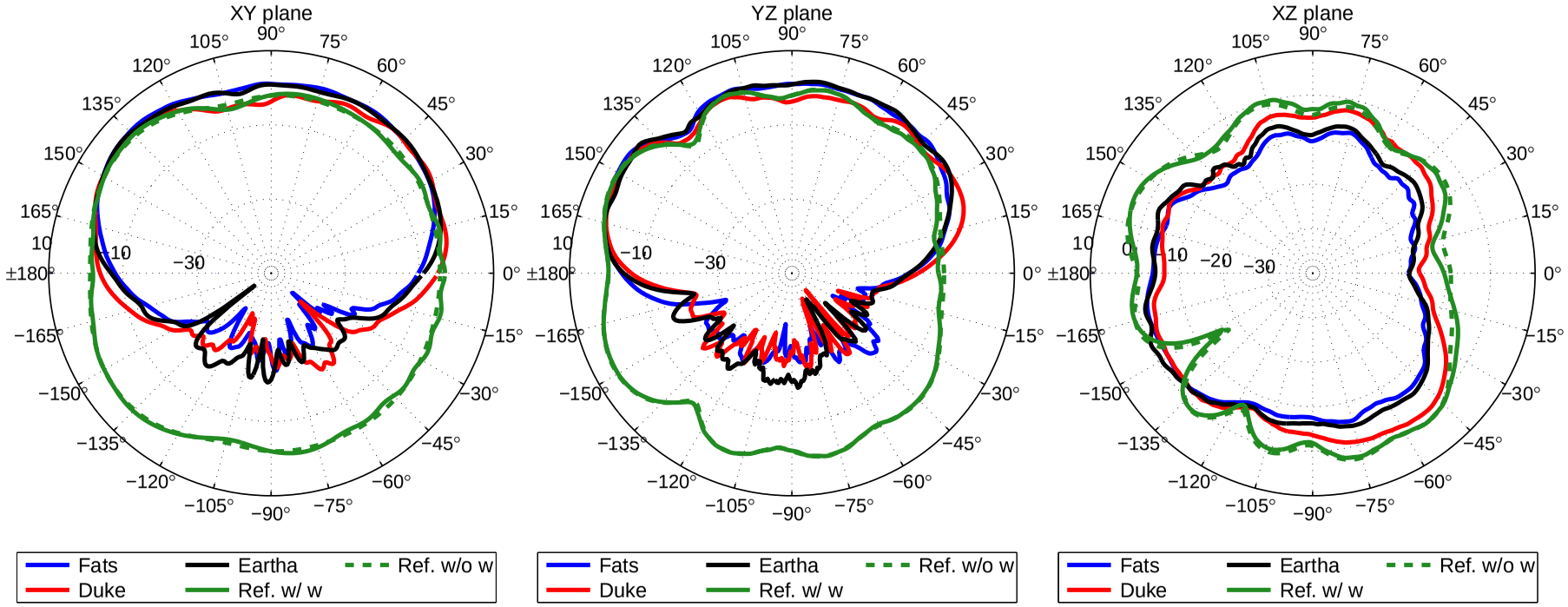

Figure 119: All Models compared to reference – bodypack monopole with wire (Ref. w/ w) and bodypack monopole without wire (Ref. w/o w)– at 6000 MHz.

B.6 Radiation patterns per frequency, for Duke, front and back position, to device in free space

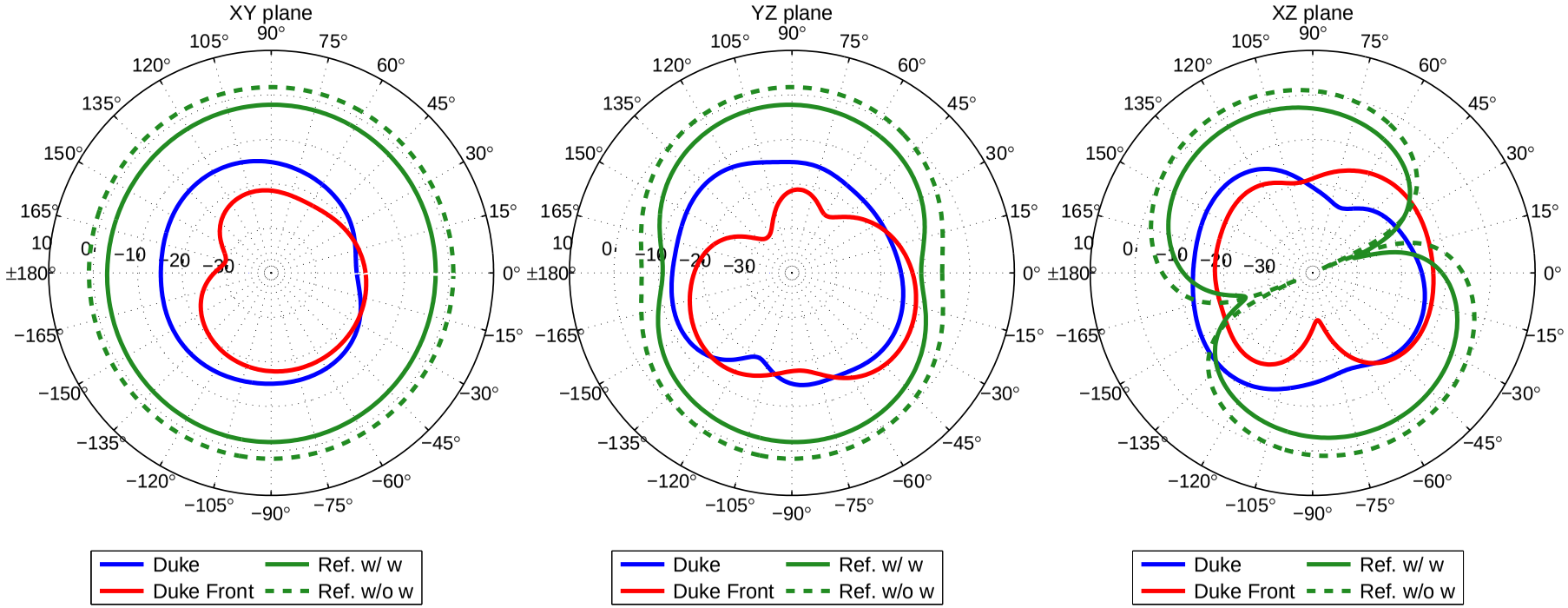

Figure 120: All Models compared to reference – bodypack monopole with wire (Ref. w/ w) and bodypack monopole without wire (Ref. w/o w)– at 235 MHz.

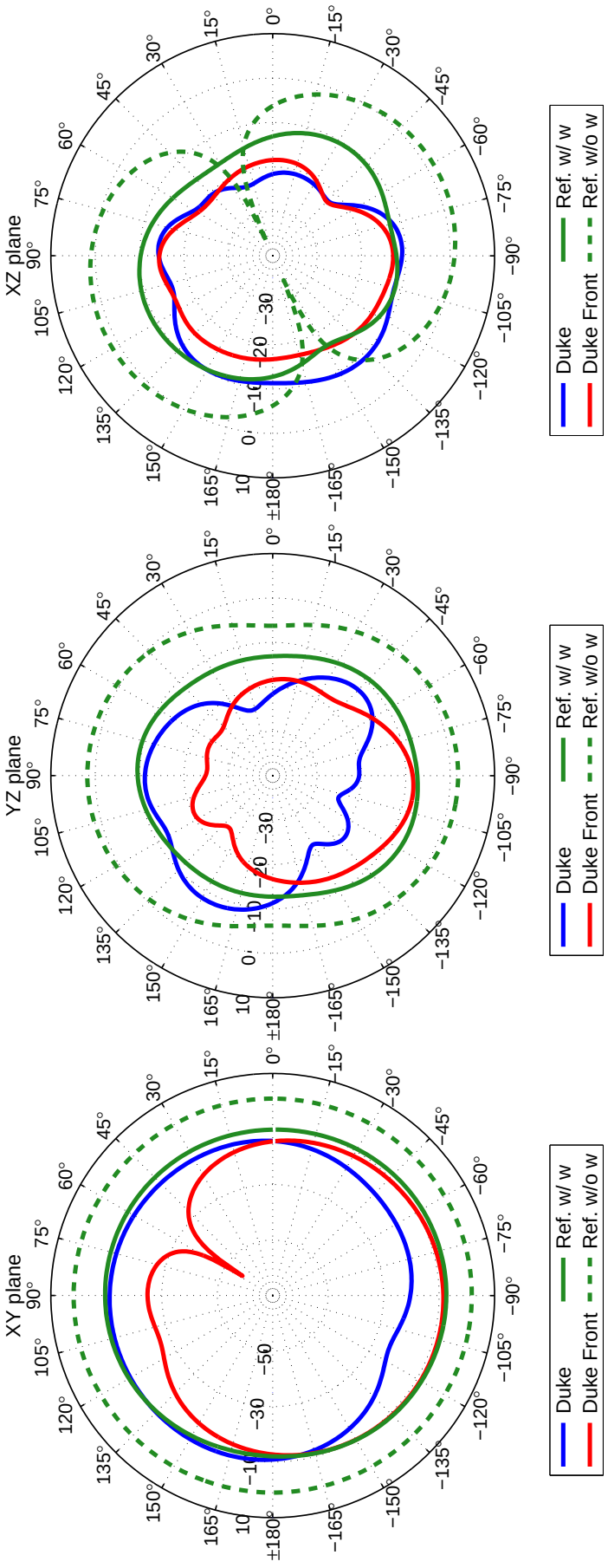

Figure 121: All Models compared to reference – bodypack monopole with wire (Ref. w/ w) and bodypack monopole without wire (Ref. w/o w)– at 300 MHz.

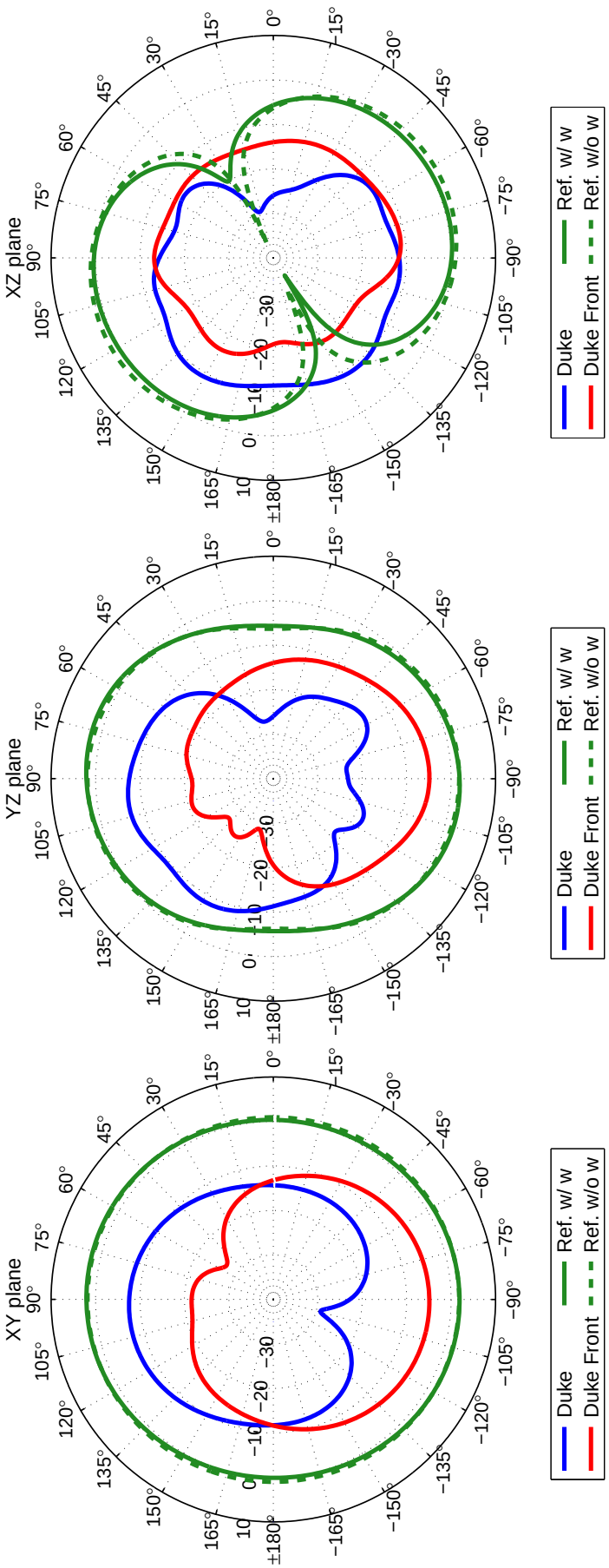

Figure 122: All Models compared to reference – bodypack monopole with wire (Ref. w/ w) and bodypack monopole without wire (Ref. w/o w)– at 375 MHz.

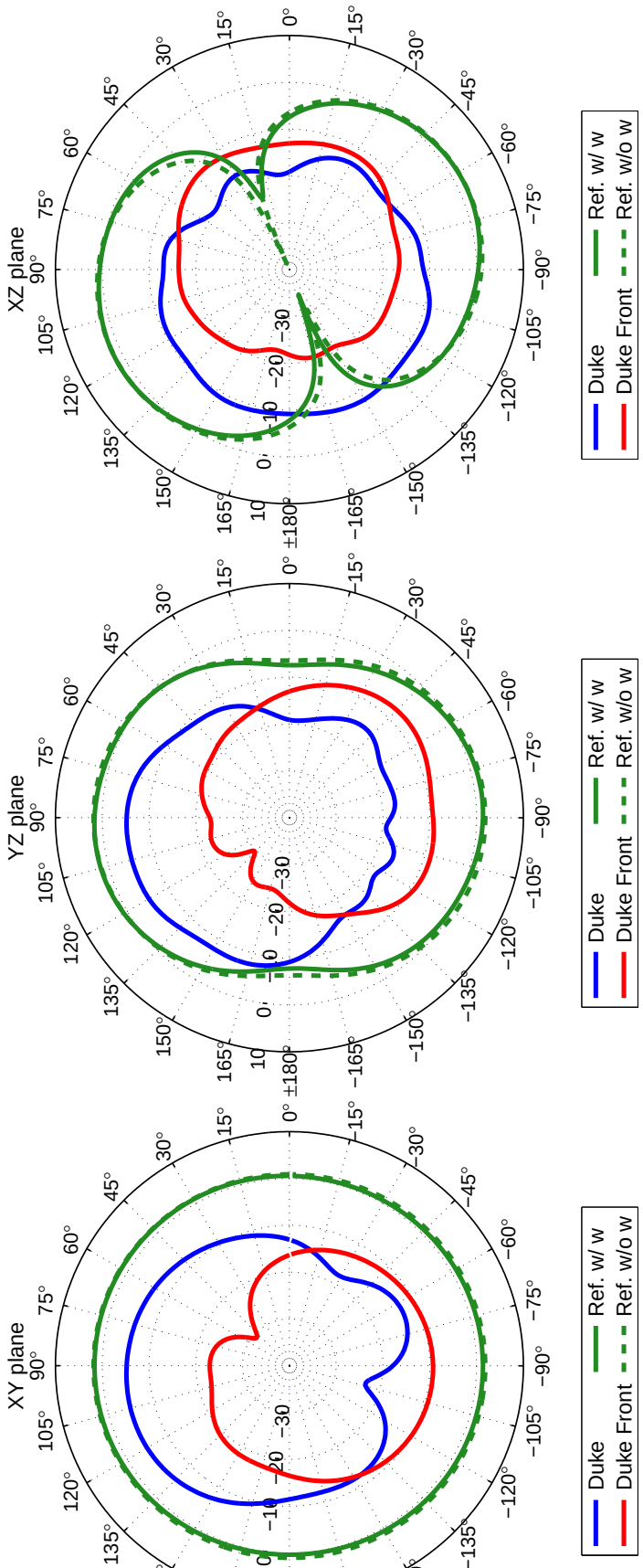

Figure 123: All Models compared to reference – bodypack monopole with wire (Ref. w/ w) and bodypack monopole without wire (Ref. w/o w)– at 470 MHz.

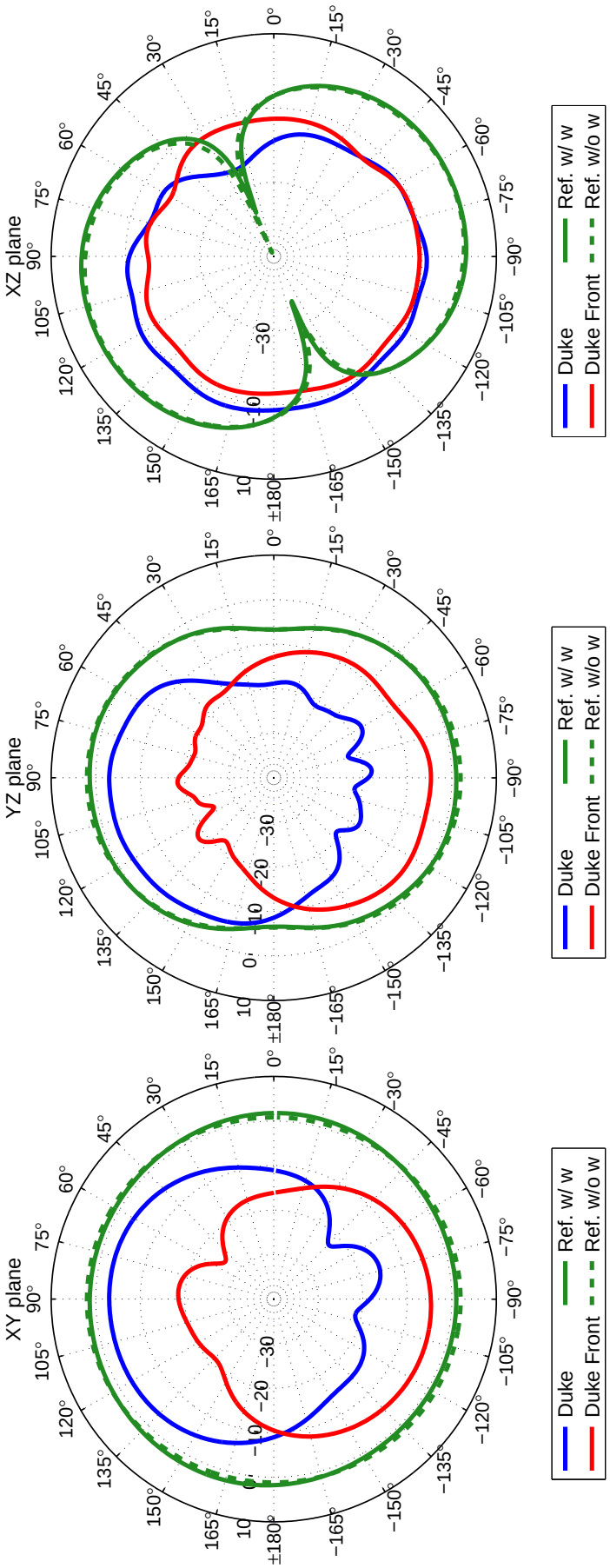

Figure 124: All Models compared to reference – bodypack monopole with wire (Ref. w/ w) and bodypack monopole without wire (Ref. w/o w)– at 595 MHz.

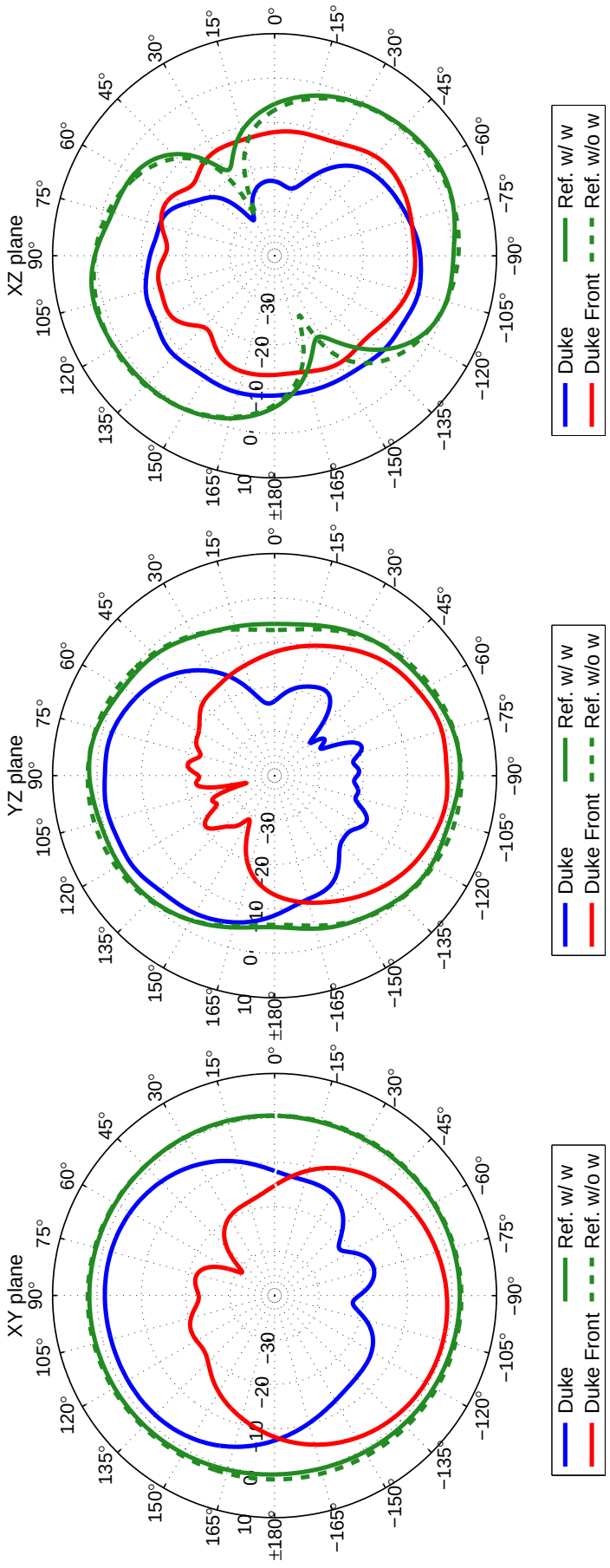

Figure 125: All Models compared to reference – bodypack monopole with wire (Ref. w/ w) and bodypack monopole without wire (Ref. w/o w)– at 750 MHz.

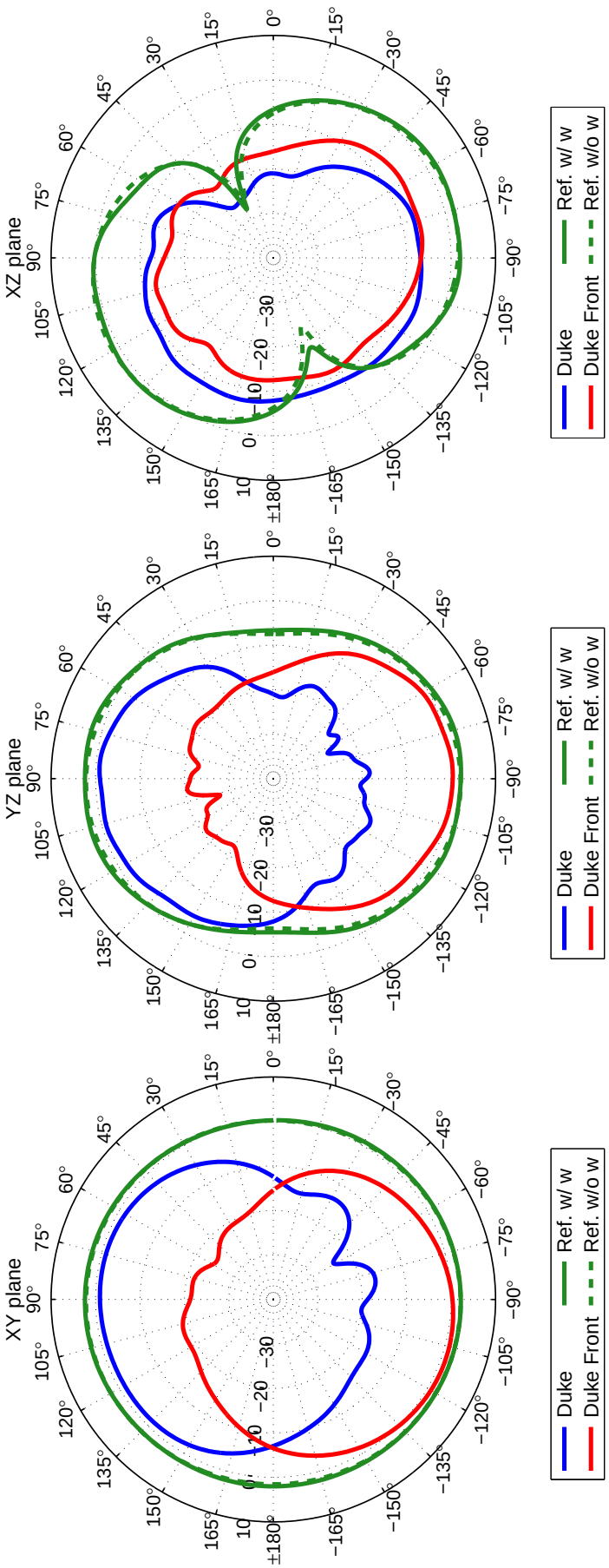

Figure 126: All Models compared to reference – bodypack monopole with wire (Ref. w/ w) and bodypack monopole without wire (Ref. w/o w)– at 825 MHz.

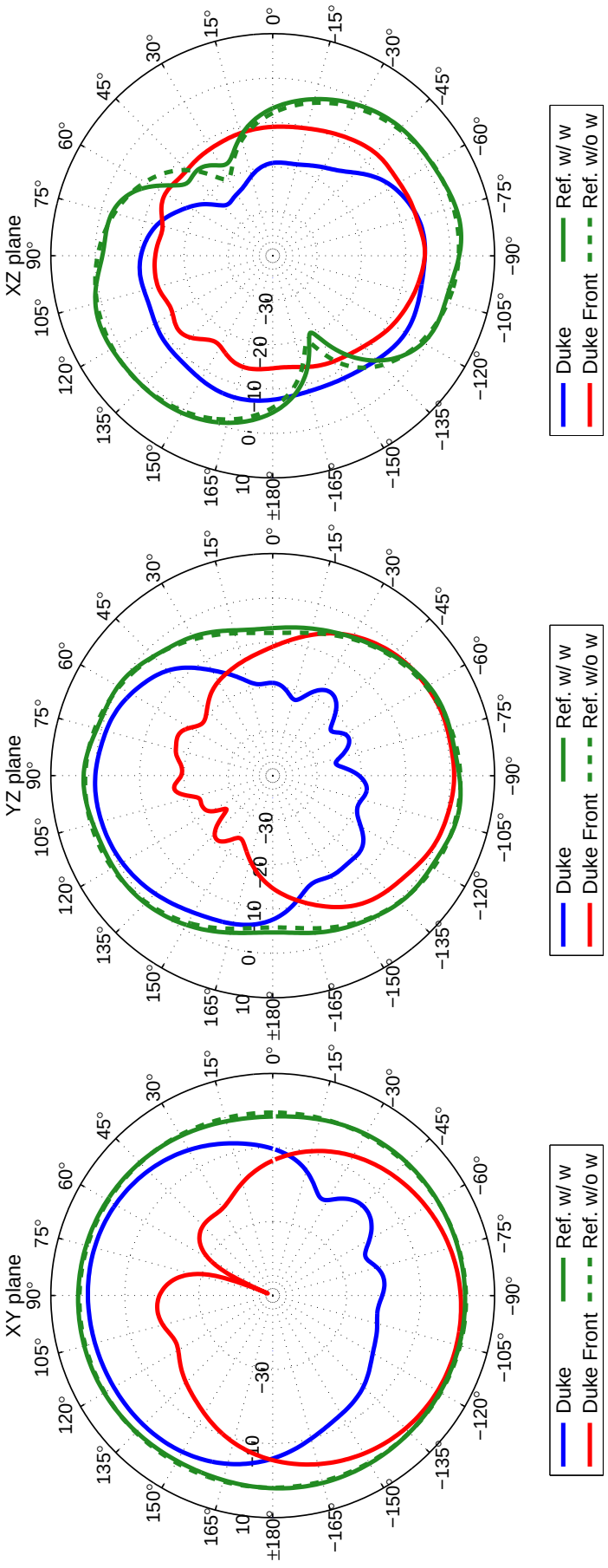

Figure 127: All Models compared to reference – bodypack monopole with wire (Ref. w/ w) and bodypack monopole without wire (Ref. w/o w)– at 945 MHz.

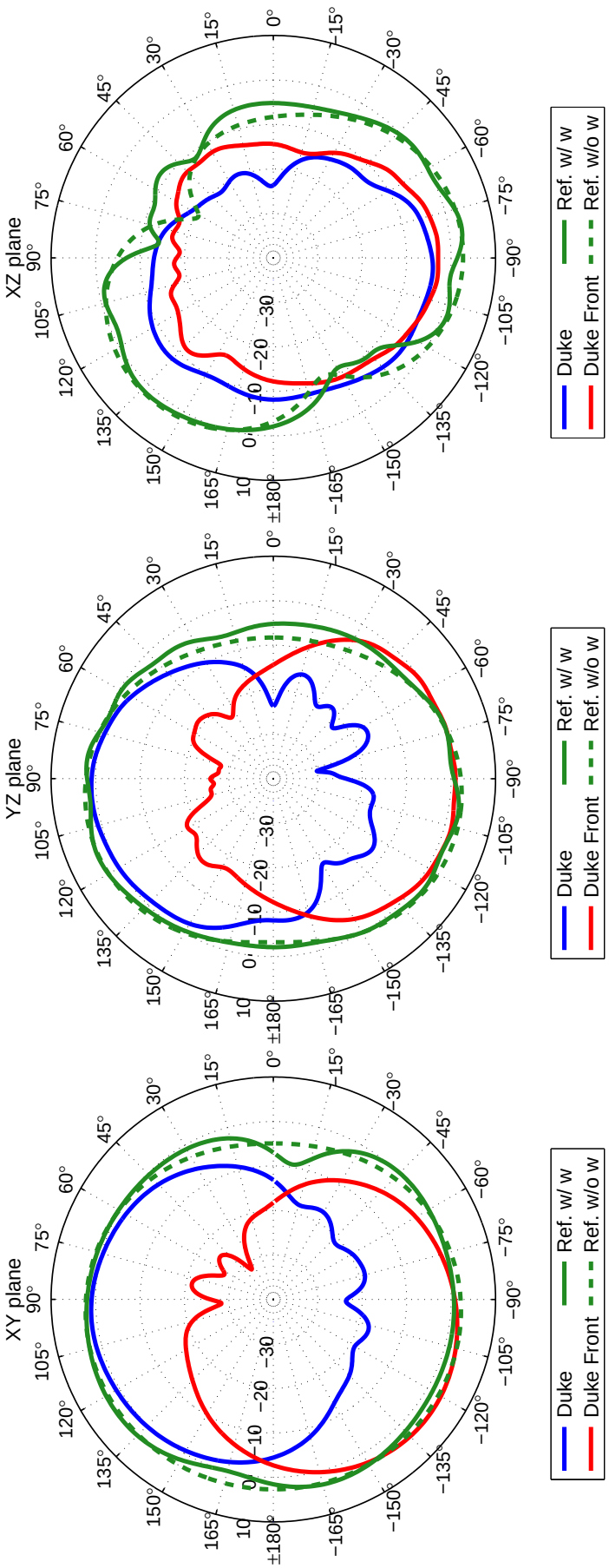

Figure 128: All Models compared to reference – bodypack monopole with wire (Ref. w/ w) and bodypack monopole without wire (Ref. w/o w)– at 1190 MHz.

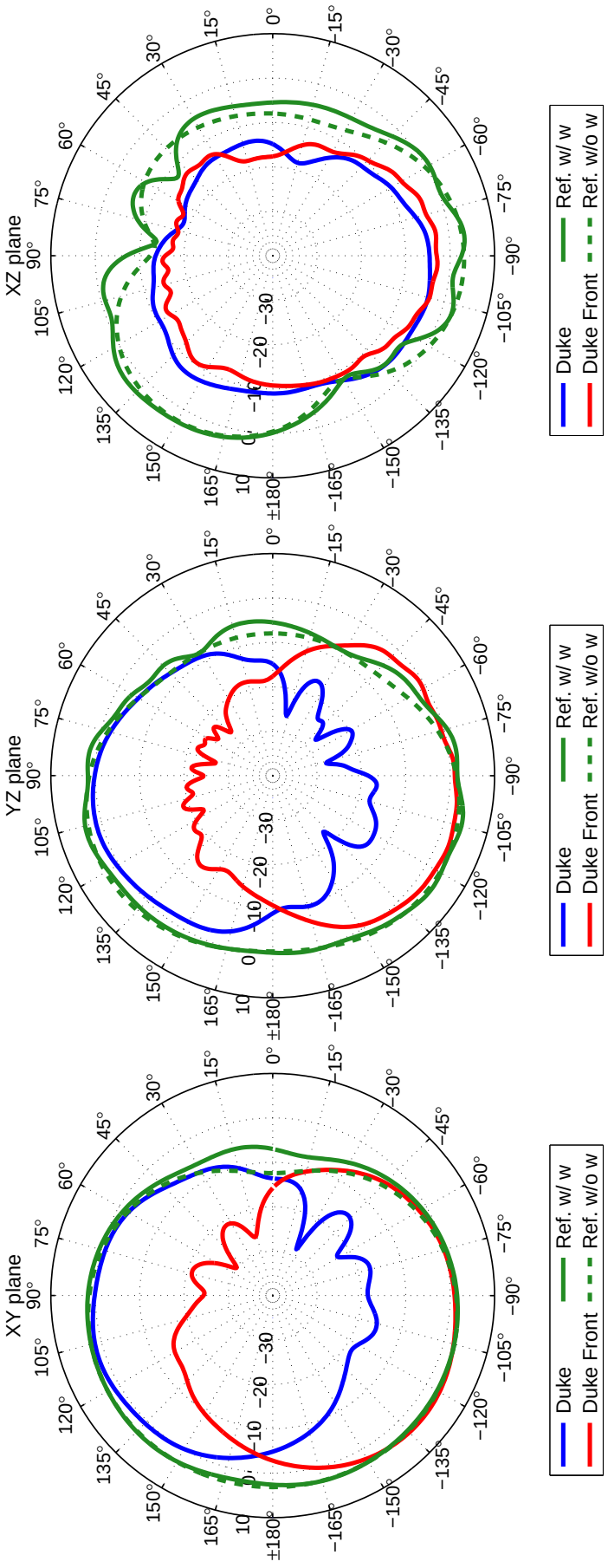

Figure 129: All Models compared to reference – bodypack monopole with wire (Ref. w/ w) and bodypack monopole without wire (Ref. w/o w)– at 1400 MHz.

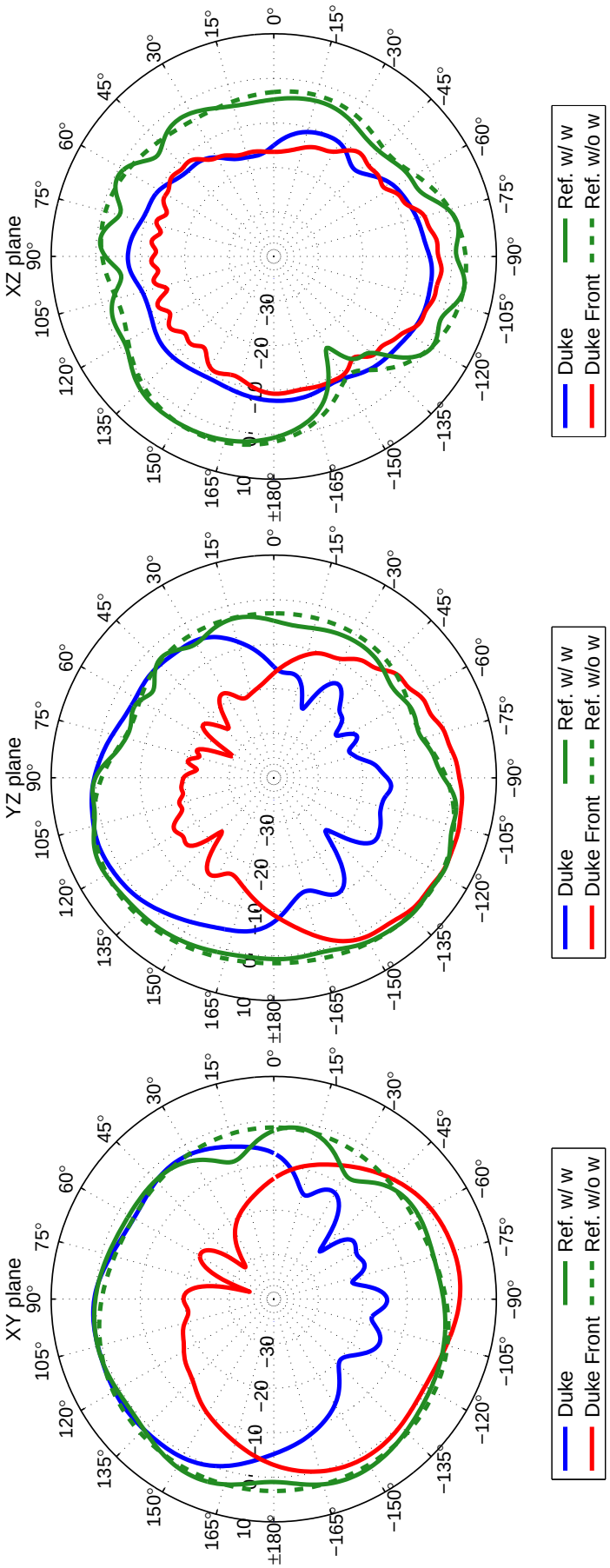

Figure 130: All Models compared to reference – bodypack monopole with wire (Ref. w/ w) and bodypack monopole without wire (Ref. w/o w)– at 1700 MHz.

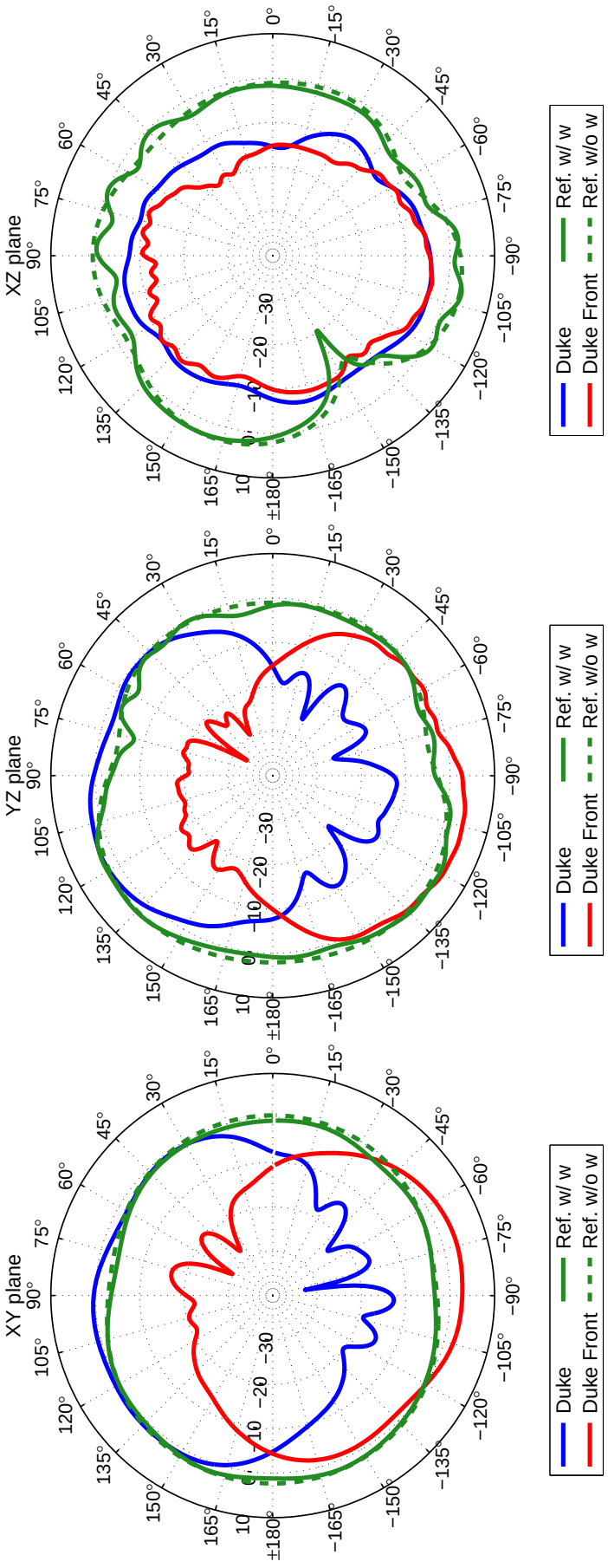

Figure 131: All Models compared to reference – bodypack monopole with wire (Ref. w/ w) and bodypack monopole without wire (Ref. w/o w)– at 1890 MHz.

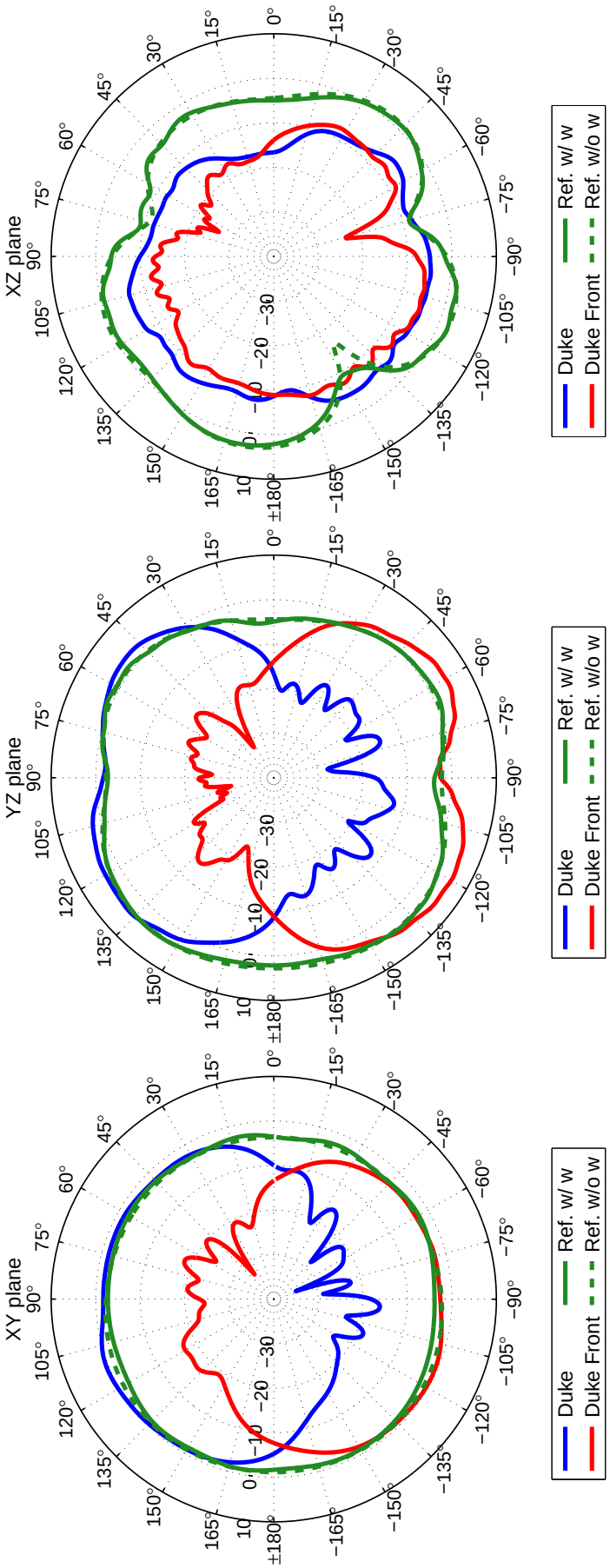

Figure 132: All Models compared to reference – bodypack monopole with wire (Ref. w/ w) and bodypack monopole without wire (Ref. w/o w)– at 2380 MHz.

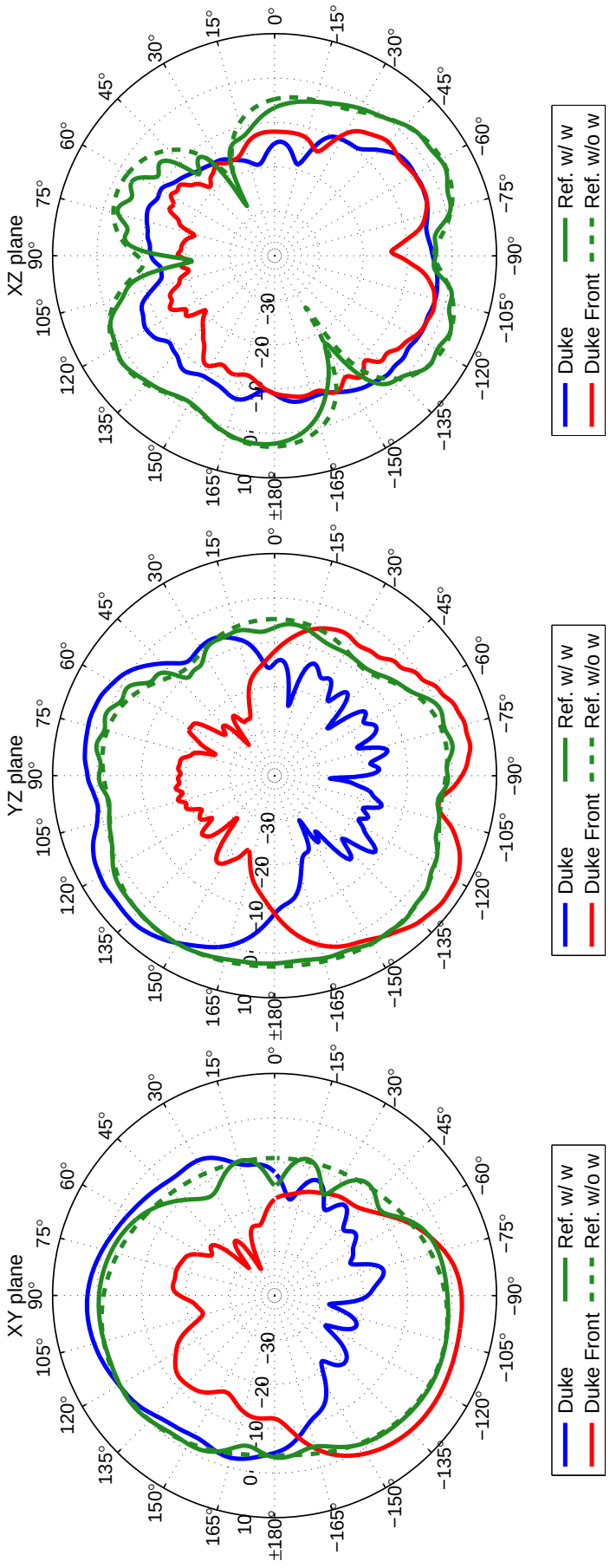

Figure 133: All Models compared to reference – bodypack monopole with wire (Ref. w/ w) and bodypack monopole without wire (Ref. w/o w)– at 3000 MHz.

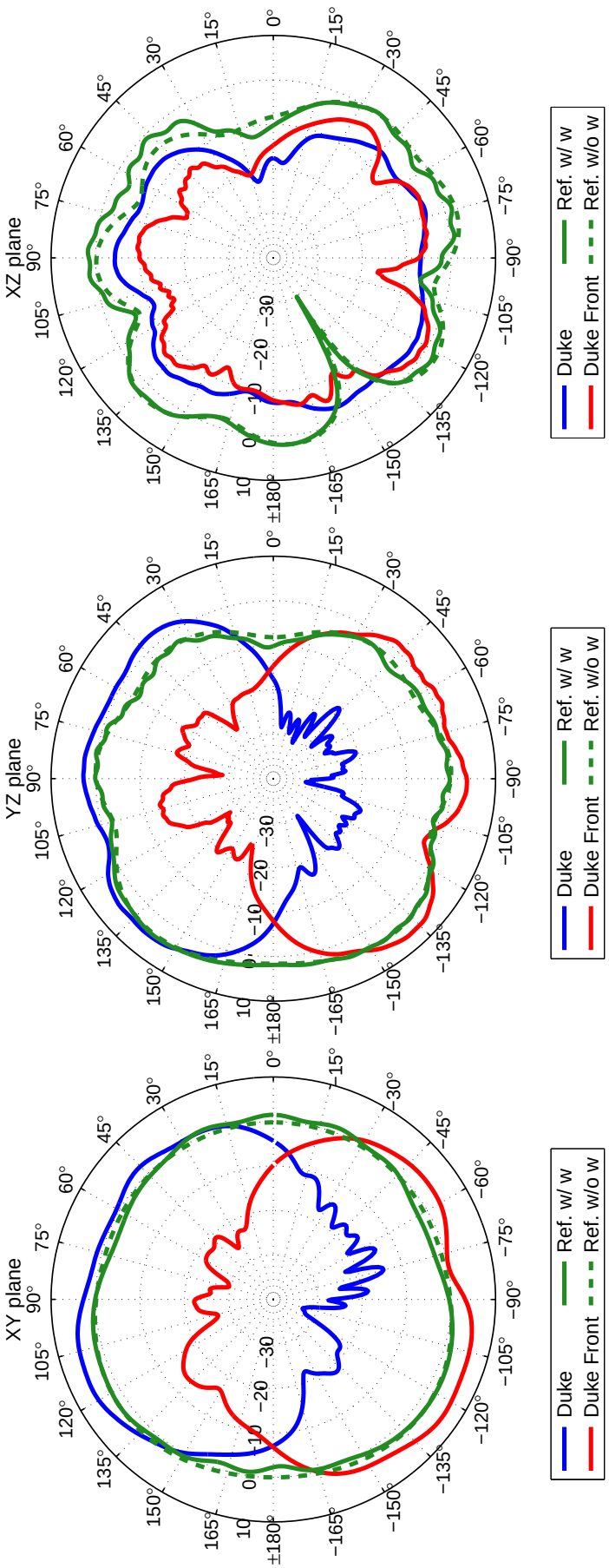

Figure 134: All Models compared to reference – bodypack monopole with wire (Ref. w/ w) and bodypack monopole without wire (Ref. w/o w)– at 3780 MHz.

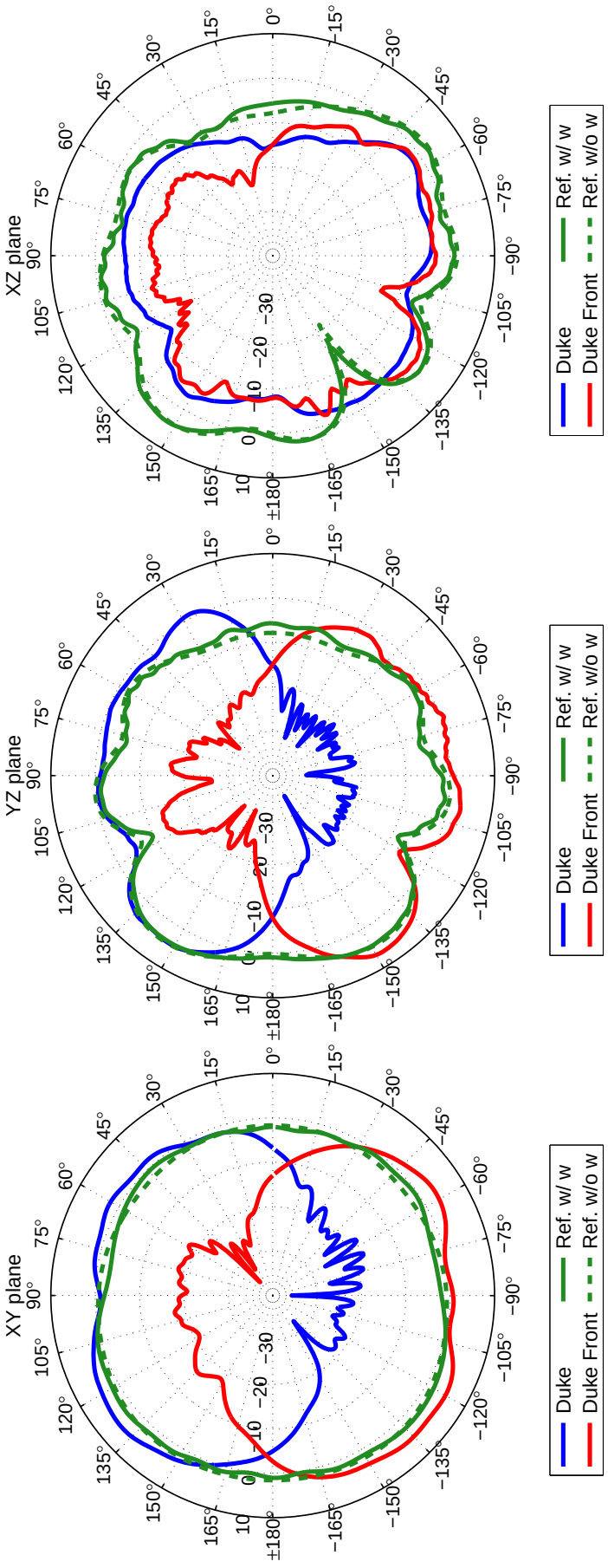

Figure 135: All Models compared to reference – bodypack monopole with wire (Ref. w/ w) and bodypack monopole without wire (Ref. w/o w)– at 4760 MHz.

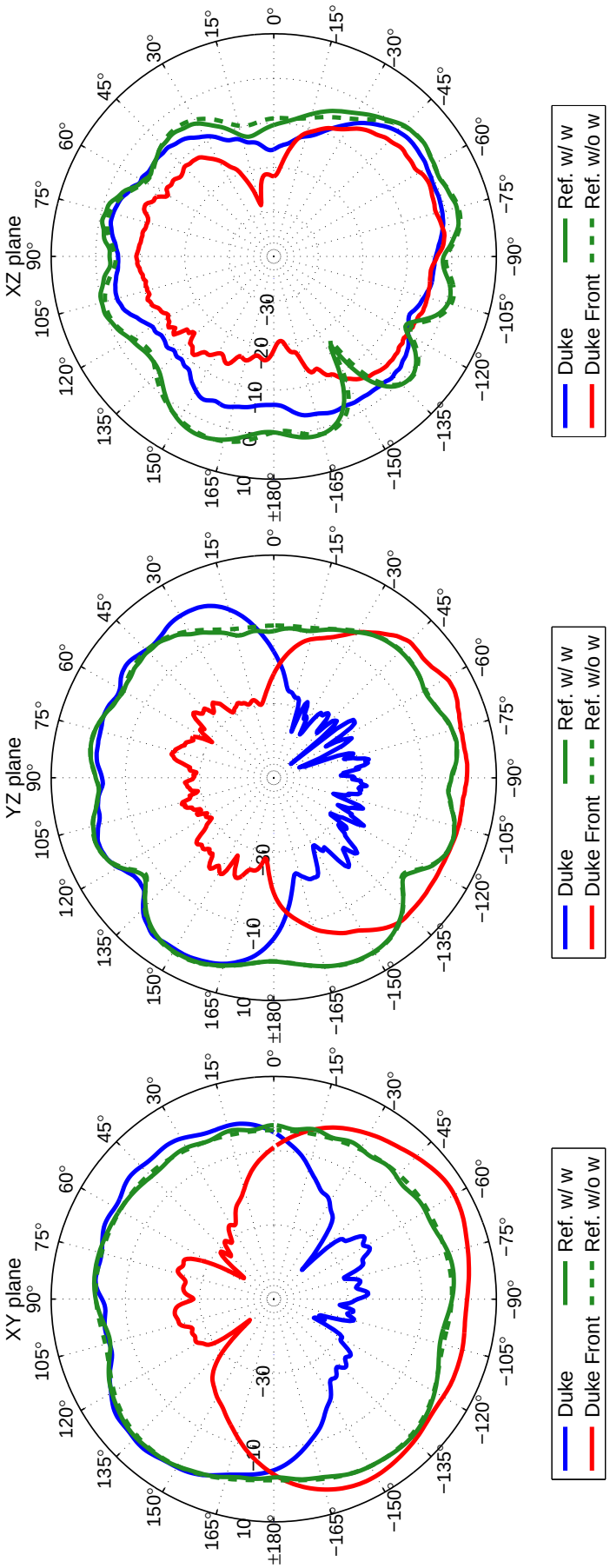

Figure 136: All Models compared to reference – bodypack monopole with wire (Ref. w/ w) and bodypack monopole without wire (Ref. w/o w)– at 6000 MHz.

References

[1] SONY. Wireless microphone package. 2008.

[2] Christ A, Kainz W, Hahn EG, Honegger K, Zefferer M, Neufeld E, Rascher W, Janka R, Bautz W, Chen J, Kiefer B, Schmitt P, Hollenbach HP, Shen J, Oberle M, Szczerba D, Kam A, Guag JW, and Kuster N. The virtual family–development of surface-based anatomical models of two adults and two children for dosimetric simulations. Physics in Medicine and Biology, 55(2):N23–38, January 2010.

[3] P.A. Hasgall, E. Neufeld, M.C. Gosselin, A. Klingenbck, and N. Kuster. It'is database for thermal and electromagnetic parameters of biological tissues. 2014.